uOttawa

L'Université canadienne
Canada's university

FACULTÉ DES ÉTUDES SUPÉRIEURES ET POSTOCTORALES

u Ottawa

L'Université canadienne
Canada's university

FACULTY OF GRADUATE AND POSDOCTORAL STUDIES

Dominique Yelle
AUTEUR DE LA THÈSE / AUTHOR OF THESIS

M.Sc. (Cellular and Molecular Medicine)
GRADE / DEGREE

Department of Cellular and Molecular Medicine
FACULTÉ, ÉCOLE, DÉPARTEMENT / FACULTY, SCHOOL, DEPARTMENT

The Role of Apoptosis in a BMPR2 Mutant Model of Pulmonary Arterial Hypertension
TITRE DE LA THÈSE / TITLE OF THESIS

Duncan Stewart
DIRECTEUR (DIRECTRICE) DE LA THÈSE / THESIS SUPERVISOR

CO-DIRECTEUR (CO-DIRECTRICE) DE LA THÈSE / THESIS CO-SUPERVISOR

Rhion Touyz

Alexandre Stewart

Gary W. Slater
Le Doyen de la Faculté des études supérieures et postdoctorales / Dean of the Faculty of Graduate and Postdoctoral Studies

The role of apoptosis in a BMPR2 mutant model of pulmonary arterial hypertension

Dominique Yelle

This thesis is submitted as a partial fulfillment of the M.Sc. program in Cellular and Molecular Medicine

Department of Cellular and Molecular Medicine
Faculty of Medicine
University of Ottawa
September 20, 2010

Your file Votre référence
ISBN: 978-0-494-79689-4
Our file Notre référence
ISBN: 978-0-494-79689-4

Abstract

Pulmonary arterial hypertension (PAH) is a rare and fatal disease caused by excessive remodelling of small pulmonary arterioles. Heterozygous loss-of-function mutations in the bone morphogenetic protein receptor 2 (BMPR2) have recently been identified in a large portion of patients with familial and idiopathic PAH. However, how mutations in this ubiquitously expressed receptor result in such a specific abnormality of the lung microcirculation is unknown. We hypothesized that loss-of-function mutations in BMPR2 lead to PAH by increasing the susceptibility of ECs to apoptosis, particularly within fragile pulmonary arterioles. To examine the consequences of BMPR2 mutations on the development of PAH, we generated mice that ubiquitously over-express an arginine to stop mutation in the receptor's C-terminal domain ($BMPR2^{R899X}$). Characterization of these mice revealed a significant increase in right ventricular systolic pressure, an indicator of pulmonary pressure, which was associated with muscularization of small pulmonary arterioles, alveolar septal thickening and pulmonary macrophage infiltration. In addition, a modest increase in apoptosis was detected in these mice. These data suggest that BMPR2 loss-of-function mutations increase the susceptibility of ECs to apoptosis and set the stage for excessive inflammation, possibly leading to spontaneous PAH. This new model will help elucidate the pathophysiological events leading to the development of PAH and provide a unique tool to evaluate novel potential treatments for this disease.

Table of Contents

List of tables and figures i
List of abbreviations iii
Acknowledgements iv
1. Introduction 1
1.1. Pulmonary arterial hypertension 1
1.2. Endothelial dysfunction and PAH 3
1.2.1. The pulmonary vascular endothelium and endothelial dysfunction 3
1.2.2. Evidence for endothelial dysfunction in PAH 4
1.2.2.1. Decreased NO production in PAH 4
1.2.2.2. Decreased prostacyclin levels in PAH 5
1.2.2.3. Increased ET-1 levels in PAH 5
1.2.2.4. Increased thromboxane A_2 production in PAH 6
1.2.3. Current PAH therapies stemming from endothelial dysfunction 7
1.3. Angioproliferative lesions and the PAH "cancer paradigm" 9
1.4. Inflammation and PAH 9
1.5. The bone morphogenetic protein receptor 2 and PAH 12
1.5.1. BMPR2 mutations and the genetic basis of PAH 11
1.5.2. BMPR2 signalling 12
1.5.3. Assessment of PAH in BMPR2 deficient mouse models 15
1.5.4. Relevance of BMPR2 signalling for vascular cells 16
1.6. Apoptosis and PAH 16
1.6.1. Evidence in support of a central role for apoptosis in PAH 16
1.6.1.1. MCT causes PAH by direct injury and apoptosis of the lung endothelium 17
1.6.1.2. VEGF survival signalling acts as a protective mechanism in PAH 17
1.6.1.3. Ang1-Tie2 EC survival pathway acts as a protective mechanism in PAH 19
1.6.2. The mechanistic link between EC apoptosis and PAH 20
1.7. $BMPR2^{R899X}$ deletional mutant mouse model 21
1.8. Hypothesis 22
1.9. Objectives 22
2. Materials and Methods 23
2.1. Mouse husbandry 23
2.2. Genotyping 23
2.3. Hemodynamic analyses 24
2.4. Tissue processing 25
2.5. Histology 26
2.5.1. Immunofluorescence 26
2.5.2. Immunohistochemistry 27
2.5.3. Hematoxylin and eosin (H&E) staining 27
2.5.4. Terminal deoxynucleotidyl transferase-mediated dUTP Nick-End-Labelling (TUNEL) staining 28
2.5.5. Microscopy 28
2.5.6. Quantification 29
2.6. Western immunoblotting 29
2.6.1. Protein extraction 29
2.6.2. Protein quantification 30

2.6.3. Gel electrophoresis 30
2.6.4. Wet transfer 31
2.6.5. Antibody detection 31
2.6.6. Quantification 32
2.7. RT-PCR 32
2.8. IL-6 administration 33
2.9. Statistical analysis 33
3. Results 34
3.1. The $BMPR2^{R899X}$ transgene is expressed in BT mice 34
3.1.1. RT-PCR revealed $BMPR2^{R899X}$ transgene expression in BT mice 34
3.1.2. $BMPR2^{R899X}$ transgene expression in BT mice could not be confirmed by Western blots with DDK and BMPR2 antibodies 34
3.1.3. Immunofluorescence staining with a DDK antibody suggests $BMPR2^{R899X}$ transgene expression in BT mice 36
3.2. Preliminary examination of BMPR2 signalling did not reveal changes in major downstream pathways 36
3.3. BT mice develop PAH with arteriolar remodelling and inflammatory infiltrates 38
3.3.1. RVSP is increased in BT mice after 1, 2 and 8 weeks of transgene induction 38
3.3.2. RV hypertrophy is not increased in BT mice 41
3.3.3. Muscularization is increased in the small pulmonary arterioles of BT mice 41
3.3.4. Morphological abnormalities including alveolar septal thickening are detected in the lungs of BT mice 43
3.3.5. The number of macrophages is increased in the lungs of BT mice 43
3.4. Temporal patterns of proliferation and apoptosis 46
3.4.1. Apoptosis is increased in the lungs of BT mice after 2 weeks and 4 weeks of transgene induction 46
3.4.2. Proliferation is increased in the lungs of BT mice after 8 weeks of transgene induction 48
3.5. IL-6 does not appear to be an efficient environmental stressor in a small cohort of $BMPR2^{R899X}$ mice 51
3.5.1. RVSP is not increased in BT mice having received IL-6 51
3.5.2. RV hypertrophy is not increased in BT mice having received IL-6 51
3.5.3. Muscularization is increased in the small pulmonary arterioles of BT mice having received IL-6 53
3.5.4. Morphological abnormalities including alveolar septal thickening are detected in the lungs of BT mice having received IL-6 53
3.5.5. The number of macrophages is not increased in the lungs of BT mice having received IL-6 53
4. Discussion 55
4.1. Lessons from BMPR2 transgenic mice 55
4.2. Ubiquitous over-expression of the $BMPR2^{R899X}$ transgene as a new model of PAH 57
4.2.1. $BMPR2^{R899X}$ mice develop typical features of PAH associated with inflammation 58

4.2.2. The transgene is expressed in $BMPR2^{R899X}$ mice 61
4.3. Mechanism by which $BMPR2^{R899X}$ over-expression may alter BMPR2 signalling and induce PAH 64
4.4. Evolving paradigms of PAH pathogenesis 66
4.4.1. Cell growth and apoptosis 66
4.4.2. Inflammation 69
4.4.3. Unifying model of disease pathogenesis in mice over-expressing the $BMPR2^{R899X}$ transgene 71
4.5. Therapeutic implications 73
4.6. Limitations 73
4.7. Future directions 74
4.8. Conclusion 75
5. References 76
Appendix 1 – Endothelial cell-specific over-expression of the $BMPR2^{R899X}$ transgene in mice using the V-Cad promoter 83
Appendix 2 – Supplemental Western blot figures 89
Appendix 3 – Solutions and Reagents 92

List of tables and figures

Table 1. Genotyping primer sequences

Figure 1. Revised clinical classification of pulmonary hypertension according to the 2003 Third World Symposium on Pulmonary Arterial Hypertension held in Venice, Italy.

Figure 2. Consequence of BMPR2 loss-of-function mutations on vascular homeostasis and the pathogenesis of PAH.

Figure 3. Expression of the $BMPR2^{R899X}$ transgene.

Figure 4. Activity of the major downstream effectors in BMPR2 signalling.

Figure 5. Progression of RVSP and RV hypertrophy over the timecourse of $BMPR2^{R899X}$ transgene induction.

Figure 6. Combined RVSP and RV/LV+S values from individual $BMPR2^{R899X}$ induction timepoints.

Figure 7. Arteriolar smooth muscle hypertrophy in BT mice following 8 weeks of transgene induction.

Figure 8. Abnormal lung morphology in BT mice following 8 weeks of transgene induction.

Figure 9. Macrophage infiltration in the lungs of BT mice following 8 weeks of transgene induction.

Figure 10. Temporal patterns of apoptosis over the timecourse of $BMPR2^{R899X}$ induction.

Figure 11. Temporal patterns of proliferation over the timecourse of $BMPR2^{R899X}$ induction.

Figure 12. Apoptosis and proliferation from combined timepoints of transgene induction.

Figure 13. Distribution of RVSP and RV/LV+S values in mice with IL-6 treatment.

Figure 14. Characterization of arteriolar muscularization, pulmonary alveolar remodelling and macrophage infiltration in mice with IL-6 treatment.

Figure 15. Proposed model for the pathogenesis of PAH in mice over-expressing the $BMPR2^{R899X}$ transgene

Figure S1.1. Expression of the $BMPR2^{R899X}$ transgene in V-Cad mice.

Figure S1.2. Distribution of RVSP and RV/LV+S values in V-Cad mice.

Figure S1.3. Arteriolar smooth muscle hypertrophy in V-Cad BT mice after 8 weeks of transgene induction.
Figure S1.4. Apoptosis is increased in V-Cad BT mice after 8 weeks of transgene induction.

Figure S2.1. Figure S2.1. Expression of the $BMPR2^{R899X}$ transgene in total protein extracts from ROSA mice.

Figure S2.2. Expression of the $BMPR2^{R899X}$ transgene in the membrane fraction of subcellular extracts from ROSA mice.

Figure S2.3. BMPR2 expression in total protein extracts from ROSA mice.

List of abbreviations

α-SMA	α-Smooth muscle actin
ALK	Acvitin receptor-like kinase
ANOVA	Analysis of variance
APAH	Associated pulmonary arterial hypertension
BCA	Bicinchoninic acid
BMP	Bone morphogenetic protein
BMPR2	Bone morphogenetic protein receptor 2
BSA	Bovine serum albumin
BT	Binary transgenic
DAB	3,3'-diaminobenzidine
DAPI	4',6-diamidino-2-phenylindole
Dox	Doxycycline
EC	Endothelial cell
eNOS	Endothelial nitric oxide synthase
EPC	Endothelial progenitor cell
ERA	Endothelin receptor antagonist
ET-1	Endothelin-1
FPAH	Familial pulmonary arterial hypertension
H&E	Hematoxylin and eosin
HPF	High power field
HRP	Horseradish peroxidase
IF	Immunofluorescence
IHC	Immunohistochemistry
IL	Interleukin
IPAH	Idiopathic pulmonary arterial hypertension
LSAB	Labelled streptavidin biotin
LV	Left ventricle
MAPK	Mitogen-activated protein kinase
MCP-1	Monocyte chemotactic protein-1
MCT	Monocrotaline
NBT	Non binary transgenic
NO	Nitric oxide
PAH	Pulmonary arterial hypertension
PBS	Phosphate buffered saline
PCR	Polymerase chain reaction
PDGF	Platelet-derived growth factor
PFA	Paraformaldehyde
PPARγ	Peroxisome proliferator-activated receptor γ
PVR	Pulmonary vascular resistance
RT-PCR	Reverse transcriptase polymerase chain reaction
rtTA	Reverse tetracycline activator
RV	Right ventricle
RVSP	Right ventricular systolic pressure
S	Septum
SEM	Standard error of the mean
SMC	Smooth muscle cell
TGF-β	Transforming growth factor-β
TNF-α	Tumor necrosis factor-α
TUNEL	Terminal deoxynucleotidyl transferase-mediated dUTP Nick-End-Labelling
VEGF	Vascular endothelial growth factor
VEGFR	Vascular endothelial growth factor receptor
WT	Wild-type

Acknowledgements

I would first and foremost like to thank my supervisor, Dr. Duncan J. Stewart, for taking me under his wing and being such an incredible mentor. Dr. Stewart, I am very grateful for the guidance and support you provided me with, as well as the countless opportunities you have given me, from attending several incredible conferences to writing a book chapter and everywhere in between. Thank you for your patience and for entrusting me with this challenging project. To Jessie and Robin, both amazing labmates, thank you for your moral support in trying times at work and outside the lab. These past two years would not have been the same without you. And thanks to the rest of the lab members for making it such a pleasant environment to work in. I would also like to thank my advisory committee members, Dr. Kursad Turksen and Dr. Rhian Touyz, for their valuable comments and suggestions and for helping me complete this project in a timely fashion. Finally, to my family and friends, thank you for your constant support and encouragement throughout this difficult but incredible journey.

1. Introduction

1.1. Pulmonary arterial hypertension

Pulmonary arterial hypertension (PAH) is an often fatal disease caused by functional or structural abnormalities involving the precapillary pulmonary arteriolar bed that result in progressive increases in pulmonary vascular resistance (PVR) [1]. Recent revision of the clinical classification of pulmonary hypertensive diseases has led to the identification of PAH as the first of five distinct groups of pulmonary hypertension (Figure 1). According to this new classification, PAH can be subclassified in three main groups: 1) idiopathic (IPAH, previously known as primary pulmonary hypertension), which occurs in the absence of any known contributing disorders; 2) heritable or familial PAH (FPAH); and 3) associated PAH (APAH, previously termed secondary PAH), which is associated with other diseases such as collagen vascular diseases (i.e. scleroderma), HIV, and systemic to pulmonary shunt (i.e. congenital heart disease) [2].

The estimated incidence of IPAH cases is 2 to 3 per million per year, with a median survival from diagnosis of only 2.8 years before the advent of modern therapies [1, 3]. The disease typically affects young women (2,3 female:1 male) with a median age at diagnosis of 36 years, although the disease can occur at any age [4].

Clinically, the pathological features of advanced PAH are characterized by medial hypertrophy, adventitial thickening, intimal fibrosis and obliteration of small pulmonary arterioles, and often include the presence of plexiform lesions, which are thought to result from dysregulated vascular cell proliferation [1, 5, 6]. Other characteristic pathological findings include *in situ* thrombosis and varying degrees of inflammation [1, 6]. The narrowing of the lumen diameter and functional pruning of pulmonary arterioles result in increased PVR and pulmonary arterial pressure, leading to right ventricular hypertrophy and

Table 3. Revised Clinical Classification of Pulmonary Hypertension (Venice 2003)

1. Pulmonary arterial hypertension (PAH)
   - 1.1. **Idiopathic** (IPAH)
   - 1.2. Familial (FPAH)
   - 1.3. Associated with (APAH):
     - 1.3.1. Collagen vascular disease
     - 1.3.2. Congenital systemic-to-pulmonary shunts**
     - 1.3.3. Portal hypertension
     - 1.3.4. HIV infection
     - 1.3.5. Drugs and toxins
     - 1.3.6. **Other** (thyroid disorders, glycogen storage disease, Gaucher disease, hereditary hemorrhagic telangiectasia, hemoglobinopathies, myeloproliferative disorders, splenectomy)
   - 1.4. **Associated with significant venous or capillary involvement**
     - 1.4.1. Pulmonary veno-occlusive disease (PVOD)
     - 1.4.2. Pulmonary capillary hemangiomatosis (PCH)
   - 1.5. Persistent pulmonary hypertension of the newborn
2. Pulmonary hypertension with left heart disease
   - 2.1. Left-sided atrial or ventricular heart disease
   - 2.2. Left-sided valvular heart disease
3. Pulmonary hypertension associated with lung diseases and/or hypoxemia
   - 3.1. Chronic obstructive pulmonary disease
   - 3.2. Interstitial lung disease
   - 3.3. Sleep-disordered breathing
   - 3.4. Alveolar hypoventilation disorders
   - 3.5. Chronic exposure to high altitude
   - 3.6. Developmental abnormalities
4. Pulmonary hypertension due to chronic thrombotic and/or embolic disease
   - 4.1. Thromboembolic obstruction of proximal pulmonary arteries
   - 4.2. Thromboembolic obstruction of distal pulmonary arteries
   - 4.3. Non-thrombotic pulmonary embolism (tumor, parasites, foreign material)
5. **Miscellaneous**

   Sarcoidosis, histiocytosis X, lymphangiomatosis, compression of pulmonary vessels (adenopathy, tumor, fibrosing mediastinitis)

Figure 1. Revised clinical classification of pulmonary hypertension according to the 2003 Third World Symposium on Pulmonary Arterial Hypertension held in Venice, Italy. *Taken from Simonneau G et al., Journal of the American College of Cardiology, 2004.*

ultimately to right heart failure [7-10]. Unfortunately, despite recent advances in therapeutic approaches which help prolong survival and improve quality of life, the prognosis for patients with PAH remains poor as many succumb to the disease within 3 to 5 years of diagnosis [11].

1.2. Endothelial dysfunction and PAH

1.2.1. The pulmonary vascular endothelium and endothelial dysfunction

The mechanisms involved in the pathogenesis of PAH remain a matter of intense debate and speculation, even today. Over the years, a substantial number of molecules have been implicated as putative candidates. However, most modern therapies were developed based on our understanding of the integral role of endothelial dysfunction in the development of this disease. Originally, endothelial dysfunction was defined as a shift in the balance of production of endothelial vasoactive factors away from vasodilator and antiproliferative agents, in favor of the release of vasoconstrictor and proliferative factors [12]. Under physiological conditions, the pulmonary vascular endothelium not only acts as a structural barrier to the passage of fluids and proteins into the interstitium, but also actively regulates the tone, growth, differentiation and migration of vascular smooth muscle cells (SMCs), in addition to exerting potent antithrombotic and anti-inflammatory influences [12]. These effects are mediated largely through the release of vasodilator substances such as the endothelium-derived relaxing factors nitric oxide (NO) and prostacyclin, as well as constricting factors, including endothelin-1 (ET-1) and thromboxane A_2 [12-15]. Consistent with endothelial dysfunction, PAH patients demonstrate an increase in ET-1 [16] and thromboxane A_2 [17] production across the pulmonary bed, as well as reduced prostacyclin and NO bioactivity [18, 19]. The initiating mechanism leading to endothelial dysfunction in

this disease is unknown, but may include hypoxia, shear stress, inflammation or response to drugs or toxins on a background of genetic susceptibility [6, 20]. Current evidence strongly suggests that endothelial dysfunction plays an integral role in mediating the pulmonary arterial structural changes observed in PAH

1.2.2. Evidence for endothelial dysfunction in PAH

1.2.2.1. Decreased NO production in PAH

NO plays an important role in modulating pulmonary vascular tone. It is a potent endogenous endothelium-derived vasodilator that directly relaxes vascular smooth muscle cells [12, 21]. In addition to its vasorelaxation effect, NO also exerts potent antiplatelet, antithrombotic and antimitogenic properties thereby preventing platelet aggregation, cell adhesion and smooth muscle cell proliferation [5, 12]. NO signals through its cytoplasmic receptor, the soluble guanylyl cyclase, which results in the generation of the second messenger cGMP that mediates most of the physiological effects of NO [22]. NO production is catalyzed by endothelial nitric oxide synthase (eNOS) [23]. Lungs from PAH patients have been reported to demonstrate reduced eNOS expression [18], although this has not been confirmed by other groups [24]. A contributory role for deficient NO production in the pathogenesis of PAH is further supported by transgenic animal models, in which over-expression of eNOS prevented hypoxia-induced PAH [25], while exposure to mild hypoxia resulted in more severe PAH in eNOS-deficient mice [26]. However, again there are conflicting findings and some groups have reported that eNOS knockout mice do not exhibit any increase in hypoxia-induced PAH, and may even show less arterial remodelling in response to chronic hypoxia than wild type mice [27].

1.2.2.2. Decreased prostacyclin levels in PAH

Prostacyclin is another important endothelium-derived vasodilator factor and has also been strongly implicated in pulmonary vascular homeostasis. In addition to promoting vasodilation in the pulmonary circulation, like NO, it is a potent endogenous inhibitor of platelet aggregation [6, 12]. The effects of NO and prostacyclin in the pulmonary vasculature are thus highly complementary. Prostacyclin also protects against pulmonary remodelling by inhibiting the growth of SMCs [21, 28]. The production of prostacyclin from prostaglandin H2 is catalyzed by prostacyclin synthase [29]. Deficiency in prostacyclin production has been strongly implicated in PAH. Prostacyclin synthase expression is decreased in lungs from patients with severe PAH [19] and prostacyclin receptor-deficient mice develop severe PAH in response to chronic hypoxia [30]. In addition, over-expression of prostacyclin synthase protects mice from chronic hypoxia-induced PAH [31]. Therefore, it is widely accepted that decreased prostacyclin levels in PAH may account for pulmonary vasoconstriction, SMC proliferation, and the pro-thrombotic state observed in this disease.

1.2.2.3. Increased ET-1 levels in PAH

ET-1 is secreted by the endothelium and is one of the most potent endogenous vasoconstrictor peptides known [5, 12]. In addition to its vasoactive properties, it also has platelet-aggregating properties as well as a growth promoting effects on SMCs and other cell types [12, 28]. The effects of ET-1 are mediated through the ET_A and ET_B receptors [21]. Activation of ET_A receptors, located mainly on vascular SMCs, causes sustained vasoconstriction and proliferation of vascular SMCs [13, 21]. In contrast, ET_B receptors which are found mainly on endothelial cells (ECs) mediate pulmonary endothelin clearance and induce the production of NO and prostacyclin by ECs [13, 21]. There is strong evidence

that ET-1 is a major player inducing vasoconstriction and remodelling in PAH. Our group was the first to demonstrate that levels of circulating ET-1 are increased in patients with PAH [16, 32], and that this was associated with massive upregulation of endothelial ET-1 expression within the pulmonary vasculature of patients with either IPAH or APAH [32]. Furthermore, in a number of experimental models, PAH is associated with selective increases in ET-1 and ET_A receptor expression in the pulmonary vasculature [33]. It has been suggested that a selective increase in the synthesis and release of ET-1 from pulmonary ECs, accompanied by a paracrine effect mediated by ET_A receptors on underlying pulmonary SMCs could contribute to both the vasoconstriction and vascular remodelling seen in PAH [12].

1.2.2.4. Increased thromboxane A_2 production in PAH

Thromboxane A_2 is another potent vasoconstrictor, as well as a smooth muscle mitogen and platelet agonist [17, 28], in many ways counteracting the effects of prostacyclin. Indeed, in endothelial dysfunction, the balance of vasodilator and vasoconstrictor prostaglandin production is shifted, and an increase in the production of thromboxane A_2 together with a decrease in prostacyclin have been reported in patients with PAH [17, 28]. The resulting imbalance between thromboxane A_2 and prostacyclin may thus contribute to the platelet activation and abnormal response of the pulmonary vascular endothelium in this disease. Whether the imbalance in the release of these mediators is a cause or a result of PAH is unknown, but it likely plays an important role in the progression of the disease.

1.2.3. Current PAH therapies stemming from endothelial dysfunction

Over the last two decades, the development of new therapies for PAH has focused on restoring the balance between vasoconstrictor and vasodilator pathways, which represent logical pharmacological targets [34].

The first such therapy to be introduced in the "modern era" of PAH management was systemic prostanoid infusion. The administration of prostacyclin by continuous intravenous infusion was pioneered by Higenbottam and his group at Papworth Hospital in the early 1980s [35], and later developed as the gold standard for treatment of severe PAH. Parenteral delivery of Flolan® via an indwelling central catheter has been shown to improve function, hemodynamics and survival in WHO class III or IV patients [36, 37]. However, this is a cumbersome and expensive treatment that is increasingly being reserved for the most difficult patients to manage, in favor of more convenient prostagladin delivery systems including subcutaneous (treprostinil) or inhaled (iloprost) prostanoids [15, 21], although these are supported by less definitive evidence of efficacy.

The next major advance came from the introduction of endothelin receptor antagonists (ERAs) which provided the first effective oral agents for patients with PAH. Bosentan is a dual (ET_A and ET_B) ERA and was the first shown to be effective in large scale clinical trials [38], and is now widely used as a first line treatment for PAH [21, 28]. More recently, a number of other ERAs have been introduced and there is an ongoing debate as to the benefits of dual versus ET_A-selective ERAs for this disease. ET_A-selective receptor blockers have the theoretical advantage of sparing the endothelial ET_B receptors, which mediate ET-1 clearance and endothelium-dependent vasodilation [21]; sitaxsentan and ambrisentan are two such ET_A-selective receptor antagonists that have been approved in

many jurisdictions for the treatment of PAH. However, to date, there is no clear evidence from clinical studies to establish the superiority of an ET_A selective strategy.

The understanding of the importance of the NO pathway has also led to the development of inhaled NO as a therapeutic strategy [39], and although useful for the acute management of PAH in a critical care setting, such as in the neonatal treatment of persistent pulmonary hypertension of the newborn, it has proven to be difficult to deliver over the long-term for the treatment of ambulatory patients. Oral phosphodiesterase type V inhibitors such as sildenafil (better known as Viagra), which increase the levels of the second messenger cGMP, have been shown to induce acute pulmonary vasodilation during short-term administration and improve exercise capacity and pulmonary hemodynamics in patients with PAH during long-term oral therapy [21, 40]. Sildenafil is now widely used in the treatment of this disease and other agents, such as tadalafil which has a longer half-life, are being introduced [41].

However, despite the proliferation of new drug therapies, nearly all patients will progress and ultimately fail medical management. For this reason, the use of combination therapy with agents acting via different mechanisms is becoming increasingly prevalent in order to maximize the clinical benefit [21]. Nonetheless, the impact of medical management on the overall prognosis of PAH has been limited; a recent systematic review of modern PAH therapies did not support any meaningful benefit on survival in these patients [42], highlighting the need for more effective treatment strategies.

Furthermore, current PAH therapies are largely addressing abnormalities in vasodilation, and do not seem to be able to modify the remodelling events that are increasingly believed to be the pathological basis of "irreversible" PAH. Indeed, only a small minority of IPAH patients (<13%) show evidence of an acute vasodilator response at

their initial hemodynamic assessments [43], again consistent with the notion that arteriolar remodelling is a dominant mechanism in the pathogenesis of PAH.

1.3. Angioproliferative lesions and the PAH "cancer paradigm"

Further support for the prevalence of remodelling mechanisms in PAH came from the recognition of the angioproliferative, cancer-like properties of vascular cells in PAH. Indeed, it was shown *in vitro* that after initial apoptosis of ECs induced by vascular endothelial growth factor receptor (VEGFR) blockade, there is increased proliferation of apoptosis resistant ECs [44]. Moreover, ECs cultured from the pulmonary arteries of PAH patients show evidence of increased proliferation and decreased apoptosis compared to those isolated from controls [45]. Lung biopsies from patients with irreversible PAH also recently revealed the presence of the anti-apoptotic protein Bcl-2, which is absent from patients with reversible PAH [45]. In parallel, experimental evidence came for the emergence of apoptosis-resistant, hyperproliferative SMCs in PAH. Pulmonary artery SMCs from PAH patients were demonstrated to be hyperproliferative and resistant to apoptosis, and these patients express the anti-apoptotic protein survivin in their pulmonary arteries [46]. Therefore, the "cancer paradigm" of PAH arose leading some to consider the presence of abnormal, hyperproliferative cells as the central feature of the disease by contributing to the formation of the characteristic plexiform lesions.

1.4. Inflammation and PAH

Inflammatory processes are also increasingly being recognized as major pathogenic components of pulmonary vascular remodelling, as they are prominent in various types of human PAH and experimental models. However, their contribution to the pathogenesis of

PAH remains poorly understood. Fortunately, substantial advances in the field are progressively illuminating the role of inflammation and the underlying cellular and molecular mechanisms that contribute to PAH.

Endothelial dysfunction in PAH can predispose to vascular inflammation by resulting in the upregulation of surface adhesion molecules involved in the trafficking of leukocytes as well as the release of cytokines and chemokines that recruit circulating inflammatory cells [47]. Indeed, several immunological disturbances have been reported in patient and experimental models with PAH. Lung sections from patients with IPAH often show extensive inflammatory infiltrates [48, 49], and the most common causes of APAH are autoimmune disorders such as scleroderma and systemic lupus erythematosus [50]. In addition, increased circulating levels of the pro-inflammatory cytokines interleukin (IL)-1, IL-6 and tumor necrosis factor (TNF)-α have been reported in patients with IPAH [6, 13]. Interestingly, IL-1 has been shown to stimulate ET-1 production and may act as a link between endothelial dysfunction and inflammation [13]. Similarly, IL-1 and IL-6 promote thrombosis and are potent SMC mitogens [14]. ET-1 itself can act as a cytokine by priming neutrophils, activating mast cells and stimulating monocytes to produce a variety of cytokines such as IL-1, IL-6, IL-8, TNF-α and transforming growth factor (TGF)-β [51]. Furthermore, macrophages and T lymphocytes are found in plexiform lesions and small arterioles in severe PAH [6]. Resident macrophages lining the alveolar walls are an important component of lung innate immunity, where they act as a clearance mechanism by mediating phagocytosis of debris and pathogens entering the lungs, but macrophages can also be recruited to the lungs by different inflammatory mediators. In support of this, a study has shown that PAH is associated with the upregulation of CX3CR1, part of a pathway

responsible for the recruitment of macrophages to the vessel wall, implying that active recruitment of macrophages plays a causal role in the development of idiopathic PAH [48].

A contributory role for IL-6 in the pathogenesis of PAH has also been demonstrated experimentally. Delivery of recombinant IL-6 protein in rats resulted in PAH associated with luminal occlusion of the small pulmonary arteries, formation of microvascular thrombi and localized hemorrhage [52]. In another study, mice treated with recombinant IL-6 demonstrated increased right ventricular systolic pressure (RVSP) and right ventricular hypertrophy, which was further augmented upon hypoxic exposure [53]. Moreover, IL-6 knockout mice demonstrated decreased hypoxia-induced PAH which was associated with attenuated macrophage recruitment within the lungs [54], whereas IL-6 over-expressing mice developed spontaneous PAH associated with the formation of neointimal occlusive lesions and inflammatory cell infiltration within the peri-arteriolar vasculature [55]. It is also of interest to note that this genetic model represents the only model that recapitulated the pathophysiological changes observed in IPAH patients in the absence of an exogenous trigger. This model may be particularly useful in further elucidating the role of chronic inflammation in PAH progression.

With the advent of these findings, it has become clear that inflammatory processes involving chemokines and cytokines play a significant role in the vascular remodelling characteristic of PAH. Nevertheless, knowledge of the exact role of inflammation in the pathogehesis of PAH remains elusive and requires further investigation.

1.5. The bone morphogenetic protein receptor 2 and PAH

1.5.1. BMPR2 mutations and the genetic basis of PAH

Arguably, the most significant advance in understanding the molecular basis of PAH has been the recent identification of the 'PAH gene'. Two independent groups have identified heterozygous mutations in the bone morphogenetic protein receptor 2 (BMPR2), a ubiquitously expressed member of the TGF-β superfamily of receptors [56, 57]. These mutations are found in up to 70% of patients with FPAH and up to 40% of patients with IPAH [7]. However, the penetrance of the PAH phenotype is variable; the likelihood that carriers of BMPR2 mutations develop clinical PAH is less than 20% [14]. Thus, it has been suggested that "multiple-hits" are required for the development of overt PAH, whereby a susceptible person with genetic predisposition may need to be exposed to additional environmental triggers before the disease is manifested [5, 34]. Over 160 different mutations have been reported involving many different regions of the BMPR2 gene, but all of the mutations identified to date are likely to produce loss of function of the BMPR2 receptor [58]. However, how haploinsufficiency in this ubiquitously expressed receptor leads to the very unique functional and morphological abnormalities in PAH is unknown.

1.5.2. BMPR2 signalling

BMPR2 is a ubiquitously expressed member of the TGF-β superfamily of receptors [59]. In addition to BMPR2, four other type II and seven type I receptors have been identified in mammals [60]. TGF-β type II receptor is the specific receptor for TGF-β [60]. Conversely, BMPR2 specifically binds to bone morphogenetic proteins (BMPs), while activin type II and type IIB receptors can also serve as type II receptors for BMPs but are

shared with other members of the family, namely activins [60]. Type I receptors are comprised of activin receptor-like kinases (ALK) [60]. Of interest, ALK-2, ALK-3 (BMPR1A) and ALK-6 (BMPR1B) function as BMP type I receptors, while ALK-1 and ALK-5 serve as type I receptors for TGF-β [60].

Members of the TGF-β superfamily share common mechanisms of signal transduction. They bind to two different type II and type I serine/threonine kinase receptors, both of which are required for signal transduction, and modulate their signals through Smad-dependent and Smad-independent pathways [59]. In the absence of ligand, both types of receptors are homomeric and found in the surface membrane of cells [10]. Ligand binding induces formation of a hetero-tetramer complex constituted of two type I and two type II receptors [60]. Subsequently, constitutively active type II receptors phosphorylate and thereby activate type I receptor kinases [59]. Therefore, the specificity of intracellular signals is mainly determined by type I receptors. Smads are the major signal transducers for the serine/threonine kinase receptors [59]. Upon ligand stimulation and activation by type II receptors, type I receptors phosphorylate receptor-regulated Smads (R-Smads), which in turn form a complex with common-partner Smads (Co-Smads) [59]. This complex then translocates to the nucleus to regulate transcription of target genes in a tissue- and cell-specific manner, by interacting with various transcription factors and transcriptional co-activators or co-repressors [59].

Despite sharing common signalling mechanisms, BMPs and TGF-β/activins typically signal via distinct pathways. Of the different R-Smads identified, Smad1, Smad5 and Smad8 are activated by BMP type I receptors, whereas Smad2 and Smad3 are activated by activin and TGF-β type I receptors [59]. However, Smad4 is the only Smad that is shared by both

BMP and TGF-β/activin signalling pathways, and can therefore mediate cross-talk between these two pathways [59].

Regulation of BMP signalling occurs at many levels. Firstly, the activity of BMPs can be regulated extracellularly by BMP-binding proteins, Noggin and Chordin [61]. These proteins can antagonize the action of BMPs by forming inactive complexes before binding of BMPs to their receptors [61]. In addition, a third class of Smads, inhibitory Smads (I-Smads) can negatively regulate signalling by interfering with R-Smads and Co-Smads [59]. Smad6 and Smad7 function as such I-Smads [59]. These can regulate cellular responses through multiple mechanisms, namely by physically interacting with type I receptors and competing with R-Smads for activation, or by interacting with activated R-Smads and preventing their complex formation with Co-Smads [59]. Expression of I-Smads is regulated by various stimuli, including TGF-β, BMP, interferon-γ, NF-κB signalling and shear stress [59].

Non-Smad pathways may also be important in understanding the diversity of signals generated by BMPR2. Of note, p38 and p44/42 mitogen-activated protein kinase (MAPK) pathways are known to be activated by BMPs in various cells [62]. The long C-terminal tail that distinguishes BMPR2 from other type II receptors has poorly understood functions, including the regulation of these pathways [63].

Signalling through BMPR2 is thus very complex and results in pleiotropic effects depending on the cell type, the specific ligand, and the environmental context [58]. This receptor has been shown to have control over a wide variety of developmental processes such as embryogenesis, bone and cartilage morphogenesis, vasculogenesis, angiogenesis, and haematopoiesis in addition to regulating cell proliferation and apoptosis [9, 10].

1.5.3. Assessment of PAH in BMPR2 deficient mouse models

Several attempts have been made to investigate the impact of BMPR2 deficiency on the development of PAH in mice. Most of these studies focused on mice heterozygous for a BMPR2 null allele ($BMPR2^{+/-}$), since the homozygous state is embryonic lethal and the BMPR2 genetic evidence indicates that haploinsufficiency is the molecular basis of the disease in humans [64]. However, in unstressed conditions $BMPR2^{+/-}$ mice fail to develop overt PAH [65]. In general, these mice exhibit moderate elevations in right ventricular systolic pressure and some level of muscularization of small arteries, but for unknown reasons they do not fully recapitulate the pathological features of frank PAH patients such as occlusion of arteries or formation of plexiform lesions [7]. Similarly, transgenic mice expressing only 5-10% of BMPR2 compared to wild-type (WT) mice did not spontaneously develop PAH [66]. These data indicate that reduced BMPR2 gene dosage alone is insufficient to cause PAH in mouse models. In contrast, transgenic mice over-expressing a "dominant negative" mutant BMPR2 gene targeted to SMCs exhibited significant elevation in RVSP compared to WT controls under basal conditions, but this occurred in the absence of significant arterial medial remodelling of the pulmonary microvasculature [67]. A more recent study from the same group has demonstrated the presence of obliterative luminal lesions in a small proportion of mice over-expressing the $BMPR2^{R899X}$ deletional mutation in SMCs [63]. To explain the increased penetrance of the phenotype in these mice, the authors have suggested that loss of the BMPR2 C-terminal cytoplasmic tail results in a stronger phenotype when the more proximal kinase domain function is preserved. Furthermore, consistent with the "multiple-hit" hypothesis, serotonin exposure alone and together with hypoxic exposure has been reported to result in exaggerated PAH and arterial remodelling in $BMPR2^{+/-}$ mice, which otherwise have a phenotype similar to their WT littermate controls

[65]. Adenoviral over-expression of 5-lipoxygenase, a pro-inflammatory gene, alone [68] and in combination with monocrotaline [69] also resulted in more severe PAH in BMPR2-deficient compared to WT littermate mice. Therefore, a reduction in BMPR2 activity appears to increase the susceptibility of mice to PAH, but by itself does not produce overt PAH.

1.5.4. Relevance of BMPR2 signalling for vascular cells

Based on recent loss- and gain-of-function studies in vascular cells *in vitro*, opposing roles for BMPR2 and its ligands, the BMPs, in vascular homeostasis have been reported. BMPs were shown to have an antiproliferative effect on pulmonary arterial smooth muscle cells, which was partly mediated through induction of apoptosis [10]. In contrast, BMPR2 signalling promotes pulmonary arterial endothelial cell survival [58]. Loss-of-function mutations in BMPR2 are thus thought to enhance pulmonary remodelling and play a significant role in the early endothelial dysfunction in patients with PAH (Figure 2). Consequently, this paradigm in BMPR2 function suggests that the BMPR2 pathway may play a critical role in preventing EC apoptosis and maintaining the integrity of the lung microvasculature.

1.6. Apoptosis and PAH

1.6.1. Evidence in support of a central role for apoptosis in PAH

Consistent with the important role of the BMPR2 pathway with respect to vascular homeostasis and EC survival, several studies have emerged that support a central role for apoptosis in the pathogenesis of PAH.

1.6.1.1. MCT causes PAH by direct injury and apoptosis of the lung endothelium

It has been recognized for many years that injury to the endothelium is likely a critical initial step in the pathogenesis of PAH. In the rat monocrotaline (MCT) model, which is one of the most widely used experimental models of this disease, PAH is thought be caused by direct injury to the lung endothelium, leading to apoptosis. Experimental models have shown that the administration of MCT induces increased vasoconstrictor responsiveness in the lungs of rats, increased vascular permeability, inflammation and endothelial cell injury [70]. Earlier reports have shown that administration of an active MCT metabolite causes EC apoptosis in cultured cells [71], and that EC apoptosis is present in larger elastic pulmonary arteries in MCT-treated rats [72]. Recently, another study showed a progressive temporal increase in apoptosis in the small pulmonary arterioles of rats post MCT treatment, which was attenuated by the use of a pan-caspase inhibitor, corresponding with a significant reduction in RVSP [70]. Together, these studies suggest that not only endothelial injury but also endothelial apoptosis may be a triggering event in PAH.

1.6.1.2. VEGF survival signalling acts as a protective mechanism in PAH

A central role for EC apoptosis was further supported in the seminal study of Taraseviciene-Stewart et al, in which hypoxic rats treated with a VEGFR2 receptor antagonist demonstrated worsening of hypoxia-induced PAH associated with marked potentiation of arterial remodelling [73]. In particular, the authors described an early increase in EC apoptosis followed by the appearance of proliferative intimal lesions, which in some cases obliterated small pulmonary arterioles [73]. Moreover, treatment with a pan-caspase inhibitor prevented the development of severe PAH as well as the remodelling changes induced by vascular endothelial growth factor (VEGF) blockade in the chronic hypoxia

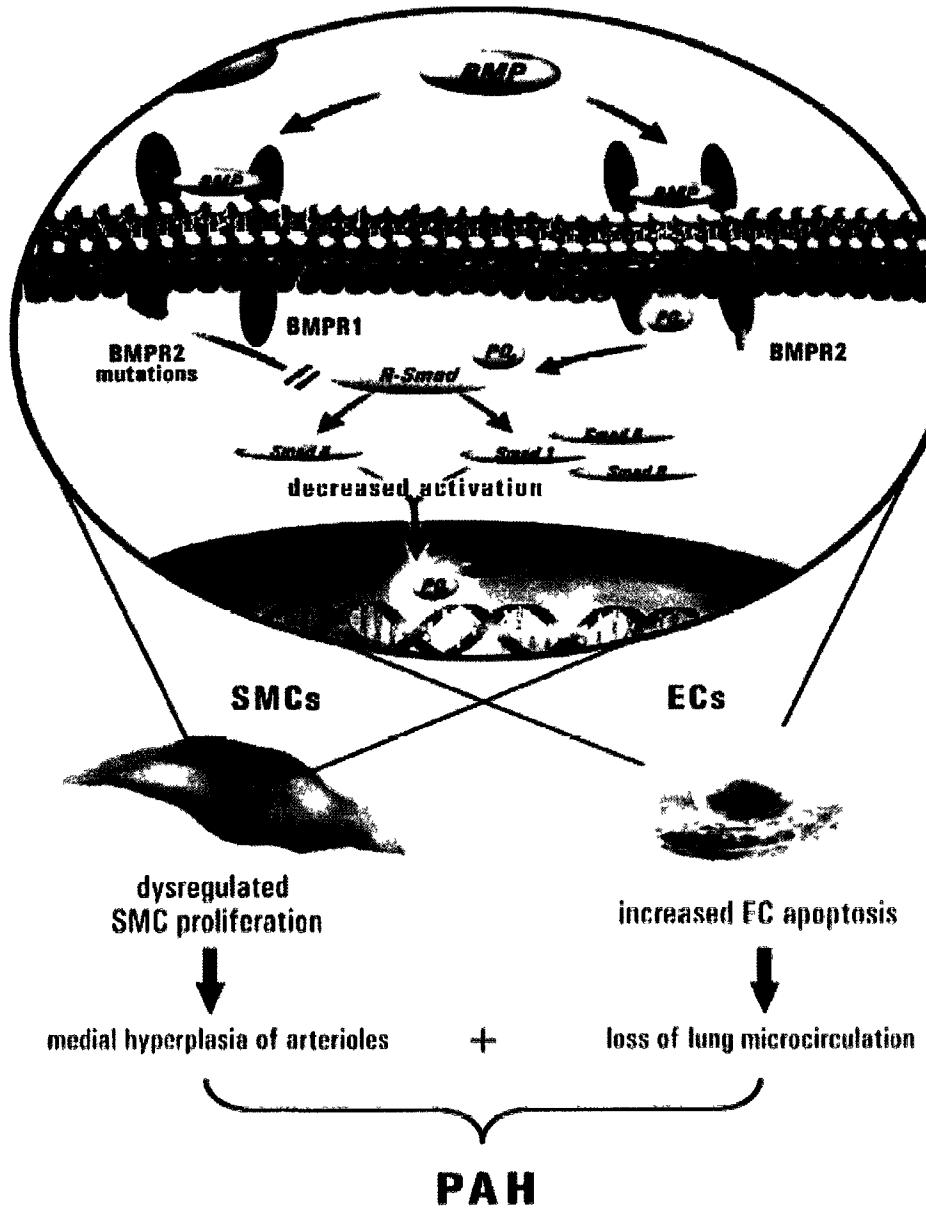

Figure 2. Consequence of BMPR2 loss-of-function mutations on vascular homeostasis and the pathogenesis of PAH. *Taken from Teichert-Kuliszewska K et al., Circulation Research, 2006.*

model [73]. The authors suggested that widespread EC apoptosis triggered by withdrawal of VEGF survival signalling together with chronic hypoxia led to the emergence of abnormal apoptosis-resistant and hyperproliferative ECs, and the development of the characteristic intimal lesions [73]. A protective role for VEGF was further supported by gene transfer experiments in both the chronic hypoxia and MCT-induced models of PAH [74, 75]. These findings suggest that VEGF survival signalling acts as a protective mechanism in PAH and support a significant role for EC apoptosis in the pathogenesis of this disease.

1.6.1.3. The Angl-Tie2 EC survival pathway acts as a protective mechanism in PAH

Additional support for the role of endothelial cell apoptosis in the pathogenesis of PAH comes from the protective role of the Angl-Tie2 pathway in this disease. Angl acts as an angiogenic and endothelial cell survival factor by activating the endothelial selective Tie2 receptor, and is thought to promote postnatal vascular homeostasis by protecting against EC apoptosis and inflammation [76, 77]. Thus, it is logical to expect that the Angl/Tie2 axis would protect against pulmonary vascular disease. However, the role this pathway plays in PAH has been controversial, largely due to a series of studies from a group implicating Angl in the pathogenesis of PAH [78-81]. Thistlethwaite et al. suggested that Angl played a causal role in the development of PAH based on their initial observations that Angl expression in the lung was negligible in healthy individuals, but significantly upregulated in PAH patients [78, 79]. Expression levels of Angl protein and Tie2 activity were also found to strongly correlate with increased pulmonary vascular resistance. However, some of this work has since been refuted, and there is now emerging consensus in the field that Angl is highly expressed in the normal human lung and its expression is not changed in the lungs of PAH patients [82, 83]. Recently, Tie2 deficient mice were observed to develop significant

elevation in RVSP following exposure to the relevant triggers of PAH, serotonin or IL-6, and exhibit significantly higher rates of apoptosis in the periphery of the lung compared to wild-type mice [84]. Since Tie2 is known to play an important role in EC survival signalling, this is consistent with the concept that predisposition to endothelial apoptosis is paramount in the pathogenesis of this disease. Moreover, inhibition of apoptosis using Z-VAD, a pan-caspase inhibitor, rescued the PAH phenotype in Tie2-deficient mice. Lung Tie2 expression and activation are also significantly downregulated in pulmonary hypertensive rats after exposure to MCT or hypoxia [83, 85-87]. In addition, it was demonstrated that enhanced Ang1 expression through cell-based gene transfer can protect against the development of MCT- or hypoxia-induced PAH, potentially through the prevention of early EC death [83, 85]. Thus, these findings highlight the role of endothelial cell survival-signalling via the Ang1-Tie2 pathway as a protective mechanism in PAH and further emphasize the importance of endothelial cell apoptosis in the onset of this disease.

1.6.2. The mechanistic link between EC apoptosis and PAH

As discussed above, several lines of evidence point to endothelial damage and apoptosis as a central trigger for the development of PAH. However, the mechanisms by which EC apoptosis can lead to a full PAH phenotype, including the typical pathological vascular lesions characterized by abnormal EC proliferation, remain unclear. The following model could be proposed to bring together many of the seemingly divergent ideas surrounding the role of EC apoptosis in PAH. Firstly, this paradigm suggests that EC apoptosis could contribute directly to classical endothelial dysfunction, since it has been previously demonstrated that regenerated endothelium following denudation-induced injury exhibits reduced vasodilator function, with the attendant consequences of vasoconstriction

and arterial remodelling [88]. In addition, these changes could potentiate the loss of vascular SMC growth inhibition that may arise as a consequence of mutations in the TGF-β receptor superfamily of genes. Secondly, loss of endothelial cells, particularly at the level of the fragile precapillary arteriole, could lead directly to the degeneration of these fragile EC structures which normally have little or no mural supporting cells. A progressive loss of functional continuity at the precapillary arteriolar level would result in loss of efficient perfusion of the distal lung microvasculature, and thus reduced effective cross sectional vascular area. In turn, this would compromise the ability of the pulmonary bed to accommodate the cardiac output, particularly during exercise, and result in elevated pulmonary vascular resistance. Finally, widespread and recurrent pulmonary vascular EC apoptosis could also set up the conditions that favor the selection of apoptosis resistant and hyperproliferative ECs, which could contribute to the intimal and plexiform lesions found in many PAH patients. At present, it is not clear which of these potential consequences of EC apoptosis may be most important in the pathogenesis of PAH. However, the evidence supporting a central role for EC apoptosis is becoming increasingly compelling and this may suggest novel strategies to detect, prevent, and treat PAH.

1.7. BMPR2^{R899X} deletional mutant mouse model

Despite these advances in our knowledge, the precise molecular mechanisms by which reduced BMPR2 signalling, endothelial apoptosis and inflammation are linked to the functional and morphological abnormalities of PAH are uncertain, and *in vivo* models have yet to provide a clear mechanistic explanation. To gain insight into these mechanisms, we have generated mice that over-express a BMPR2^{R899X} transgene, in which an arginine to stop

mutation is inserted at amino acid 899 (R899X) in the receptor's C-terminal domain. This model will help us determine the effect of conditional over-expression of a BMPR2 mutation on EC survival and microvascular loss in relation to the development of PAH *in vivo*, and hopefully elucidate some of the outstanding questions in the field.

1.8. Hypothesis

Over-expression of BMPR2 loss-of-function mutations will lead to PAH by increasing the susceptibility of ECs to apoptosis, particularly at the level of fragile pulmonary arterioles.

1.9. Objectives

1.9.1. Confirm the expression of the $BMPR2^{R899X}$ transgene.

1.9.2. Determine the impact of over-expression of the $BMPR2^{R899X}$ transgene on normal BMPR2 signalling

1.9.3. Determine the effect of abnormal BMPR2 signalling on the structural and functional integrity of the pulmonary microcirculation.

1.9.4. Examine the temporal and spatial patterns of EC apoptosis and proliferation in the lung during the progression of PAH and verify whether they are consistent with a causal role in the disease.

1.9.5. Examine the effect of an additional environmental stressor (ie. IL-6) on the severity of the PAH phenotype

2. Materials and Methods

Unless stated otherwise, all procedures were performed by Dominique Yelle.

2.1. Mouse husbandry

All experiments were approved by the University of Ottawa's Animal Care ethics committee and adhere to the Guidelines of the Canadian Council on Animal Care. $TetO_7$-$BMPR2^{R899X}$ mice, which express murine BMPR2 with an arginine to stop mutation at amino acid 899 ($BMPR2^{R899X}$) labeled with a C-terminal FLAG tag, were generously provided by Dr. James West at Vanderbilt University and bred in-house at the University of Ottawa. B6.Cg-*Gt(ROSA)*$^{26Sortm1(rtTA*M2)}$Jae/J mice (referred to herein as ROSA-rtTA mice) were purchased from Jackson Laboratories (stock 006965). Heterozygotes in $TetO_7$-$BMPR2^{R899X}$ were crossed to homozygotes in ROSA-rtTA with ubiquitous expression of the reverse tetracycline transactivator (rtTA). This resulted in mice that were universally heterozygous for ROSA-rtTA, and approximately half of which were heterozygous for $TetO_7$-$BMPR2^{R899X}$. In this system, the BMPR2 transgene should only be expressed by binary transgenic (BT) animals containing both rtTA and $BMPR2^{R899X}$. Those containing only rtTA (NBT-ROSA) or $BMPR2^{R899X}$ (NBT-BMPR2) were considered non-binary transgenic and used as littermate controls. Mice were fed doxycycline (Dox) in the chow (400 mg/kg, Teklad diet 06264, Harlan Laboratories) starting at 5 weeks of age until sacrifice to induce $BMPR2^{R899X}$ over-expression.

2.2. Genotyping

Tail clippings were collected from each mouse at weaning for genotyping. DNA was isolated and amplified by polymerase chain reaction (PCR) using the REDextract-N-Amp™ Tissue PCR kit (Sigma, XNATR). ROSA primer sequences were used as recommended by

Jackson Laboratories. $BMPR2^{R899X}$ primers were designed against a region specific to the transgenic construct using the NCBI primer-BLAST tool. Genotyping primer sequences are illustrated in Table 1.

Table 1. Genotyping primer sequences

	Sequence		
Primers	Forward	Reverse	Product
ROSA wt	AAAGTCGCTCTGAGTTGTTAT	GGAGCGGGAGAAATGGATATG	500 bp
ROSA mut	AAAGTCGCTCTGAGTTGTTAT	GCGAAGAGTTTGTCCTCAACC	300 bp
R899X	ACCGGGACCGATCCAGCCTC	CAGCCAGGGCACCCGAAAGG	334 bp

2.3. Hemodynamic analyses

Following the endpoints of doxycycline administration, mice were anaesthetized using a mixture of ketamine (100 mg/kg, Ketalean, DIN 00612316) and xylazine (10 mg/kg, Rompun, DIN 02169592) and shaved to expose the surgical area. An incision was made extending from the animal's chin down to the right armpit and the jugular vein was exposed and freed from adherent tissues. The cranial end of the jugular was tied off completely, and a loose tie was made at the caudal end of the exposed jugular. A small incision was then made in the medial aspect of the vein. A Scisense 1.2 French pressure microtip catheter transducer (111B-B072, Scisense, London, ON) was then inserted through the incision and gently threaded down into the right ventricle. Proper placement of the catheter within the ventricle was determined through observation of the pressure loop obtained from the catheter. The loose caudal suture was then tightened to secure the catheter in place, and data was collected using LabScribe2 software (Scisense). RVSP was calculated by averaging the amplitude of three pressure loops. Mice were then culled by dissecting the abdominal aorta. Subsequently, the right ventricle (RV) was dissected from the left ventricle and septum

(LV+S) and both were individually weighed to calculate the RV/LV+S ratio as an indicator of RV hypertrophy. Importantly, all measurements described herein were performed in a blinded fashion. Furthermore, lung tissue was harvested from every mouse. Right lung tissue was harvested for protein or mRNA extraction, placed into cryogenic vials (Corning, 430488), flash frozen in liquid nitrogen and stored at -80°C. The remaining left lung was perfused with a 1:1 PBS:OCT solution via the trachea. Half of the left lung was processed for histological analyses and the remainder embedded in OCT medium (TissueTek 4583) for frozen sections. All hemodynamic analyses and tissue harvesting were graciously performed by Yupu Deng.

2.4. Tissue processing

Lung tissues harvested for histological analysis were fixed in 4% paraformaldehyde (PFA, Appendix 3) at 4°C overnight. The next day, tissues were washed and soaked in phosphate buffered saline (PBS, Appendix 3) all day, then transferred into 70% ethanol overnight. Tissues were then transferred into cassettes (Fisher, 15182702D) and sequentially passaged through 80% ethanol (1 x 30 min), 90% ethanol (2 x 30 min), 95% ethanol (2 x 30 min and 1 x 1h), 100% ethanol (1 x 30 min and 2 x 1h), xylene:100% ethanol 1:1 (1 x 30 min), xylene (1 x 30 min and 2 x 1h), and finally placed in paraffin (TissuePrep, Fisher, T565) overnight at 65°C. Samples were then embedded into paraffin blocks, solidified and cut into 5μm sections collected onto Superfrost® Excell microscope slides (Fisher, 22-034-985) using a microtome (Microm, HM 330). Tissue processing was graciously performed by Anli Yang.

2.5. Histology

For all histological analyses, samples were initially deparaffinized and rehydrated by sequential dips in xylene (3 x 5 min), 100% ethanol (2 x 2 min), 90% ethanol (1 x 1 min), 70% ethanol (1 x 1 min), dH_2O (1 x 5 min) and PBS (1 x 5 min). When antigen retrieval was required, slides were soaked in citrate buffer (Antigen unmasking solution, 1:100, Vector, H-3300) and microwaved 15 min, then cooled to room temperature for 30 min and washed 2 x 5 min in PBS and 1 x 5 min in dH_2O. Permeabilization was done by incubating the sections with 0.25% Trition X-100 (Fisher, BP151-100) in PBS for 15 min at room temperature.

2.5.1. Immunofluorescence

Following deparaffinization, antigen retrieval and permeabilization, sections were blocked by incubating with 5% normal goat serum (Sigma, G9023) and 3% BSA (Cell Signaling Technologies, 9998) in PBS for 1h at room temperature in preparation for immunofluorescence (IF) staining. Primary antibodies were diluted in blocking buffer and incubated in a humid chamber for 1h at room temperature (anti-DDK mouse monoclonal, OriGene, TA50011, 1:200; anti-α-SMA mouse monoclonal Cy3 conjugate, Sigma, C6198, 1:400). Slides were then washed 3 x 5 min in PBS, and incubated with the appropriate secondary antibodies when necessary (goat anti-mouse Alexa 488, Invitrogen, A-11001, 1:500) diluted in PBS for 1h at room temperature in the dark. Afterwards, slides were washed again in PBS 3 x 5 min, counterstained with DAPI diluted in PBS (Molecular Probes, D21490, 1:4000) for 15 min at room temperature, then washed in PBS 3 x 5 min and 1 x 5 min in dH_2O. Finally, slides were coverslipped with Mowiol mounting medium (Appendix 3) and stored in the dark at 4°C.

2.5.2. Immunohistochemistry

Slides were initially deparaffinized and rehydrated followed by antigen retrieval as described above, and subjected to a 3% hydrogen peroxide (Sigma 216763) treatment for 10 min at room temperature. After being washed 3 x 5 min in PBS, slides were blocked at room temperature for 10 min (Protein Block Serum-Free Ready-to-use, Dako, X0909). Slides were then incubated overnight at room temperature in primary antibody (mouse anti-human Ki67, BD Biosciences, 550609, 1:5; anti-CD68 rat monoclonal, AbD Serotec, MCA1957T, 1:100) diluted in antibody diluent (Dako, S3022). The next day, slides were washed 3 x 5 min in PBS then subjected to immunohistochemistry (IHC). The following IHC reactions were performed at room temperature using the labelled streptavidin biotin (LSAB) method (LSAB + System-HRP, K0679, Dako). Slides were incubated in biotinylated link 20 min, washed 3 x 5 min in PBS, then incubated with streptavidin-horseradish peroxidase (HRP) 20 min, washed again 3 x 5 min in PBS and finally incubated with DAB (1 drop DAB chromogen + 1000 µL DAB substrate buffer) for 5 min and placed in water to stop the reaction. Slides were dehydrated by rapid sequential dips in 70% ethanol, 90% ethanol and 100% ethanol, followed by two 5 min dips in xylene. Slides were coverslipped with Mowiol mounting medium and stored at room temperature.

2.5.3. Hematoxylin and Eosin (H&E) staining

Following deparaffinization and rehydration, slides were stained with concentrated hematoxylin (Vector, H-3404) for 5 min, rinsed under flowing tap water for 10 min, quickly dipped in acid alcohol (Appendix 3), transferred back to tap water for 5 min, dipped in Scott's solution (Appendix 3) for 2 min, rinsed under flowing tap water for 5 min, stained in eosin (Fisher, E-511) for 4 min and finally rinsed under flowing tap water for 7 min. Once

desired staining was achieved, slides were dehydrated by rapid sequential dips in 70% ethanol, 90% ethanol and 100% ethanol, followed by two 5 min dips in xylene. Slides were coverslipped with Permount (Fisher, SP15-100) and stored at room temperature.

2.5.4. Terminal deoxynucleotidyl transferase-mediated dUTP Nick-End-Labelling (TUNEL) staining

Following deparaffinization and rehydration, slides were permeabilized with a 20 μg/μL proteinase K solution (Sigma, P8044) for 10 min at room temperature then subjected to DNA fragmentation analysis to identify cells undergoing apoptosis using a TUNEL assay kit (Dead End™ Fluorometric TUNEL System, Promega, G3250). Positive controls were first incubated with DNase I (Ambion, AM1906) at 10 units/mL in DNase I buffer for 10 min at room temperature, while negative controls were incubated without rTdT enzyme. The tailing reaction took place for 1h at 37°C. Nuclear counterstaining was performed for 15 min at room temperature using DAPI (Molecular Probes, D21490, 1:4000). Slides were coverslipped with Mowiol mounting medium and stored at 4°C.

2.5.5. Microscopy

For IHC and H&E staining, whole sections were scanned to create digital images using the Aperio ScanScope CS. For α-SMA and TUNEL staining, pictures were acquired by confocal microscopy using the Fluoview FV1000 (Olympus, model BX61WI). Pictures of DDK IF staining were acquired with an Axio Observer.Z1 inverted microscope (Zeiss). Figures were compiled using Adobe Photoshop CS3. Manipulations of brightness and intensity were made equally to all treatment groups.

2.5.6. Quantification

For α-smooth muscle actin (α-SMA) IF, pictures of small vessels (~40 μm diameter) were taken at 20X magnification with 4X zoom. α-SMA staining was quantified by measuring the smooth muscle thickness at four diametrically opposite points around each vessel, then averaging these values for individual animals and genotype groups. For quantification of IHC slides, snapshots from fields of interest were taken from the digital images. For Ki67, a 10x magnification field with an even distribution of cells was selected on every lung lobe (4/slide), preferably towards the centre of the lobe and avoiding large gaps such as airways or vessels, and the number of Ki67-positive cells was counted. Cells were considered Ki67-positive if there was strong brown staining. Similarly, a 20X magnification field was selected for CD68 slides (4/slide) and positively stained brown cells were counted. H&E images were quantified by taking snapshots at 40X magnification, and measuring average alveolar septal thickness along a hairline drawn vertically across the centre of the field. TUNEL images were captured at 20X magnification with 2X zoom and the number of positive cells per high power field (HPF) was quantified. Only cells with colocalization of staining with DAPI were counted as positive. All quantification was performed in a blinded fashion.

2.6. Western immunoblotting

2.6.1. Protein extraction

For protein extraction, lung tissues were ground into a fine powder in liquid nitrogen using a pestle and mortar. Approximately 50 mg of tissue was used for total protein extracts. Once homogenized, tissues were immediately resuspended in cold RIPA lysis buffer (Appendix 3) supplemented with protease inhibitor cocktail (Sigma, P8340) and incubated

on ice for 20 min. Samples were then centrifuged at 4°C for 20 min at 12 000 rpm, after which the supernatants were collected. Subcellular proteins were extracted using the ProteoExtract® Subcellular Proteome Extraction Kit (Calbiochem, 539790). Extracts were collected from 50 mg of flash-frozen fragmented tissue prepared as described above, then processed according to the procedures detailed in section 8.3 of User Protocol 539791. Cytosolic, membrane, nuclear and cytoskeleton fractions were collected.

2.6.2. Protein quantification

Protein extracts were quantified using a bicinchoninic acid (BCA) assay. For each sample, 100 µL BCA reagent mix (Appendix 3) prepared immediately before use was combined to 4 µL of protein extract. Duplicates of each sample as well as a bovine serum albumin (BSA) standard were loaded onto a 96-well plate (Corning, 3598) and incubated for 30 min at 37°C. Absorbance was read at 562 nm using a POLARstar Omega microplate reader (BMG Labtech).

2.6.3. Gel electrophoresis

Protein samples were prepared in Laemmli buffer (Appendix 3) and boiled for 10 min at 95°C before being loaded on 10% Tris-SDS polyacrylamide gels (Appendix 3). Unless specified otherwise, 80 µg of total protein and 50 µg of subcellular membrane proteins were used for respective blots. Gels were initially run at 90V for 20 min or until samples migrated from the stacking gel into the separating gel, then at 160V for 90 min or until the 42 kDa ladder marker (Spectra multicolor broad range protein ladder, Fermentas, SM1841) reached the bottom of the gel. All gels were migrated in Mini-PROTEAN® Tetra Cell chambers (BioRad, 165-8004) with running buffer (Appendix 3).

2.6.4. Wet transfer

Gels were initially equilibrated in transfer buffer (Appendix 3) for 15 min at room temperature, and then transferred onto Hybond-C Extra nitrocellulose membranes (GE Healthcare, RPN303E) in a Mini Trans-Blot® cell (BioRad, 170-3930) at 80V for 2 hours. Once the transfer was complete, membranes were stained with Ponceau-S red (Sigma, P7170) for 1 min to visualize the proteins and assess the quality of the transfer.

2.6.5. Antibody detection

For transgene expression studies, membranes were blocked in 5% nonfat dry milk in 0.1% TBS-T (Appendix 3) for 1h at room temperature. Primary antibodies were incubated overnight at 4°C in 5% nonfat milk in 0.1% TBS-T (anti-DDK mouse monoclonal, OriGene, TA50011, 1:1000; anti-BMPR2 mouse monoclonal, BD Biosciences, 612292, 1:500). Membranes were then washed in 0.1% TBS-T (3 x 5 min) and incubated with the appropriate HRP-conjugated secondary antibody in 5% nonfat milk in 0.1% TBS-T for 1h at room temperature (anti-mouse HRP conjugate, Promega, W4021, 1:2500). Where applicable, membranes were stripped with Re-blot Plus mild buffer (Millipore, 60513) for 15 min at room temperature then re-probed with β-actin (Sigma, A5441, 1:10000) to confirm equal protein loading.

For BMRP2 signalling studies, membranes were blocked in 5% BSA in 0.1% TBS-T for 1h at room temperature. Primary antibodies were incubated overnight at 4°C in 5% BSA in 0.1% TBS-T (anti-Smad1 rabbit polyclonal, Cell Signalling, 9743, 1:1000; anti-phospho-Smad1/5/8 rabbit polyclonal, Cell Signalling, 9511, 1:1000; anti-p38 MAPK rabbit polyclonal, Cell Signalling, 9212, 1:1000; anti-phospho-p38 MAPK rabbit polyclonal, Cell Signalling, 9211, 1:1000; anti-p44/42 MAPK mouse monoclonal, Cell Signalling, 9107,

1:2000; anti-phospho-p44/42 MAPK rabbit polyclonal, Cell Signalling, 9101, 1:1000). Membranes were then washed in 0.1% TBS-T (3 x 5 min) and incubated with the appropriate HRP-conjugated secondary antibody in 5% BSA in 0.1% TBS-T for 1h at room temperature (anti-rabbit HRP conjugate, Promega, W4011, 1:5000; anti-mouse HRP conjugate, Promega, W4021, 1:5000). Following detection of total antibodies, membranes were stripped and re-probed with phospho-antibodies. For all blots, detection was performed using Amersham ECL Plus (GE Healthcare, RPN2132). Images were captured with the FluorChem HD2 imaging system (Alpha Innotech).

2.6.6. Quantification

Western blots were quantified by spot densitometry using the AlphaEaseFC software. The pixel intensity value (termed integrated density value) for each band was measured on non-saturated blots. The values for phospho-proteins were normalized to those of total protein for each sample, and averaged within each group. Fold change was calculated by normalizing BT to NBT values.

2.7. RT-PCR

RNA was isolated using the RNeasy® Plus Mini Kit (Quiagen, 74134). Lung tissue was homogenized in RLT Plus buffer supplemented with 10μL β-mercaptoethanol/mL using a Sonic Dismembrator (Fisher, model 500, 15-338-550) at an amplitude of 30% for 2 x 45 sec. Samples were spun through the gDNA eliminator spin column provided in the kit to eliminate genomic DNA contamination. RNA quantification was done using the NanoDrop 2000 spectrophotometer (Thermo Scientific, ND2000). Reverse transcriptase (RT)-PCR was performed with the SuperScript® One-Step RT-PCR kit (Invitrogen, 10928-034). Total

RNA (1 μg) was used in each reaction. cDNA synthesis was performed at 50°C for 30 min followed by a 2 min initial denaturation step at 94°C. This was followed by 40 cycles at 94°C for 15 s, 50°C for 30 s, and 72°C for 20 s, with a final extension step at 72°C for 5 min. Gel images were captured using the Alpha Imager imaging system (Alpha Innotech).

2.8. IL-6 administration

A small selected cohort of BT mice and NBT controls received daily subcutaneous injections of recombinant murine IL-6 (200 ng/kg, Sigma-Aldrich, I9646) over a 2 week period starting 6 weeks after the administration of doxycycline, i.e. 2 weeks before sacrifice. The IL-6 solution for injection was prepared by resuspending the stock into 10 mL of 0.9% saline for injection USP (Baxter, JB1301) and making 200 μL aliquots which were brought to 1.5 mL with saline on the day of use.

2.9. Statistical analysis

All data are presented as mean ± standard error of the mean (SEM). Statistical analyses were performed using GraphPad Prism software version 5.0. Differences amongst multiple means were determined by analysis of variance (ANOVA), and when overall differences were detected, the Bonferroni post-hoc analysis was used to determine the difference between individual means. For IL-6 treatments, means of the two groups were compared using an unpaired t-test with Welch's correction for unequal variances when appropriate.

3. Results

3.1. The BMPR2^{R899X} transgene is expressed in BT mice

3.1.1. RT-PCR revealed BMPR2^{R899X} transgene expression in BT mice

To examine whether BMPR2^{R899X} transgene expression was detectable at the mRNA level, an RT-PCR using primers directed against a region specific to the BMPR2^{R899X} construct was performed (Figure 3B, n=3). BMPR2^{R899X} expression was detected in BT mice, albeit at variable levels, at both 1 week and 8 weeks of transgene induction. Lower expression levels were also detected in some NBT-BMPR2 mice, consistent with a degree of 'leakiness' of the responder transgenic mice. However, as expected, there was a complete absence of transgene expression in NBT-ROSA controls. Primers against ribosomal subunit 18S were used as a loading control.

3.1.2. BMPR2^{R899X} transgene expression in BT mice could not be confirmed by Western blots with DDK and BMPR2 antibodies

In an initial attempt to confirm whether the BMPR2^{R899X} transgene was expressed at the protein level in BT mice, Western blots using an antibody against the C-terminal flag tag (DDK) were performed on total lung protein extracts. These blots did not reveal any band specific to BT mice (Appendix 2, figure S2.1, n=2). In an effort to enrich the extracts for the BMPR2^{R899X} transgene, subcellular membrane fractions were isolated from mice following 1 week and 8 weeks of transgene induction. However, Western blots with the DDK antibody still did not reveal any specific bands in BT mice in membrane extracts (Figure 3A and

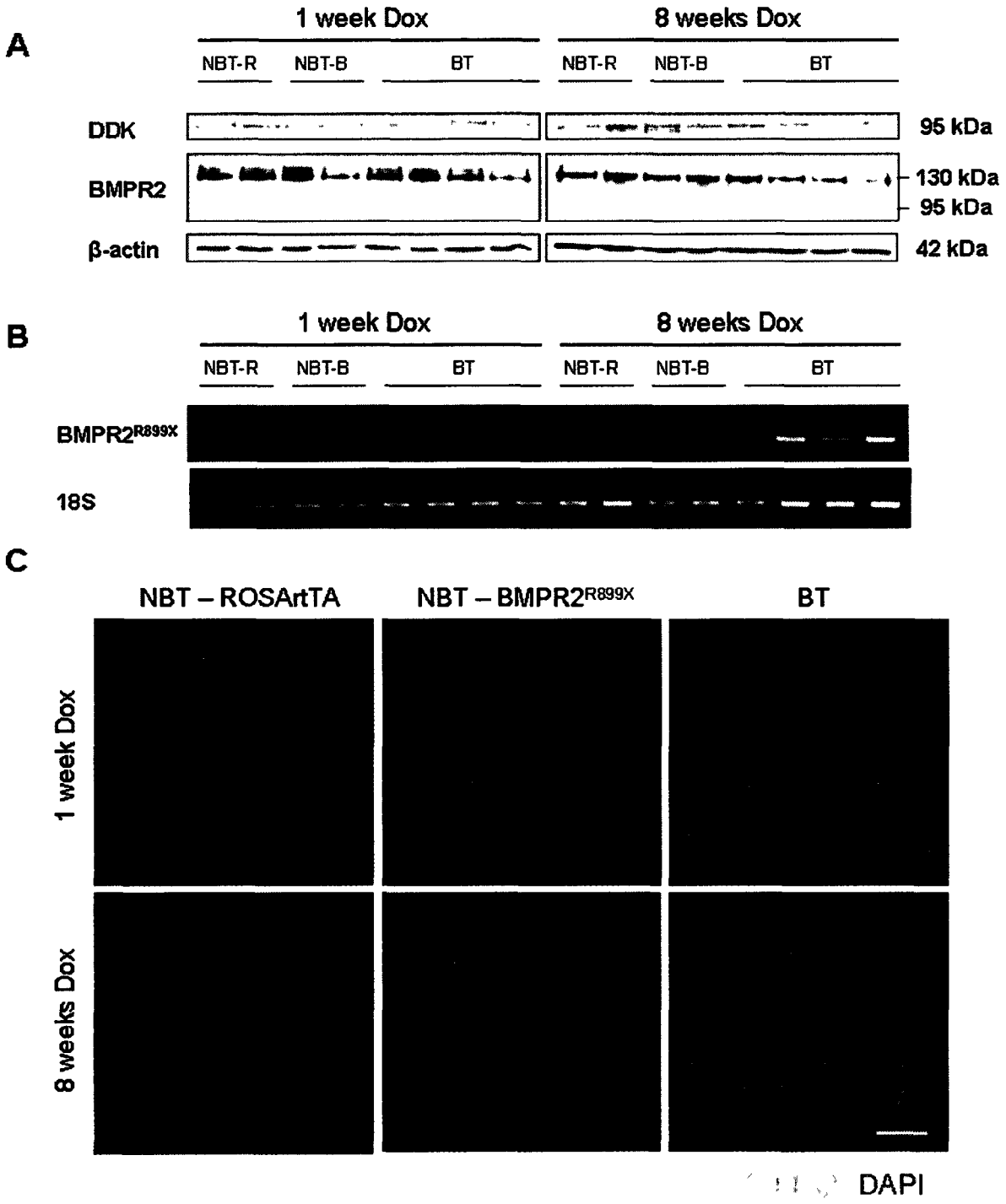

Figure 3. Expression of the BMPR2^{R899X} transgene. **(A)** Western blot with an anti-DDK (Flag) antibody on subcellular membrane extracts from the lungs of NBT-ROSA (n=2), NBT-BMPR2 (n=2) and BT (n=4) mice following 1 and 8 weeks of transgene induction. The same membrane was stripped and re-probed with an anti-BMPR2 antibody. β-actin was used as a loading control. These experiments were performed in triplicate. **(B)** RT-PCR on RNA from lung samples of NBT-ROSA (n=2), NBT-BMPR2 (n=2) and BT (n=4) mice following 1 and 8 weeks of transgene induction using primers specific for the BMPR2^{R899X} construct. 18S was used as a loading control. These experiments were performed in triplicate. **(C)** Immunofluorescence using an anti-DDK (Flag) antibody with DAPI nuclear counterstaining on paraffin lung sections from NBT-ROSA (n=2), NBT-BMPR2 (n=2) and BT (n=4) mice following 1 and 8 weeks of transgene induction. Bar = 120 μm.

appendix 2, figure S2.2, n=3). In parallel, Western blots were performed with an antibody against BMPR2 to try to distinguish the native receptor from the truncated transgene. The native receptor was successfully detected, but no band corresponding to the transgene was detected in BT mice in total extracts (Appendix 2, figure S2.3, n=4) or membrane fractions (Figure 3A, n=3). β-actin was used as a loading control in all the aforementioned blots.

3.1.3. Immunofluorescence staining with a DDK antibody suggests BMPR2^{R899X} transgene expression in BT mice

In another attempt to confirm whether the BMPR2^{R899X} transgene was expressed at the protein level, immunofluorescence using the same DDK antibody as above was performed on lung sections. Staining was detected in BT mice (n=4) after 1 week and 8 weeks of transgene induction, with lower levels or absent staining in NBT-BMPR2 mice (n=2) and NBT-ROSA controls (n=2) (Figure 3C).

3.2. Preliminary examination of BMPR2 signalling did not reveal changes in major downstream pathways

To examine the impact of over-expressing the BMPR2^{R899X} transgene on normal BMPR2 signalling, Western blots with antibodies for major downstream signalling targets were performed. When the fold change of phospho protein normalized to total protein was calculated for each blot, no difference (fold change greater than 1.2 or lesser than 0.8) was observed in Smad 1/5/8 (0.92 fold change, n=1), p38 MAPK (0.99 fold change, n=1) or p44/42 MAPK activity (0.92 fold change, n=1) in BT mice compared to NBT-ROSA controls (Figure 4).

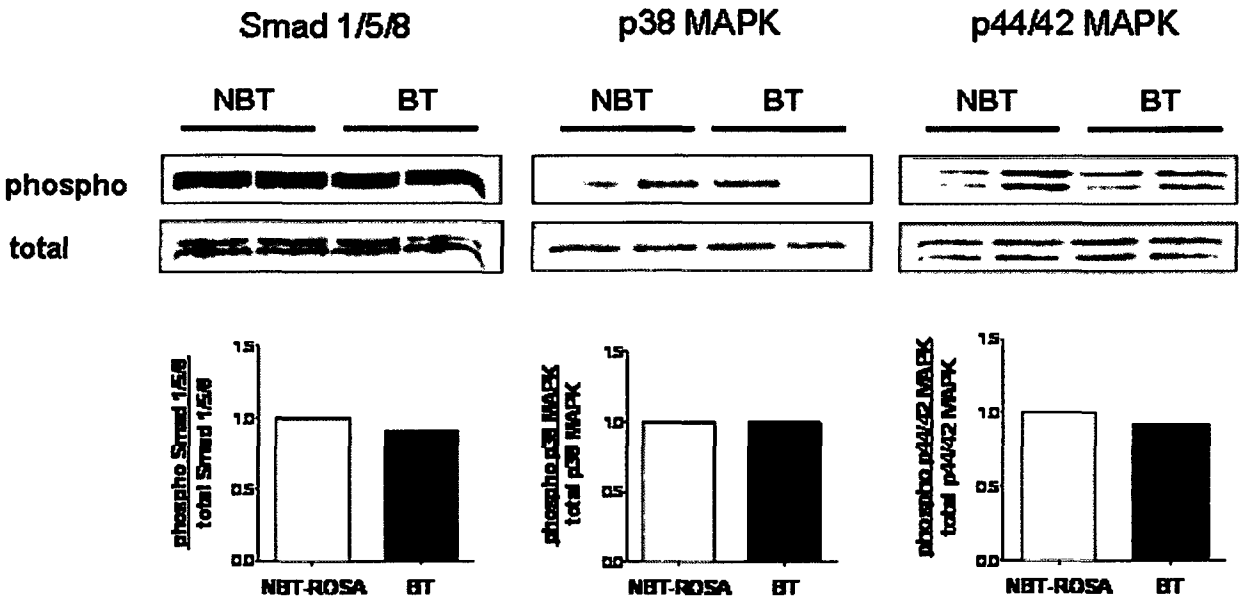

Figure 4. Activity of the major downstream effectors in BMPR2 signalling. (A) Western blots using anti-phospho-Smad1/5/8, anti-phospho-p38 MAPK and anti-phospho-p44/42 MAPK antibodies on total lung protein extracts from NBT-ROSA (n=2) and BT (n=2) mice following 1 week of transgene induction. Membranes were stripped and re-probed with corresponding total antibodies. These experiments were only performed once. **(B)** Quantification of the relative fold change in protein expression in BT compared to NBT-ROSA mice by spot densitometry. Phospho-proteins were normalized to total proteins in individual samples.

3.3. BT mice develop PAH with arteriolar remodelling and inflammatory infiltrates

3.3.1. RVSP is increased in BT mice after 1, 2 and 8 weeks of transgene induction

To determine whether mice over-expressing the $BMPR2^{R899X}$ transgene developed PAH, right ventricular systolic pressure (RVSP) was measured by right ventricle catheterization as an indicator of pulmonary pressure. RVSP values are summarized in scatter (Figure 5A) and box plots (Figure 5B) following 1, 2, 4 and 8 weeks of transgene induction. RVSP was significantly increased in BT mice compared to NBT-ROSA controls after 1 week of transgene induction (25 ± 0.4 mmHg, n= 9, 21 ± 0.9 mmHg, n= 4, respectively, $p<0.01$), while NBT-BMPR2 mice had an intermediate value (23 ± 0.6 mmHg, n=4). After two weeks of transgene induction, RVSP was again significantly increased in BT mice compared to NBT-ROSA controls (24 ± 0.5 mmHg, n=10, 20 ± 0.6 mmHg, n=3, respectively, $p<0.01$) with NBT-BMPR2 mice at an intermediate value (21 ± 1.3 mmHg, n=3). However, no significant increase in RVSP values was detected after 4 weeks of transgene induction in BT mice compared to NBT-BMRR2 or NBT-ROSA controls (25 ± 1.2 mmHg, n=9, 25 ± 1.7 mmHg, n=4, 23 ± 0.3 mmHg, n=3, respectively). By 8 weeks of transgene induction, RVSP returned to being significantly increased in BT mice compared to both NBT-BMPR2 mice and NBT-ROSA controls (25 ± 0.5 mmHg, n=14, 24 ± 0.5 mmHg, n=11, 23 ± 0.3 mmHg, n=4, respectively, $p<0.05$). When all timepoints were pooled, RVSP was again significantly increased in BT mice compared to both NBT-BMPR2 and NBT controls (25 ± 0.3 mmHg, n=42, 23 ± 0.4 mmHg, n=22, 22 ± 0.5 mmHg, n=14, respectively, $p<0.01$, Figure 6A). Of note, the baseline RVSP of mice treated with doxycycline was comparable to that of WT mice not receiving the treatment (not shown).

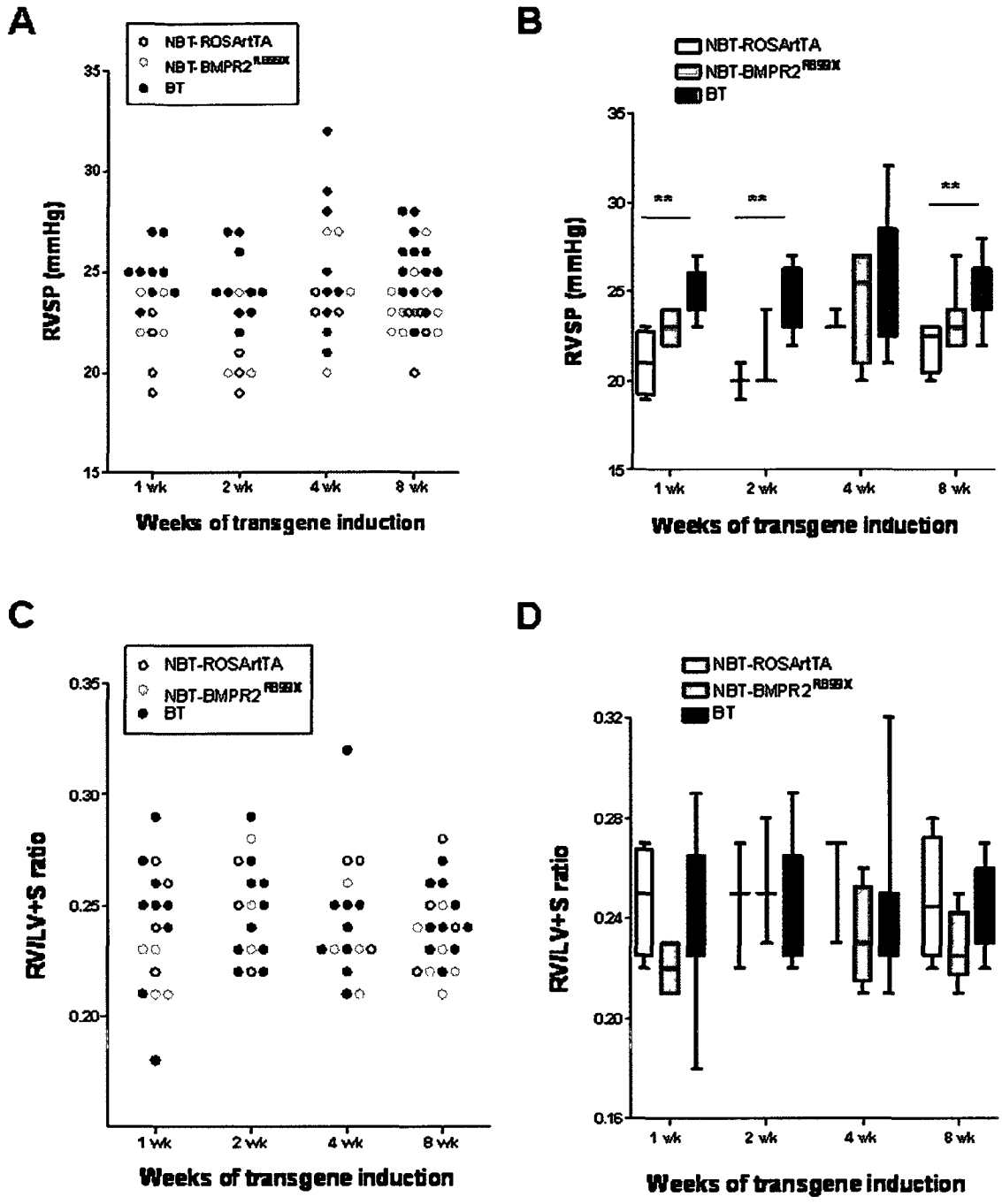

Figure 5. Progression of RVSP and RV hypertrophy over the timecourse of BMPR2^{R899X} transgene induction. **(A)** Scatter plot showing the distribution of RVSP values after different periods of transgene induction. **(B)** Box plots summarizing RVSP values of each group. Whiskers represent sample minimum and maximum, line at sample median. ** = $p<0.01$ by ANOVA with Bonferroni post-hoc analysis. **(C)** Scatter plot showing the distribution of RV/LV+S values after different periods of transgene induction. **(D)** Box plots summarizing RV/LV+S values of each group. Whiskers represent sample minimum and maximum, line at sample median.

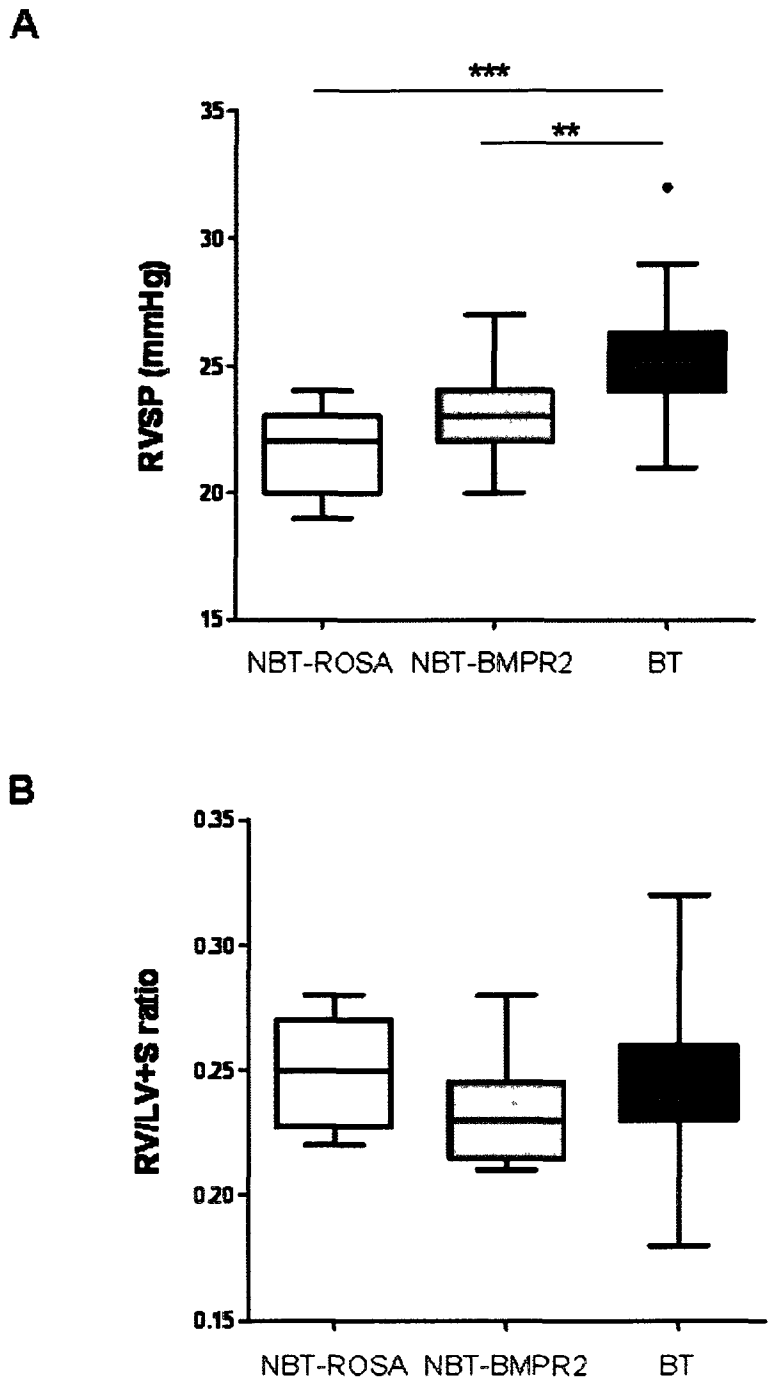

Figure 6. Combined RVSP and RV/LV+S values from individual BMPR2^{R899X} induction timepoints. **(A)** Box plots showing RVSP distribution in pooled NBT-ROSA (n=14), NBT-BMPR2 (n=22) and BT (n=42) mice. Whiskers represent sample minimum and maximum, line at sample median. ** = $p<0.01$ and *** = $p<0.001$ by ANOVA with Bonferroni post-hoc analysis. **(B)** Box plots showing RV/LV+S distribution in pooled NBT-ROSA (n=14), NBT-BMPR2 (n=17) and BT (n=37) mice. Whiskers represent sample minimum and maximum, line at sample median.

3.3.2. RV hypertrophy is not increased in BT mice

The weight ratio of the right ventricle to left ventricle plus septum (RV/LV+S) was calculated as an indicator of RV hypertrophy. Again, summary data is depicted in scatter (Figure 5C) and box plots (Figure 5D) following 1, 2, 4 and 8 weeks of transgene induction. No significant increase in RV hypertrophy was detected in BT mice compared to NBT-BMPR2 mice or NBT-ROSA controls after 1 week (0.24 ± 0.011, n=9, 0.22 ± 0.0058, n=4, 0.25 ± 0.011, n=4, respectively), 2 weeks (0.25 ± 0.0080, n=9, 0.25 ± 0.015, n=3, 0.25 ± 0.015, n=3, respectively), 4 weeks (0.24 ± 0.011, n=9, 0.23 ± 0.010, n=4, 0.26 ± 0.013, n=3, respectively) or 8 weeks of transgene induction (0.24 ± 0.0049, n=10, 0.23 ± 0.0060, n=6, 0.25 ± 0.013, n=4, respectively). Similarly, no significant increase in RV hypertrophy was detected in BT mice compared to NBT-BMPR2 mice or NBT-ROSA controls when all timepoints were pooled (0.25 ± 0.0042, n=37, 0.23 ± 0.0047, n=17, 0.25 ± 0.0057, n=14, respectively, Figure 6B).

3.3.3. Muscularization is increased in the small pulmonary arterioles of BT mice

As muscularization of small pre-capillary arterioles is a key feature in several models of PAH as well as human disease, it was of interest to see whether this feature would be reproduced in mice over-expressing the $BMPR2^{R899X}$ transgene. Muscularization was assessed by immunofluorescence for α-smooth muscle actin on lung sections from mice following 8 weeks of transgene induction. Quantification of small vessels (~40μm diameter) revealed that muscularization was significantly increased in BT mice compared to NBT-BMPR2 mice and NBT-ROSA controls (4.7 ± 0.38 μm, n= 10, 1.9 ± 0.11 μm, n= 6, 1.7 ± 0.16 μm, n=4, respectively, $p<0.0001$, Figure 7).

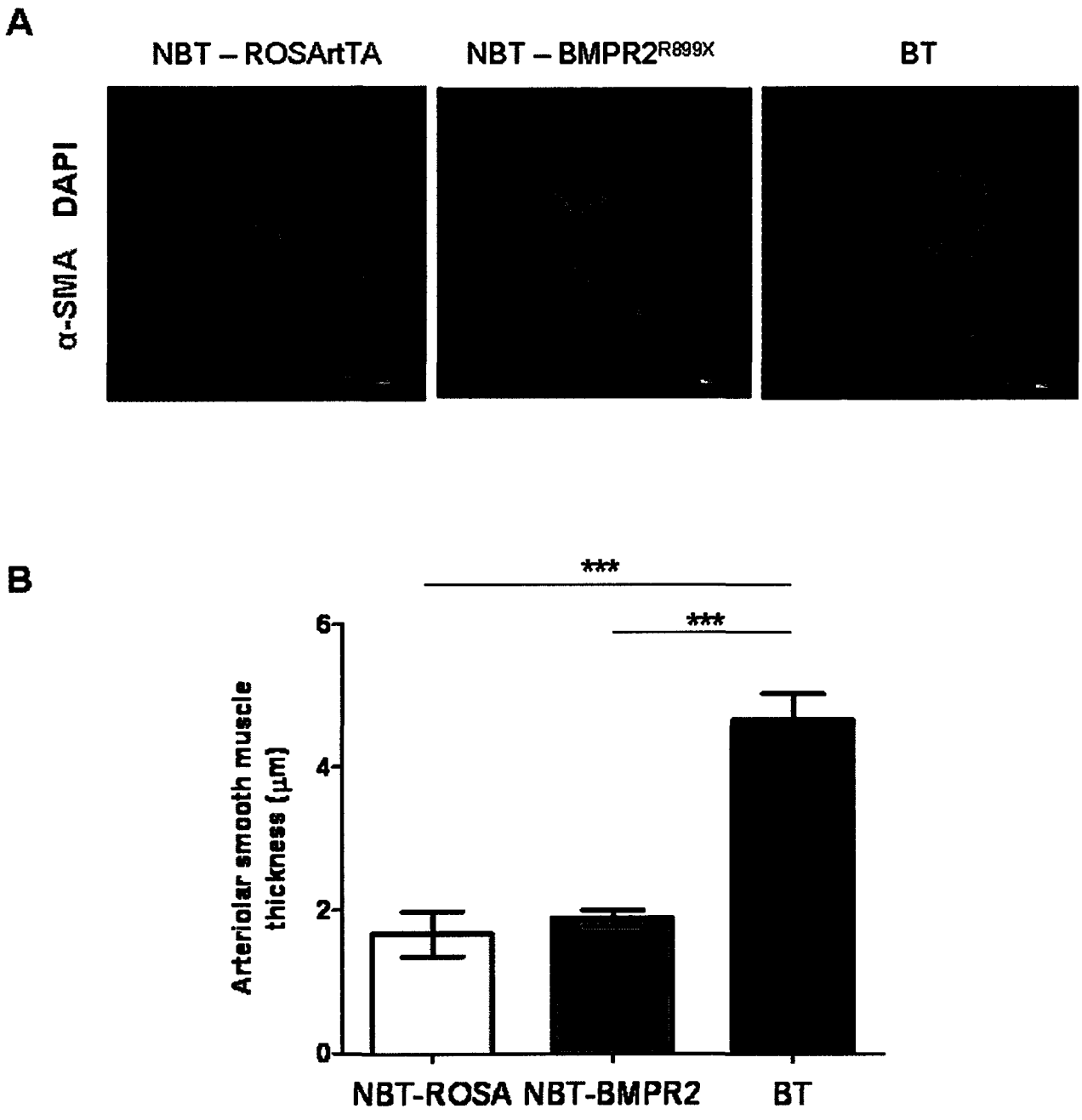

Figure 7. Arteriolar smooth muscle hypertrophy in BT mice following 8 weeks of transgene induction. **(A)** Immunofluorescence using an antibody against α-smooth muscle actin (α-SMA, red) combined with DAPI counterstaining (blue) on paraffin lung sections after 8 weeks of transgene induction. Bar = 30μm **(B)** Quantification of arteriolar smooth muscle thickness in NBT-ROSA (n=4), NBT-BMPR2 (n=6) and BT (n=10) mice. Bar = mean ± SEM. *** = $p<0.001$ by ANOVA with Bonferroni post-hoc analysis.

3.3.4. Morphological abnormalities including alveolar septal thickening are detected in the lungs of BT mice

Plexiform lesions are another interesting feature of PAH that are found on rarer occasions, and we sought to examine whether these were present in mice over-expressing the $BMPR2^{R899X}$ transgene. To examine gross lung morphology, H&E staining was performed on lung sections from mice 8 weeks post-transgene induction. No plexiform-like lesions were detected, but other marked morphological abnormalities were observed, notably alveolar septal thickening and cellular infiltration in several BT mice (Figure 8A). Although the severity of this phenotype was variable amongst the different animals, quantification of average alveolar septal thickness revealed a significant increase in BT mice compared to NBT-BMPR2 mice and NBT-ROSA controls (3.4 ± 0.17 μm, n=10, 2.2 ± 0.13 μm, n=5, 2.1 ± 0.12 μm, n=4, respectively, $p<0.0001$, Figure 8B).

3.3.5. The number of macrophages is increased in the lungs of BT mice

To determine whether inflammatory cells such as macrophages could be responsible for the alveolar septal thickening and cellular infiltrates detected by H&E staining, immunohistochemistry for CD68, a macrophage marker, was performed on lung sections of mice 8 weeks post transgene induction. The number of macrophages was significantly increased in BT mice compared to both NBT-BMPR2 mice and NBT-ROSA controls (101 ± 6 cells/field, n=10, 63 ± 5 cells/field, n=6, 38 ± 1 cells/field, n=4, respectively, $p<0.0001$, Figure 9).

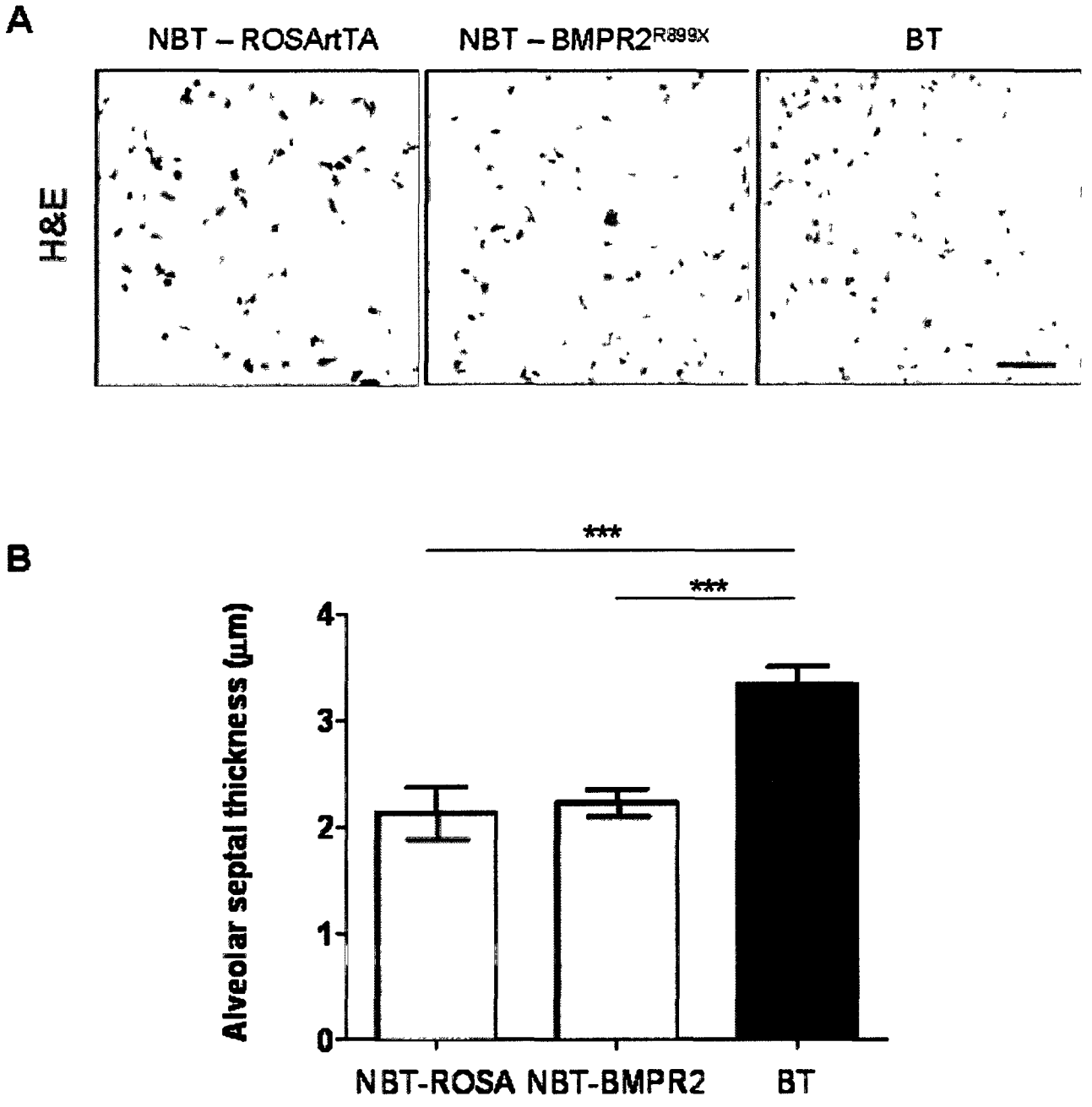

Figure 8. Abnormal lung morphology in BT mice following 8 weeks of transgene induction. **(A)** Hematoxylin and eosin (H&E) staining on paraffin lung sections after 8 weeks of transgene induction. Bar = 30µm **(B)** Quantification of alveolar septal thickness in NBT-ROSA (n=4), NBT-BMPR2 (n=5) and BT (n=10) mice. Bar = mean ± SEM. *** = $p<0.001$ by ANOVA with Bonferroni post-hoc analysis.

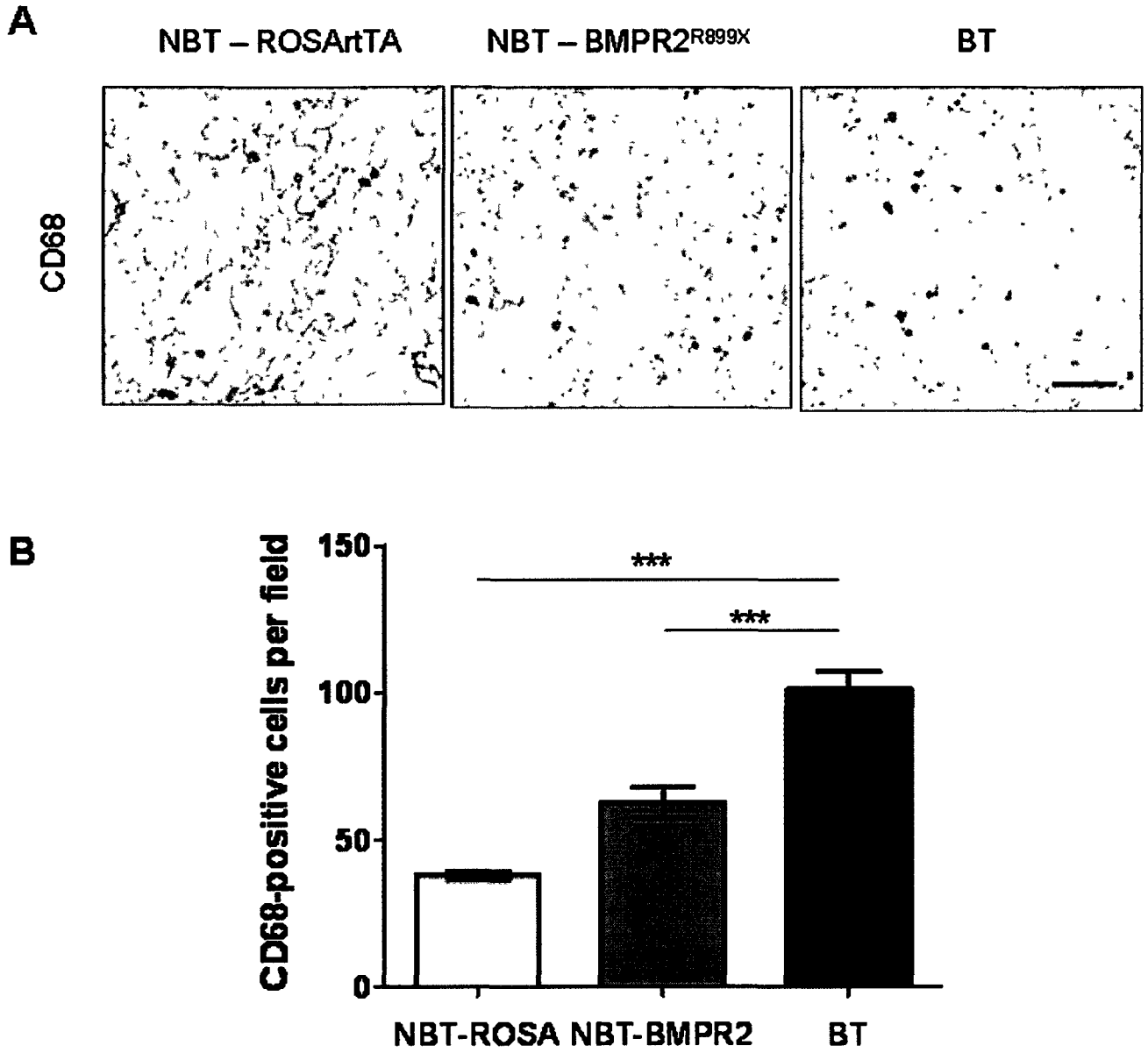

Figure 9. Macrophage infiltration in the lungs of BT mice following 8 weeks of transgene induction. **(A)** Immunohistochemistry with an antibody against CD68 on paraffin lung sections after 8 weeks of transgene induction. Bar = 60μm **(B)** Quantification of the number of CD68-positive cells in NBT-ROSA (n=4), NBT-BMPR2 (n=6) and BT (n=10) mice. Bar = mean ± SEM. *** = $p<0.001$ by ANOVA with Bonferroni post-hoc analysis.

3.4. Temporal patterns of proliferation and apoptosis

3.4.1. Apoptosis is increased in the lungs of BT mice after 2 weeks and 4 weeks of transgene induction

As there is accumulating evidence to suggest that apoptosis plays a major role in the pathogenesis of PAH and we believe that it may be central to disease progression in this model, we sought to evaluate the levels of apoptosis at various timepoints following transgene induction. To examine the temporal patterns of apoptosis, Terminal deoxynucleotidyl transferase-mediated dUTP Nick-End-Labeling (TUNEL) staining was performed on lung sections at 1, 2, 4 and 8 weeks following transgene induction. Representative staining is shown at early and late timepoints, as well as quantification for all timepoints (Figure 10). When comparing levels of apoptosis in BT mice to those in NBT-BMPR2 mice or NBT-ROSA controls, no significant increase was detected after 1 week (2 ± 1 cells/HPF, n=9, 4 ± 1 cells/HPF, n=4, 1 ± 0 cells/HPF, n=4, respectively) or 8 weeks of transgene induction (3 ± 1 cells/HPF, n=10, 3 ± 0 cells/HPF, n=6, 3 ± 1 cells/HPF, n=4, respectively). However, the number of apoptotic cells was significantly increased in BT mice compared to NBT-ROSA controls after 2 weeks of transgene induction (4 ± 0 cells/HPF, n=9, 1 ± 0 cells/HPF, n=3, respectively, $p<0.05$) as well as in NBT-BMPR2 mice compared to NBT-ROSA controls (4 ± 1 cells/HPF, n=3, 1 ± 0 cells/HPF, n=3, respectively, $p<0.05$). Similarly, apoptosis was significantly increased in BT mice compared to NBT-ROSA controls after 4 weeks of transgene induction (5 ± 1 cells/HPF, n=9, 0 ± 0 cells/HPF, n=3, respectively, $p<0.05$), this time with NBT-BMPR2 mice having an intermediate value (2 ± 0 cells/HPF, n=4). When all timepoints were pooled, an overall increase in the number of apoptotic cells was detected in BT mice compared to NBT-ROSA controls (4 ± 0

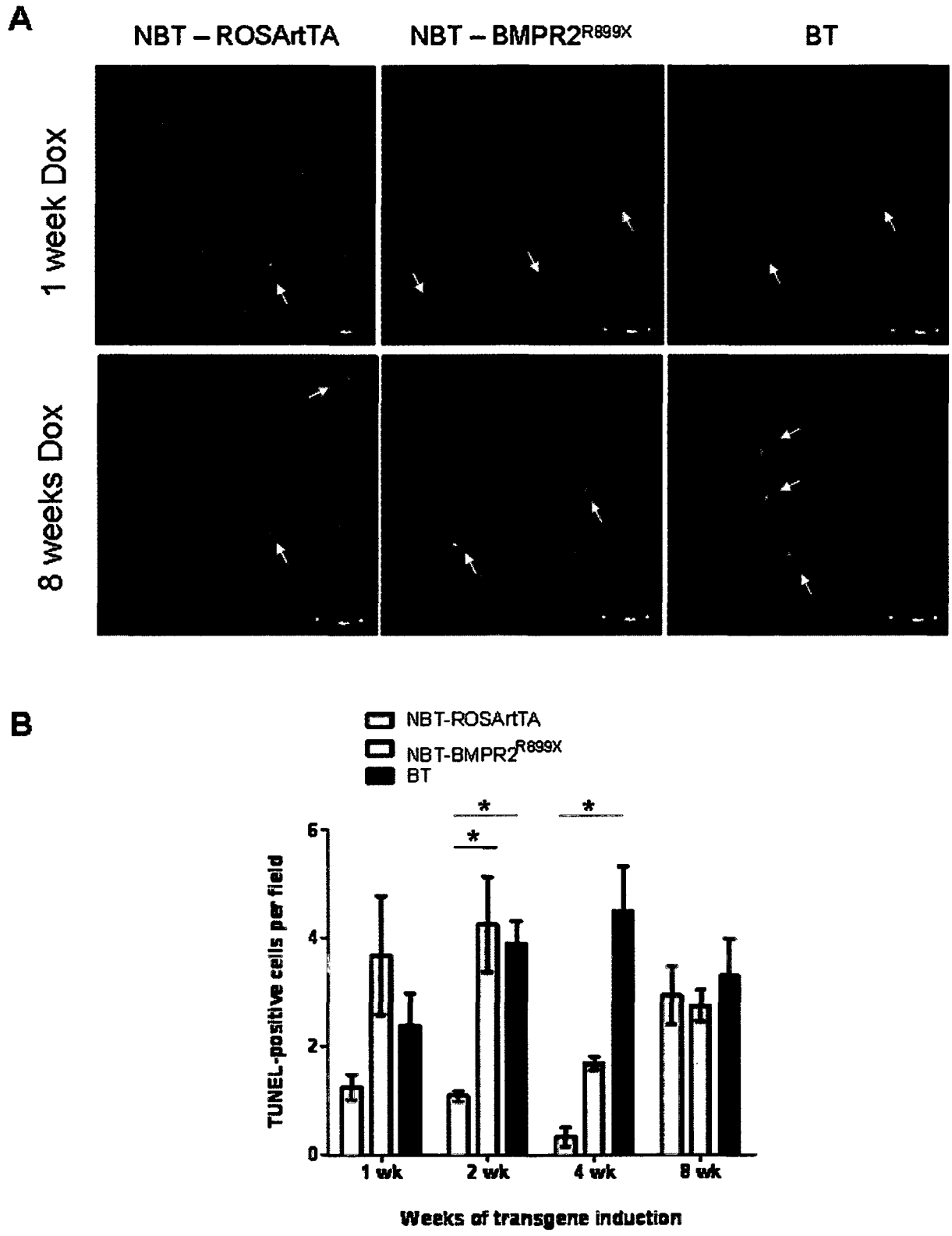

Figure 10. Temporal patterns of apoptosis over the timecourse of BMPR2^{R899X} induction. **(A)** TUNEL staining combined with DAPI nuclear counterstaining on paraffin lung sections of NBT-ROSA, NBT-BMPR2 and BT mice after 1 week (n=4, n=4 and n=9, respectively) and 8 weeks (n=4, n=6 and n=10, respectively) of transgene induction. Bar = 30μm. **(B)** Quantification of TUNEL-positive cells. Bar = mean + SEM. * = $p<0.05$ by ANOVA with Bonferroni post-hoc analysis.

cells/HPF, n=37, 2 ± 0 cells/HPF, n=13, respectively, $p<0.01$, Figure 12A) again with NBT-BMPR2 mice at an intermediate value (3 ± 0 cells/HPF, n=16).

3.4.2. Proliferation is increased in the lungs of BT mice after 8 weeks of transgene induction

Having recognized that apoptosis was deregulated in mice over-expressing the $BMPR2^{R899X}$ transgene, it was of interest to see whether this was also the case for proliferation. To examine the temporal patterns of proliferation, Ki67 staining was performed on lung sections at 1, 2, 4 and 8 weeks following transgene induction. Representative staining is shown at early and late timepoints, as well as quantification for all timepoints (Figure 11). When comparing levels of proliferation in BT mice to NBT-ROSA controls, a significant increase is only observed following 8 weeks of transgene induction (114 ± 20 cells/field, n=10, 22 ± 14 cells/field, n=4, respectively, $p<0.05$). There was no significant increase in proliferation in BT mice compared to NBT-BMPR2 mice and NBT-ROSA controls after 1 week (89 ± 24 cells/field, n=9, 111 ± 2 cells/field, n=4, 35 ± 11 cells/field, n=4, respectively), 2 weeks (82 ± 25 cells/field, n=10, 153 ± 78 cells/field, n=3, 42 ± 23 cells/field, n=3, respectively) or 4 weeks of transgene induction (64 ± 16 cells/field, n=9, 14 ± 3 cells/field, n=4, 24 ± 13 cells/field, n=3, respectively). Nevertheless, when all timepoints were pooled, there was a significant increase in the number of proliferative cells in BT mice compared to NBT-ROSA controls (88 ± 11 cells/field, n=38, 30 ± 7 cells/field, n=14, respectively, $p< 0.05$, Figure 12B).

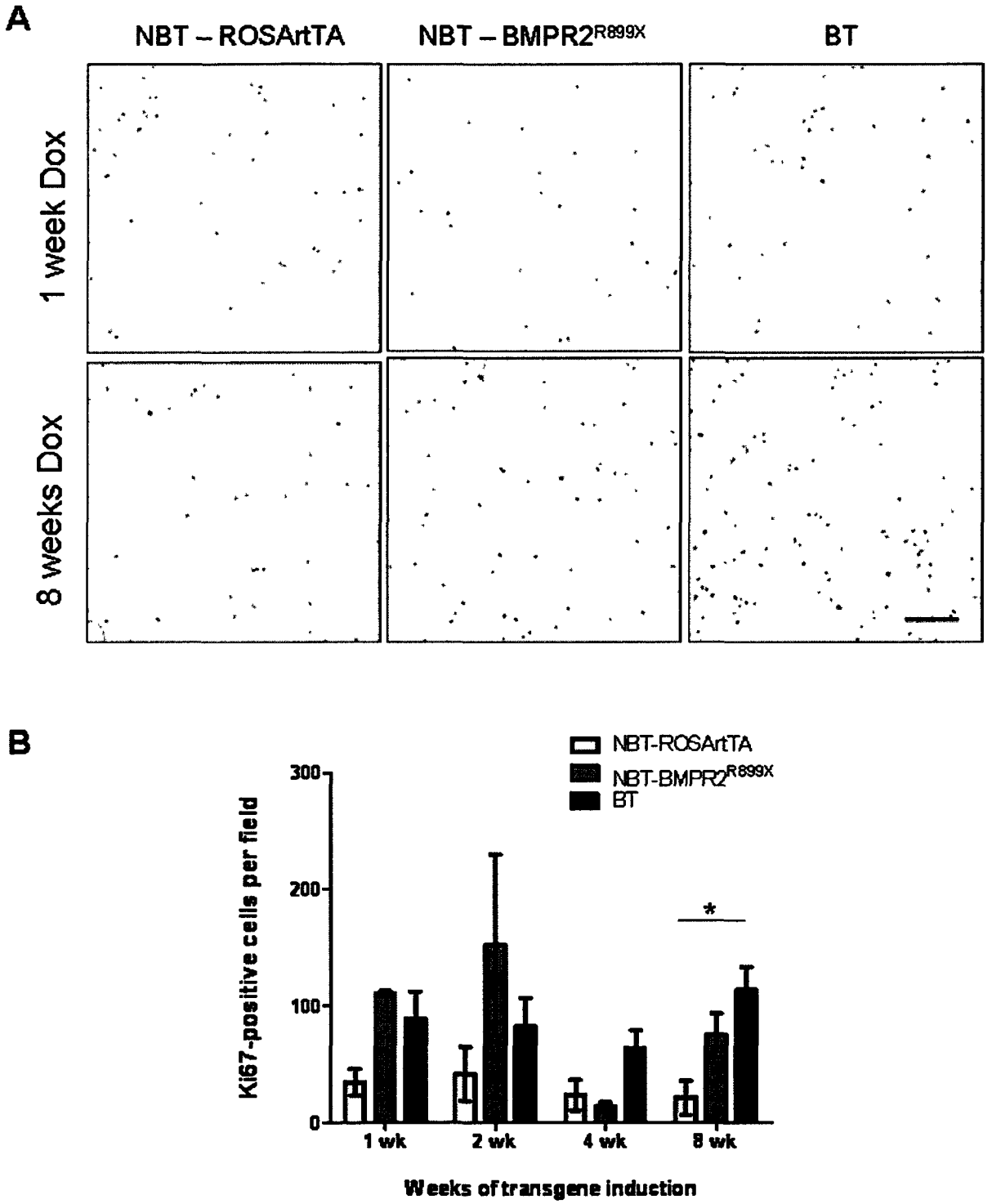

Figure 11. Temporal patterns of proliferation over the timecourse of BMPR2^{R899X} induction. (A) Immunohistochemistry with an antibody against Ki67 on paraffin lung sections of NBT-ROSA, NBT-BMPR2 and BT mice after 1 week (n=4, n=4 and n=9, respectively) and 8 weeks (n=4, n=6 and n=10, respectively) of transgene induction. Bar = 120μm **(B)** Quantification of Ki67-positive cells. Bar = mean + SEM. * = $p<0.05$ by ANOVA with Bonferroni post-hoc analysis.

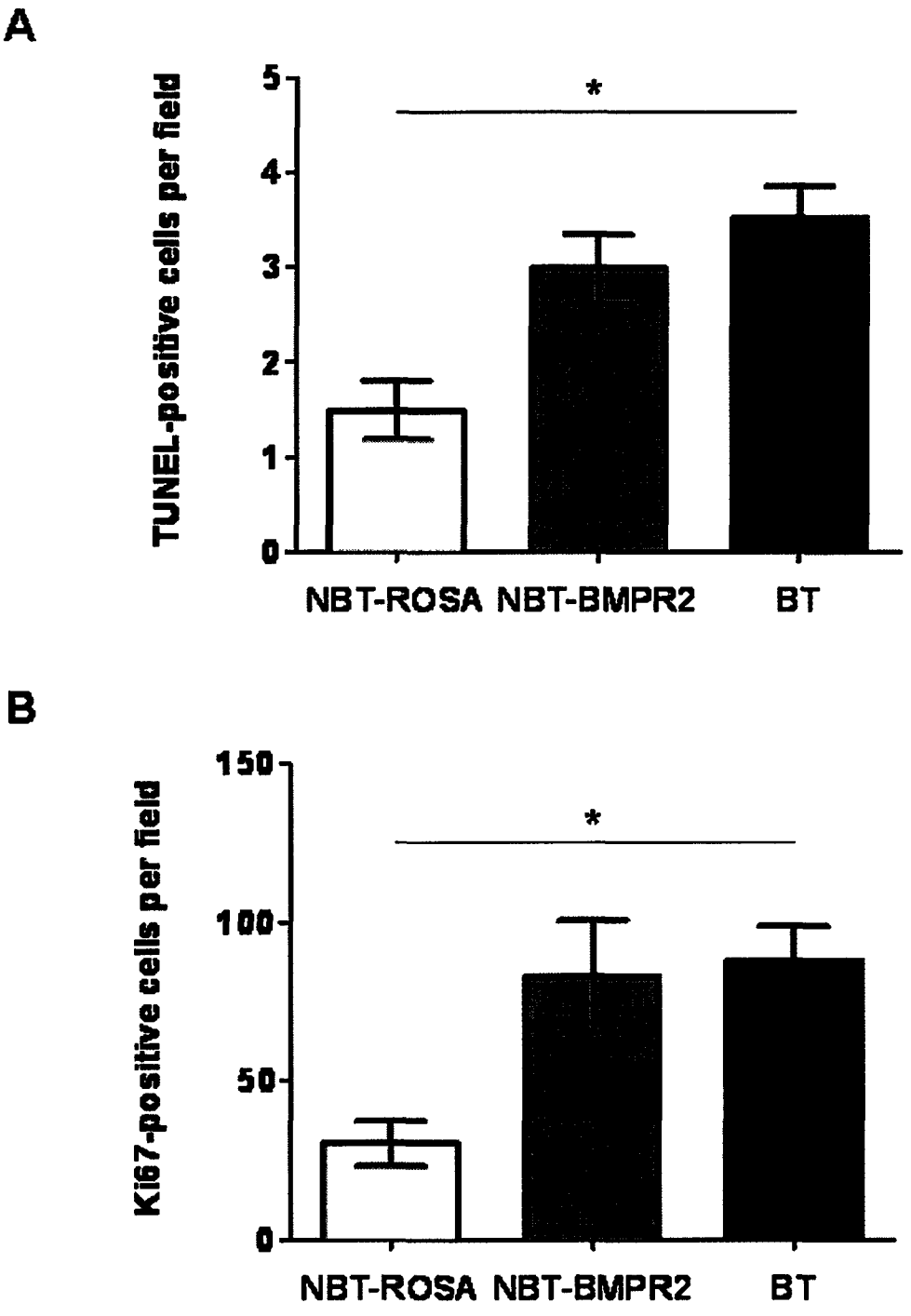

Figure 12. Apoptosis and proliferation from combined timepoints of transgene induction. **(A)** Average number of TUNEL-positive cells in NBT-ROSA (n=13), NBT-BMPR2 (n=16) and BT (n=37) mice from pooled timepoints. **(B)** Average number of Ki67-positive cells in NBT-ROSA (n=14), NBT-BMPR2 (n=17) and BT (n=38) mice from pooled timepoints. Bar = mean ± SEM. * = $p<0.05$ by ANOVA with Bonferroni post-hoc analysis.

3.5. IL-6 does not appear to be an efficient environmental stressor in a small cohort of $BMPR2^{R899X}$ mice

3.5.1. RVSP is not increased in BT mice having received IL-6

Because IL-6 has been involved as a relevant environmental stressor or "second hit" in PAH, we sought to determine whether it would produce a more severe phenotype in mice over-expressing the $BMPR2^{R899X}$ transgene. Mice receiving IL-6 were characterized similarly to mice without treatment. RVSP was again measured as an indicator of pulmonary pressures after 2 weeks of IL-6 administration and a total of 8 weeks of transgene induction, and values are summarized in scatter (Figure 13A) and box plots (Figure 13B). Surprisingly, IL-6 only markedly increased RVSP in 1 of 8 BT mice, and average RVSP was not significantly increased in BT mice compared to NBT-ROSA controls (25 ± 1.6 mmHg, n= 8, 21 ± 1.9 mmHg, n=4, respectively). Furthermore, IL-6 appears to have induced spontaneous PAH in 1 of the 4 NBT-ROSA controls.

3.5.2. RV hypertrophy is not increased in BT mice having received IL-6

RV hypertrophy was assessed by measuring RV/LV+S ratios in mice having received IL-6. Summary data is depicted in scatter (Figure 13C) and box plots (Figure 13D). Similar to RVSP data, the ratios were highly variable within each group, and no significant increase was detected in BT mice compared to NBT-ROSA controls (0.25 ± 0.010, n=8, 0.23 ± 0.022, n=4, respectively).

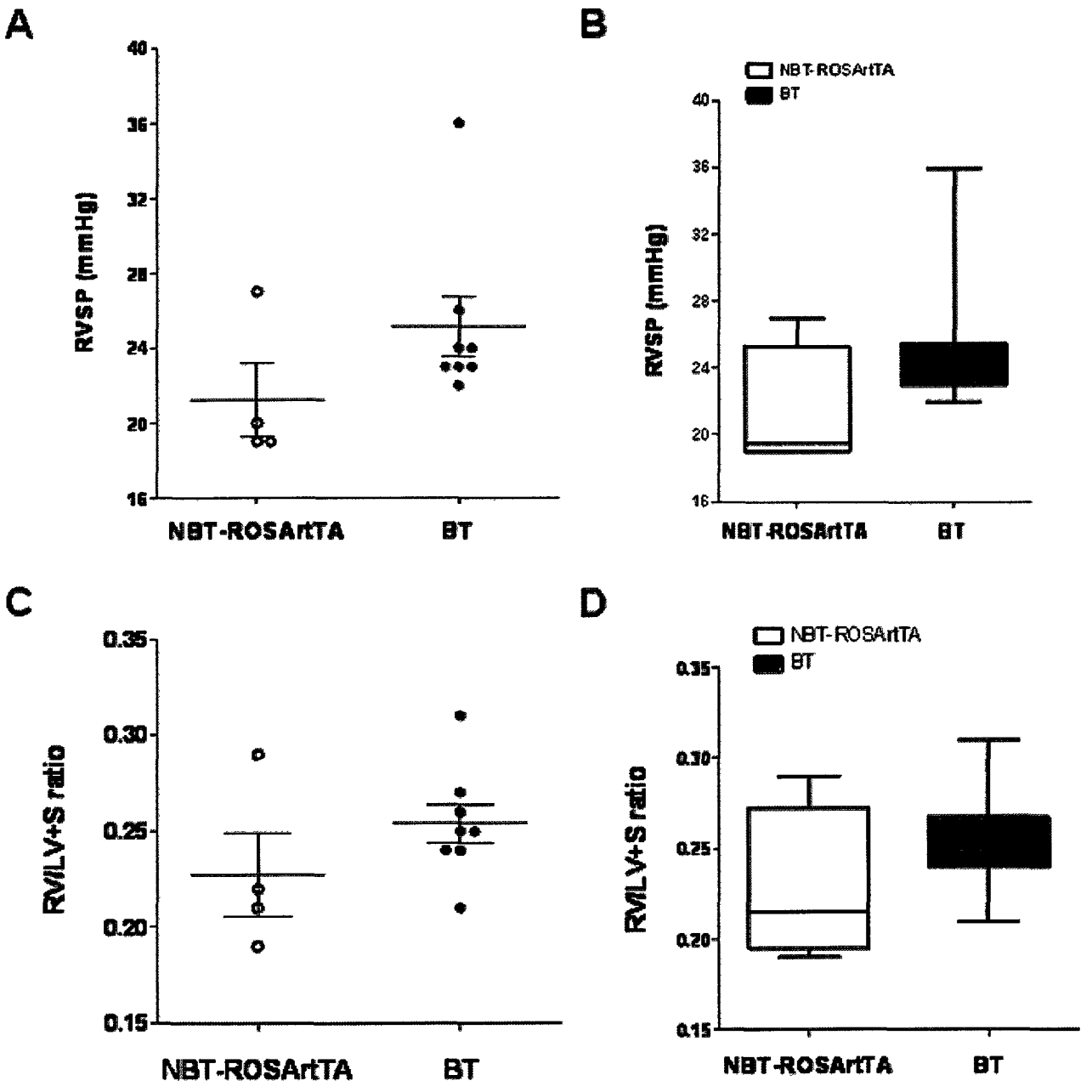

Figure 13. Distribution of RVSP and RV/LV+S values in mice with IL-6 treatment. **(A)** Scatter plot showing the distribution of RVSP values in BT mice (n=8) compared to NBT-ROSA controls (n=4). Line shows the mean of each group. **(B)** Box plots summarizing RVSP values of each group. Whiskers represent sample minimum and maximum, line at sample median. **(C)** Scatter plot showing the distribution of RV/LV+S values in BT mice (n=8) compared to NBT-ROSA controls (n=4). Line shows the mean of each group. **(D)** Box plots summarizing RV/LV+S values of each group. Whiskers represent sample minimum and maximum, line at sample median.

3.5.3. Muscularization is increased in the small pulmonary arterioles of BT mice having received IL-6

Once again muscularization of small pre-capillary arterioles in mice having received IL-6 was assessed by immunofluorescence for α-smooth muscle actin on lung sections. Quantification of small vessels (~40μm diameter) revealed that muscularization was significantly increased in BT mice compared to NBT-ROSA controls (4.3 ± 0.47 μm, n=8, 1.8 ± 0.12 μm, n=4, respectively, p=0.001, Figure 14A, D and G).

3.5.4. Morphological abnormalities including alveolar septal thickening are detected in the lungs of BT mice having received IL-6

Lung morphology was also examined in these mice by H&E staining. Similar to mice without IL-6 treatments, no plexiform-like lesions were detected, but there was notable alveolar septal thickening and cellular infiltration (Figure 14B and E). Quantification of average septal thickness revealed a significant increase in BT mice compared to NBT-ROSA controls (2.9 ± 0.18 μm, n=8, 1.2 ± 0.095 μm, n=4, respectively, p<0.0001, Figure 14H).

3.5.5. The number of macrophages is not increased in the lungs of BT mice having received IL-6

The presence of inflammatory infiltrates in mice having received IL-6 was again detected by immunohistochemistry for CD68. Interestingly, the number of macrophages was not significantly increased in BT mice compare to NBT-ROSA controls (59 ± 5 cells/field, n=8, 46 ± 7 cells/field, n=4, Figure 14C, F and I).

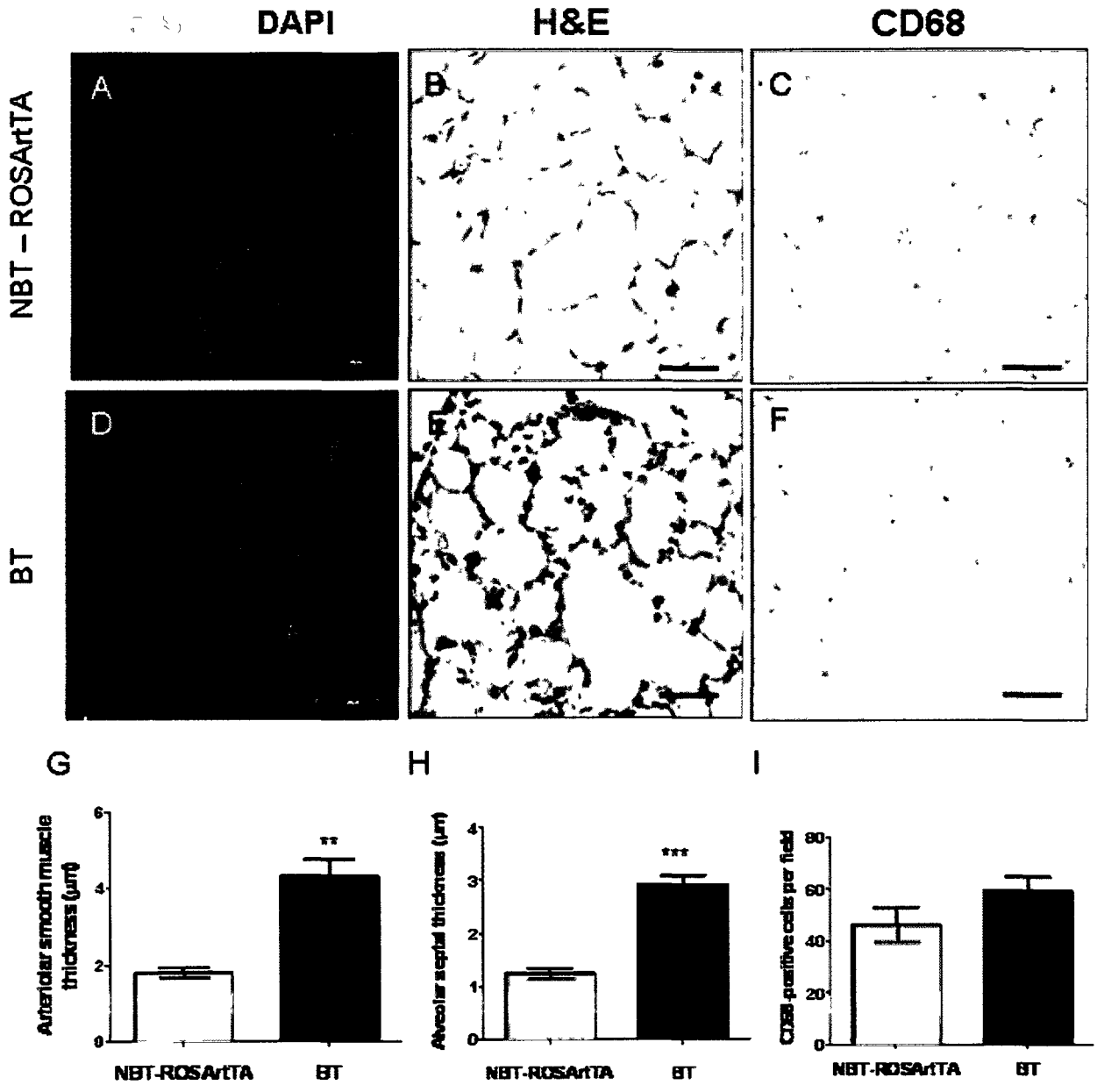

Figure 14. Characterization of arteriolar muscularization, pulmonary alveolar remodelling and macrophage infiltration in mice with IL-6 treatment. (A and D) Immunofluorescence using an antibody against α-smooth muscle actin (α-SMA, red) combined with DAPI counterstaining (blue) on paraffin lung. Bar = 30µm **(B and E)** Hematoxylin and eosin (H&E) staining on paraffin lung sections. Bar = 30µm **(C and F)** Immunohistochemistry with an antibody against CD68 on paraffin lung sections. Bar = 60µm **(G)** Quantification of arteriolar smooth muscle thickness in BT mice (n=8) compared to NBT-ROSA controls (n=4). Bar = mean ± SEM. ** = $p<0.01$ by t-test with Welch's correction. **(H)** Quantification of alveolar septal thickness in BT mice (n=8) compared to NBT-ROSA controls (n=4). Bar = mean ± SEM. *** = $p<0.001$ by t-test with Welch's correction. **(I)** Quantification of the number of CD68-positive cells in BT mice (n=8) compared to NBT-ROSA controls (n=4). Bar = mean ± SEM.

4. Discussion

PAH is a rare disease with a very complex and multifactorial pathogenesis that remains largely undefined. Current PAH therapies have been developed based on advances in our understanding of the concepts behind PAH pathogenesis. Earlier beliefs that PAH was largely a disease of excessive pulmonary vasoconstriction led to the introduction of calcium channel blockers as a treatment option [89]. Subsequently, the discovery of the importance of endothelial dysfunction in PAH then led to the introduction of therapies to restore the balance between vasoconstrictor and vasodilator factors, including the administration of prostaglandins, endothelin receptor antagonists and phosphodiesterase inhibitors [89]. More recent ideas about the development of this disease are mainly focused on the role of pulmonary arteriolar remodelling and abnormal cell growth and survival; this has led to the testing of novel agents that have been developed for cancer therapies, including Gleevec and Sorafenib [89].

However, despite all these advances, we are far from having a truly effective treatment for this progressive and usually lethal disease, and there is still no consensus about the mechanisms underlying its pathogenesis. Arguably, the most significant insight should have come from the recent discovery of mutations in the BMPR2 receptor associated with both familial and sporadic cases, which were found in up to half of all patients (~80% of FPAH and almost 40% of IPAH). Nevertheless, even a decade after this seminal discovery, we are still not much closer to understanding how these mutations may cause this disease.

4.1. Lessons from BMPR2 transgenic mice

Several studies have examined the role of BMPR2 signalling in the context of pulmonary vascular cells and PAH. Mice heterozygous for a BMPR2 null allele ($BMPR2^{+/-}$)

or those expressing only 5-10% of BMPR2 compared to WT mice exhibited modest elevations in RVSP and some level of arteriolar muscularization, but showed no evidence of arteriolar occlusion or plexiform lesions under unstressed conditions [7, 66]. However, the presence of obliterative luminal lesions was demonstrated in mice over-expressing the $BMPR2^{R899X}$ deletional mutation in SMCs, which also had significantly increased RVSP and arteriolar muscularization [63]. Exaggerated PAH and arterial remodelling was also reported in $BMPR2^{+/-}$ mice exposed to serotonin or hypoxic conditions [65]. These studies suggest that a reduction in BMPR2 activity increases the susceptibility of mice to PAH and give support to the notion that remodelling mechanisms play a role in the pathogenesis of this disease. Further support for the prevalence of remodelling mechanisms in PAH came from the identification of hyperproliferative and apoptosis-resistant vascular cells in patients with the disease [45, 46]. Moreover, consistent with the important role of the BMPR2 pathway with respect to vascular homeostasis and EC survival, several studies have emerged that support a central role for apoptosis in the pathogenesis of PAH. In the rat MCT model of PAH, a progressive temporal increase in apoptosis in the small pulmonary arterioles was observed, which was attenuated by the use of a pan-caspase inhibitor, corresponding with a significant reduction in RVSP [70]. Furthermore, treatment of hypoxic rats with a VEGFR2 antagonist resulted in worsening of hypoxia-induced PAH associated with an early increase in EC apoptosis, marked potentiation of arterial remodelling and the appearance of proliferative lesions [73]. Treatment of these rats with a pan-caspase inhibitor prevented the development of severe PAH and the remodelling changes induced by VEGFR2 blockade [73]. The Ang1-Tie2 EC survival pathway was also shown to act as a protective mechanism in PAH, where Tie2 deficient mice developed PAH associated with increased apoptosis when exposed to serotonin or IL-6, and the phenotype was rescued by the use of apoptosis

inhibitors [84]. Together, these studies have shown the critical role of the BMPR2 pathway in maintaining vascular homeostasis, and have implicated BMPR2 mutations and abnormal cell growth and survival as key factors in the pathogenesis of PAH. Yet, to date, the precise mechanisms leading to the onset and progression of PAH remain unknown.

4.2. Ubiquitous over-expression of the BMPR2^{R899X} transgene as a new model of PAH

In an attempt to examine the impact of BMPR2 loss-of-function mutations on vascular remodelling and the development of PAH, we generated mice over-expressing the BMPR2^{R899X} transgene. Previous work by West et al. examined the effect of SMC-specific over-expression of the BMPR2^{R899X} transgene, which was shown to result in the development of PAH associated with vascular remodelling [63]. Since there is considerable evidence to suggest that ECs are central in disease pathogenesis, studies were initiated in mice over-expressing the BMPR2^{R899X} transgene specifically in ECs to see whether we could reproduce the PAH phenotype (Appendix 1). Using this new model, the unique focus of our study was to address the role of apoptosis in the pathogenesis of the disease, which was not examined by West et al. Although this model did produce PAH associated with increased peripheral cell apoptosis, the phenotype was modest and there were difficulties in confirming transgene protein expression. This led us to use a ubiquitous promoter to drive expression of the BMPR2^{R899X} transgene, in hopes of achieving more robust transgene expression and thus a stronger PAH phenotype. We therefore pursued characterization of mice over-expressing the BMPR2^{R899X} transgene under the ROSA promoter. This model also better mimics the clinically relevant scenario in which BMPR2 mutations are expressed ubiquitously in cells throughout the body, and yet pathology is seen only in the lung vasculature.

4.2.1. BMPR2^{R899X} mice develop typical features of PAH associated with inflammation

One of the main objectives of this study was to determine whether BMPR2^{R899X} mice developed PAH. Therefore, hemodynamic parameters were measured and lungs were characterized to see whether these mice reproduced typical features of PAH. First, RVSP was measured by right ventricle catheterization as a surrogate measure of pulmonary pressures. As early as 1 week of transgene expression, BT mice were already showing increased RVSP compared to NBT-ROSA controls. This was also the case after 2 weeks and up to 8 weeks of transgene induction. NBT-BMPR2 mice generally had intermediate values, consistent with a phenotype resulting from transgene leakiness. Although RVSP was not significantly increased after 4 weeks of transgene induction, the pattern of RVSP distribution between each group was comparable to that of other time points. The lack of significant increase could be accounted for by the variability of RVSP values in BT mice, which was larger than at other time points, as well as the small sample size of NBT controls which on average had higher RVSPs than in other time points. In other words, statistical significance might be reached if sample size was increased. Indeed, when all time points were pooled, BT mice had significantly higher RVSPs than NBT-ROSA controls. Of note,

Variability in the degree of elevation of RVSP within BT mice could be due to either differences in transgene expression in individual mice, or to variability in disease penetrance, which is a typical feature in FPAH. As mentioned previously, less than 20% of BMPR2 mutation carriers develop PAH, and mice would presumably have a similar incomplete penetrance. In future experiments it would be interesting to carefully quantify transgene expression in individual mice and correlate it with the severity of the disease. A close correlation would be consistent with this being a dominant mechanism, whereas as lack of

correlation would suggest that other mechanisms account for the incomplete penetrance in our mouse model.

The next parameter characterized was RV remodelling. Surprisingly, despite the significant increase in pulmonary pressures, BT mice did not show any significant RV hypertrophy as indicated by the RV/LV+S ratio at any specific timepoint or when all time points were pooled. From previous studies, ratios from 0.3 up to 0.45 are typically indicative of substantial RV hypertrophy associated with severe PAH [67, 83]. Here, average ratios in BT mice were no higher than 0.25. RV remodelling occurs over time, as pulmonary vascular resistance increases and pressure climbs. In this model, it is possible that the degree of increase in RVSP was not severe enough to induce substantial RV hypertrophy, or that remodelling would manifest itself later in the disease progression and was not yet detectable after 8 weeks of transgene induction.

Another key feature of PAH that was reproduced in $BMPR2^{R899X}$ mice is muscularization of small pulmonary pre-capillary arterioles as determined by smooth muscle actin staining. BT mice showed significantly increased arteriolar smooth muscle thickness when compared to NBT-BMPR2 mice and NBT-controls. It is debatable whether this phenotype is attributable to increased pulmonary vascular resistance or to disrupted BMPR2 signalling. Here, the lack of RV remodelling despite increased RVSP suggests that muscularization is more likely a result of abnormal SMC proliferation rather than a direct consequence of increased pulmonary pressures. Incidentally, Hansmann et al. recently demonstrated for the first time that the anti-proliferative effects of BMPR2 signalling in pulmonary arteriolar SMCs can be attributed to activation of PPARγ [90]. Their study suggests that BMPR2 signalling prevents PDGF-BB-induced proliferation of pulmonary arteriolar SMCs by decreasing nuclear phospho-ERK and inducing DNA binding of PPARγ

that is independent of Smad1/5/8 phosphorylation [90]. They also show that mice with deletion of PPARγ in SMCs spontaneously develop PAH, and that endogenous expression of PPARγ in SMCs can protect against this [90]. These findings are consistent with the muscularization observed in mice over-expressing the $BMPR2^{R899X}$ transgene, and bring support to the concept that signalling mediated by the C-terminal portion of BMPR2 is perturbed in this model. As PPARγ-mediated events protect against PAH, PPARγ agonists could offer a new treatment possibility for patients with the disease. Indeed, rosiglitazone, a PPARγ agonist, was shown to attenuate hypoxia-induced pulmonary arterial remodelling and hypertension in mice [91].

Other than arterial remodelling, the most typical morphological abnormality observed in patients with PAH are the plexiform lesions, albeit these can occur much less consistently. These consist of lesions with multiple irregular vascular lumens composed largely of abnormally proliferating endothelial and smooth muscle-like cells. Upon careful inspection of lung morphology in BT-BMPR2 mice using H&E staining, no plexiform-like lesions or obliterated vessels were observed. This was not unexpected in view of the rather modest degree of elevation of RVSP and the fact that these lesions are not always seen clinically, even in severe end-stage disease. However, marked cellular infiltration and alveolar septal thickening was noted in several BT mice, pointing towards local infiltration of inflammatory cells. To confirm the nature of these cellular infiltrates, staining for CD68, a macrophage marker, was performed on lung sections. The significant increase in the number of macrophages in BT mice compared to controls brings further support to previous studies implicating macrophages as key players in the pathogenesis of PAH. Over-expression of the $BMPR2^{R899X}$ transgene could contribute to inflammatory cell infiltration by exerting direct effects on macrophages, or alternatively by promoting the recruitment of macrophages to the

site of injury in response to local increases in apoptosis. However, the exact mechanism of macrophage infiltration and its role are still unknown and will make the object of further studies.

In summary, $BMPR2^{R899X}$ mice have increased RVSP and muscularization of small pre-capillary arterioles, despite a lack of obvious RV hypertrophy, with alveolar septal thickening and extensive pulmonary inflammatory infiltrates by macrophages. Together, these data suggest that over-expression of the $BMPR2^{R899X}$ transgene is sufficient to induce PAH and that inflammation likely has an important contributory role in the pathogenesis of this disease. Importantly, this is the first demonstration that ubiquitous over-expression of a truncated BMPR2 receptor results in PAH with significant elevations in RVSP, extensive muscularization of small arteries and inflammation. This is in contrast to heterozygous BMPR2 knockout mice or mice expressing only 5-10% BMPR2, which do not spontaneously develop PAH, and supports previous work from West et al. with SMC-specific transgene over-expression [63].

4.2.2. The transgene is expressed in $BMPR2^{R899X}$ mice

Another main objective of this study was to confirm expression of the $BMPR2^{R899X}$ transgene. The initial strategy employed was to perform Western blots using an antibody against the C-terminal flag tag on total protein extracts from lungs. The expected molecular weight for the native BMPR2 receptor, which has a length of 1038 amino acids, is around 130 kDa [63]. The expected size of the transgene truncated at 899 amino acids and with addition of the 8 amino acid flag tag was thus calculated to be approximately 95 kDa. Therefore, it was expected that a band of this size should be detected in BT mice expressing the $BMPR2^{R899X}$ transgene, that would be absent in NBT controls which would only express

the native, full-length receptor. Originally, a Flag antibody from Sigma was used which yielded poor quality blots with very high background and many unspecific bands, making it difficult to distinguish the band of interest. In hopes of resolving this issue, a new antibody was purchased from OriGene, termed DDK, generated against the same epitope. This antibody was claimed to be more specific and have less background staining than other Flag antibodies. Unfortunately, DDK blots on total protein extracts still revealed no specific band in BT mice. Because BMPR2 is not a very high abundance protein, subcellular protein fractions were collected rather than total extracts in an effort to enrich the transgene in the membrane fraction. Once again, the $BMPR2^{R899X}$ transgene could not be detected by DDK blots on membrane fractions. A major drawback of the flag and DDK antibodies is that they were raised in mice, which is also the nature of the protein extracts used for blotting. This consequently resulted in increased background signals that could potentially have been masking the band of interest, especially since the flag tag is such a small epitope. To circumvent this problem, another approach that could be tried in the future is to immunoprecipitate the transgene using a flag or DDK antibody, then blot the isolated fraction using the same antibody. In theory, only proteins with a strong affinity for the antibody, ie the flag-tagged transgene, should remain in the isolated fraction, thereby making the blot much cleaner.

In parallel with the flag and DDK trials, membranes were probed with an antibody against BMPR2 to distinguish between the native receptor and the truncated transgene, which should run at different molecular weights as described above. As expected, the native BMPR2 receptor was detected in all samples, but no specific band corresponding to the $BMPR2^{R899X}$ transgene product was seen in BT samples. Taken together, these results

suggest that the levels of $BMPR2^{R899X}$ expression were likely too low to be detected using a Western blot approach, which although very specific lacks high sensitivity.

Therefore, a more sensitive approach was used to detect the $BMPR2^{R899X}$ transgene, i.e. RT-PCR. Primers were directed against a region specific to the transgene, and these amplified a specific band that was expressed in all Dox-stimulated BT mice. However, these experiments also suggested some degree of leakiness, since a band could also be detected in the NBT-BMPR2 mice, but at somewhat lower levels than in their BT littermates. Importantly, no specific bands for the $BMPR2^{R899X}$ transgene were seen in the NBT-ROSA mice, which do not harbour the mutant receptor transgene. However, the overall level of expression was quite low in BT mice and not substantially greater than that seen in the V-Cad model described in Appendix 1. In this regard, we were unsuccessful in establishing a more robust expressing model that is needed to fully explore the phenotype induced by the mutation. Unfortunately, we are also limited in the number of commercially available mouse strains with promoters driving ubiquitous expression of the tetracycline transactivator, and the ROSA strain that was selected has been shown to exhibit lower levels of expression in the lungs than other organs [92]. Nevertheless, our experiments did confirm that the transgene was being expressed in BT mice in a specific manner.

Knowing that the transgene was present, at least at the mRNA level, we wanted to confirm that it was also being translated into proteins. Immunostaining is a highly sensitive technique that also provides information about spatial localization. Therefore, an immunofluorescence staining using the DDK antibody was performed on a small number of samples, which revealed staining in BT mice, with much lower staining in NBT-BMPR2 mice and NBT-ROSA controls. Admittedly, unspecific background staining must be kept in mind because the antibody used was raised in mice, but levels of staining consistently

appeared higher in BT mice. In future experiments, an isotype control for the DDK antibody should be used to control for unspecific staining. Together with the RT-PCR findings, these results provide two lines of evidence that the $BMPR2^{R899X}$ transgene is being expressed, both at the mRNA and protein level.

4.3. Mechanism by which $BMPR2^{R899X}$ over-expression may alter BMPR2 signalling and induce PAH

As described previously, the kinase domain of the BMPR2 receptor signals mainly through Smad1/5/8 while the C-terminal portion of the receptor signals primarily through p38 and p44/42 MAPK pathways. Analysis of these targets by Western blots did not reveal any obvious changes in their activity in BT mice compared to NBT-ROSA controls. Because the R899X deletion is in the C-terminal portion of the receptor and the kinase domain is preserved, it was anticipated that Smad signalling would remain unchanged. On the other hand, a plethora of signalling pathways, including many of the major growth factors, converge on p38 and p44/42 MAPK, and this background stimulation might mask any alteration in signalling attributable to this mutation. Since our interest is mainly focused on vascular cell signalling, in future studies it would be possible to determine whether an imbalance in the signalling pathways could be demonstrated in pulmonary vascular cells by isolating ECs and SMCs from the lungs of $BMPR2^{R899X}$ mice using digestion and cell sorting strategies [93]. Alternatively, cultured cells could be transfected with the $BMPR2^{R899X}$ transgene, and the activity of these signalling pathways could be assessed *in vitro* in the presence and absence of BMP ligands.

The presence of a phenotype in mice over-expressing the $BMPR2^{R899X}$ transgene is suggestive of a "dominant negative" interaction of the transgene with the native receptor.

Indeed, West et al. refer to over-expression of the $BMPR2^{R899X}$ transgene specifically in SMCs as a dominantly acting mutant [63]. However, to our knowledge this group has not reported any evidence that clarifies the exact mechanism by which this deletion can result in a dominant negative effect on the remaining wild type receptors. For instance, it could be speculated that the mutant transgene interferes with normal BMPR2 signalling by integrating into the hetero-tetramer complex required for signal transduction thus preventing the efficient activation of downstream mediators, possibly by reducing oligomerization or binding of necessary factors. Alternatively, it may act by another mechanism altogether. For example, by causing an imbalance in downstream signalling pathways, it may alter the normal consequences of BMPR2 activation such that the cellular effects are reversed. In SMCs, this may result in proliferation rather than growth inhibition, whereas in ECs it may induce rather than protect against apoptosis. Indeed, the effects of TGF-β family ligands are exquisitely sensitive to this balance in signalling pathways, and the relative activation of Smads 2/3 versus 1/5/8 appears to play a key role in development of vascular malformations in hereditary hemorrhagic telangectasia (HHT), a disease which is also associated with mutations in TGF-β family receptors [94, 95]. However, in HHT this involves TGF-β ligand receptors including endoglin and ALK-1, although interestingly it has recently been reported that families harbouring ALK-1 mutations also can exhibit PAH identical to that found in families with the classical BMPR2 mutations [94]. Both ALK-1 and endoglin favour signalling by the Smad 1/5/8 pathway, which is the typical BMP pathway, and thus loss of function mutations in these receptors will shift the balance towards Smads 2/3 [95]. This mechanism may also contribute to PAH associated with many BMPR2 mutations, but as mentioned above, would be unlikely in the case of the $BMPR2^{R899X}$ mutation, unless the

deleted region of the C-terminus was involved in modulating Smad activation. Which of these possibilities may be relevant for this model is still unclear, and more detailed signalling studies will be required to elucidate this.

If the $BMPR2^{R899X}$ transgene does indeed interact in a dominant negative fashion with the native receptor, this might explain why over-expression of the transgene results in a stronger phenotype than BMPR2 haploinsufficiency. While $BMPR2^{+/-}$ mice exhibit modest elevations in RVSP and some arteriolar muscularization, but no arteriolar occlusion or plexiform lesions, our mice ubiquitously over-expressing $BMPR2^{R899X}$ show significant increases in RVSP, extensive arteriolar muscularization, alveolar remodelling and inflammatory cell infiltration under unstressed conditions. This is consistent with the findings of West et al. where over-expression of $BMPR2^{R899X}$ specifically in SMCs resulted in significantly increased RVSP, arteriolar muscularization and the presence of obliterative luminal lesions. Although our mice do not fully recapitulate the features described in SMC-$BMPR2^{R899X}$ mice, such as arteriolar occlusion, they also develop more severe PAH in comparison to $BMPR2^{+/-}$ mice. Therefore, potential dominant negative interactions with the native BMPR2 receptor may have a more profound impact on PAH pathogenesis than simply a reduction in normal BMPR2 signalling.

4.4. Evolving paradigms of PAH pathogenesis

4.4.1. Cell growth and apoptosis

Despite the recent evidence pointing to apoptosis as an important initiating factor in PAH, it is still unclear how it is involved in the early pathogenesis. Mechanisms by which apoptosis can lead to PAH were described in detail in section 1.6.2. Briefly, it has been

proposed that apoptosis can lead to PAH by contributing directly to endothelial dysfunction, in which damage to the endothelium results in reduced vasodilator function and arterial remodelling. In addition, apoptosis could lead directly to the degeneration of fragile pre-capillary arterioles, ultimately resulting in elevated pulmonary vascular resistance. Finally, widespread and recurrent EC apoptosis could result in the selection of apoptosis resistant and hyperproliferative ECs, contributing to the formation of vascular lesions.

We studied apoptosis over an 8 week time course of transgene expression to see whether an early increase in apoptosis could be demonstrated, in association with disease progression in this model. Intriguingly, an increase that was detected in BT mice, in particular after 2 and 4 weeks of transgene induction, which although significant, was modest. However, apoptosis is a transient event and the rapid clearance of apoptotic cells by a mechanism called efferocytosis [96] can further contribute to a reduction in steady-state levels, thus leading to an underestimation the actual rates of apoptosis. In an acute injury model such as monocrotaline, a large proportion of cells undergo apoptosis. Presumably, efferocytosis mechanisms are overwhelmed and clearance becomes inefficient in such circumstances. On the other hand, when levels of apoptosis are subtly increased, cells would be cleared rapidly enough that increased levels of apoptosis would barely be detectable. This is seemingly the case in this model of PAH as only a small number of apoptotic cells were detected. However, the failure of efferocytosis, which appears to be a key regulatory checkpoint for the immune system and cell proliferation, may contribute to disease pathogenesis by impeding both the resolution of inflammation and the maintenance of alveolar integrity [96]. The marked infiltration of macrophages together with alveolar septal thickening in this model might in fact indicate that efferocytosis mechanisms are indeed active in mice over-expressing the $BMPR2^{R899X}$ transgene. An obvious shortcoming of this

experiment is the lack of double-labelling, as combining TUNEL with staining for different cell type markers would have enabled us to conclude on the nature of the cell type undergoing apoptosis. Nonetheless, we believe that apoptosis is mainly associated with ECs in this model, since similar patterns were observed in our V-Cad model where over-expression of the $BMPR2^{R899X}$ transgene is restricted to ECs (Appendix 1, Figure S1.4).

In other animal models of PAH, proliferation is typically associated with disease pathogenesis via smooth muscle cell hypertrophy and vascular remodelling, and in rare cases with occlusive vascular lesions resulting from abnormal proliferation of endothelial cells. The temporal patterns of proliferation in mice over-expressing the $BMPR2^{R899X}$ transgene were therefore characterized to see whether they were also consistent with a causal role in disease progression. Although trends pointed towards a consistent increase in proliferation in BT mice at early time points, proliferation was only significantly increased after 8 weeks of transgene induction. Many factors could be accounting for this marked increase in proliferation. The significant arteriolar muscularization in this model suggests that a portion of the proliferating cells are smooth muscle cells. However, the large number of proliferating cells and their disperse localization in BT mice suggests that other cell types must be involved. Another possibility is the reactive proliferation of endothelial cells as a consequence of apoptosis. If proliferation occurred as a reactive response of endothelial cells to apoptosis, an initial wave in apoptosis at earlier time points would be expected, followed by a wave of proliferation at later time points. Interestingly, this is indeed the pattern that was observed, where apoptosis was significantly increased after 2 and 4 weeks of transgene induction, while proliferation peaked after 8 weeks. Alternatively, macrophages or other inflammatory cells could be proliferating in response to an increase in local inflammatory stimuli. The fairly large number of cells undergoing proliferation makes the

last possibility more likely. However, it could very well be a combination of all processes. Again, double-labelling the proliferating cells with different cell type markers would have been useful in identifying which cells are proliferating. Overall, despite the exact cause remaining unknown, the excessive proliferation could contribute to vascular occlusion, a phenomenon that might be detected later on during the course of the disease in this model.

To the best of our knowledge, this is the first study examining the early patterns of apoptosis and proliferation in a genetic model of PAH. Although the mechanisms remain unclear, preliminary data suggests that the patterns of apoptosis and proliferation are both consistent with a role in disease pathogenesis in this model. These results emphasize the importance of abnormalities in vascular cell growth and apoptosis, in accordance with recently emerged studies in the field, and further studies using this model will likely divulge valuable insight into the early mechanisms of PAH pathogenesis.

4.4.2. Inflammation

Over the years, there has been increasing evidence to suggest a role for inflammation in PAH, and several pro-inflammatory cytokines, amongst them IL-6, were implicated in disease pathogenesis. A correlation between regulation of the BMP pathway and regulation of inflammation in the context of PAH was recently shown, where heterozygous BMPR2 knockout mice had increased susceptibility to PAH caused by stimulation with 5-lipoxygenase [68]. This finding suggests that dysregulation in BMPR2 signalling conceivably causes vulnerability to an inflammatory second hit. In support of this, Hagen et al. have recently demonstrated the presence of a negative feedback loop between IL-6 and BMPR2 signalling, in which increased IL-6 induces BMP pathway activity, while increased BMP activity suppresses IL-6 [97]. The BMP pathway must therefore normally prevent

positive feedback loops in inflammatory cytokines, and in the absence of functional BMPR2 signalling, these pathways might become uncontrolled and lead to disease.

In light of this evidence, a small cohort of $BMPR2^{R899X}$ mice were subjected to treatment with IL-6 to see whether the addition of an inflammatory stimulus would enhance the PAH phenotype in this model. The surprising lack of overall increase in RVSP in BT mice probably owes to the high variability within each group, which might be reduced if the size of the cohort had been larger. Part of this variability is also due to the spontaneous PAH that appears to have been induced by IL-6 in a control mouse. This is not necessarily unexpected, as IL-6 has previously been shown to induce spontaneous PAH in rats [52]. The lack of increase in RV hypertrophy is not surprising either in the absence of a significant increase in RVSP. Overall, IL-6 mice had a phenotype very similar to that of mice without treatment, in terms of small pre-capillary arteriolar muscularization and alveolar septal thickening. Interestingly, they did not show a significant increase in the number of pulmonary macrophages. It could be speculated that the pro-inflammatory nature of IL-6 caused macrophage infiltration in NBT-ROSA mice in addition to BT mice, as both groups were receiving the treatment. Based on the results from previous studies, a repeat of this experiment using IL-6 at a higher dose, with larger cohorts of mice and including saline control groups would expectantly result in the potentiation of PAH, and be very useful in investigating precisely how inflammation is linked to disease pathogenesis.

The detection of an increased number of macrophages in mice over-expressing the $BMPR2^{R899X}$ transgene also further underlines the role of inflammation in the pathogenesis of PAH. Although the molecular mechanism of macrophage infiltration and its role remain elusive, macrophage accumulation and activation may promote the release of a variety of proinflammatory cytokines such as monocyte chemotactic protein (MCP)-1, which was

shown to be elevated in PAH, and is capable of causing vasoconstriction, increasing vascular permeability and inducing proliferation [98]. This candidate offers a possible link between inflammation and the pathogenesis of PAH. Importantly, the recognition of complex inflammatory disturbances in the vascular remodelling process opens up several avenues for future work in characterizing the role of different inflammatory mediators in PAH pathogenesis, in addition to offering potential new targets for therapy.

4.4.3. Unifying model of disease pathogenesis in mice over-expressing the BMPR2^{R899X} transgene

Based on the results of this study and previous findings gathered from the literature, we propose the following model for disease pathogenesis (Figure 15). An initial insult either by hypoxia, shear stress, inflammation, viral infection or other unidentified environmental triggers in genetically predisposed individuals (i.e. those with BMPR2 mutations) leads to excessive EC injury and apoptosis, which cascades into a complex series of interactions resulting in PAH. EC apoptosis is central to disease pathogenesis in this model by contributing directly to endothelial dysfunction and microvascular dropout, and indirectly to the formation of plexiform lesions. The ensuing disruption of fragile pre-capillary arterioles results in altered release of several cytokines, chemokines and growth factors, leading to SMC hyperplasia and the onset of inflammation. Increased production of these endothelial mediators also directly contributes to further vascular remodelling and recruitment of inflammatory cells. Concomitantly, BMPR2 mutations directly contribute to SMC hyperplasia and promote inflammation by disrupting the protective feedback loop between BMPR2 and IL-6. Eventually, excessive local inflammation together with vascular remodelling and microvascular dropout by apoptosis could conceivably result in increased

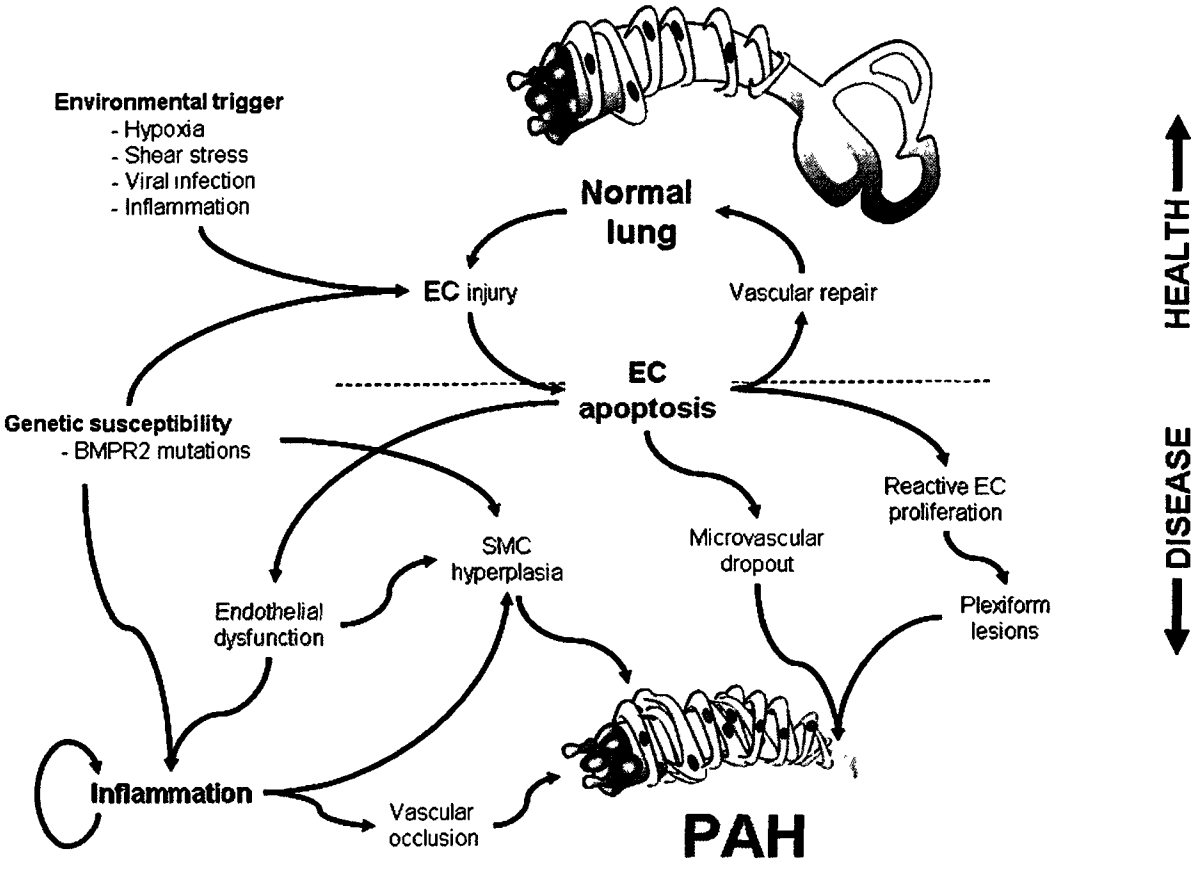

Figure 15. Proposed model for the pathogenesis of PAH in mice over-expressing the BMPR2^{R899X} transgene. BMPR2, bone morphogenetic protein receptor 2. EC, endothelial cell. PAH, pulmonary arterial hypertension. SMC, smooth muscle cell.

pulmonary vascular resistance and ultimately lead to PAH.

4.5. Therapeutic implications

To the extent that apoptosis represents the initiating mechanism underlying the pathogenesis of PAH, strategies designed to enhance vascular repair may represent an attractive therapeutic approach. Indeed, alternative approaches to pharmacological treatment of PAH are currently being explored, including cell therapy using endothelial progenitor cells (EPCs). Given the accumulating evidence supporting a role for circulating EPCs in repairing and regenerating damaged blood vessels throughout the body, exploiting the potential of these progenitor cells alone or in combination with genetic engineering represents a prospective future in PAH therapy. A number of clinical trials using progenitor cell therapy for PAH have been registered in clinicaltrials.gov, including the PHACeT trial (NCT00469027), which is currently enrolling patients. A recent pilot randomized trial has been reported showing that transplantation of autologous EPCs into patients with IPAH is safe, and the authors noted that the patients receiving EPC therapy had significant improvements in both primary and secondary endpoints of 6 minute walk test and mean pulmonary arterial pressure [99]. Therefore, EPC therapy may be a promising avenue for the treatment of PAH.

4.6. Limitations

In addition to some of the limitations discussed above, a major shortcoming of this study is the lack of strong transgene expression in $BMPR2^{R899X}$ mice. This could very well be a limiting factor to the severity of the phenotype that was observed in these mice. However, the presence of a phenotype despite low levels of transgene expression

demonstrates the importance of abnormal BMPR2 signaling in the development of a disease state. In terms of the impact of IL-6 administration of the development of PAH, interpretation of the results was difficult due to the small size of the groups, which increased variability, and the lack of saline controls, which would have been essential to help discern the effect of IL-6 from that of the transgene alone. The absence of a markedly more severe phenotype in response to IL-6 also made the effectiveness of the treatments questionable, as a larger proportion of BT mice were expected to develop overt PAH. Admittedly, the IL-6 delivery might not always have been efficient as it was administered at very low concentrations and in small volumes. These issues were not overlooked in previous data interpretations and will be addressed in future studies.

4.7. Future directions

This study opens up avenues for several lines of future work. First, this model could be used to pursue more detailed signalling studies to examine whether the transgene has a dominant negative interaction with the native BMPR2 receptor, or acts by a different mechanism altogether. Signalling studies could be refined by isolating vascular cells from the lungs of $BMPR2^{R899X}$ mice, or alternatively by transfecting cultured cells with the $BMPR2^{R899X}$ transgene, then examining the activity of the signalling pathways *in vitro* in the presence and absence of BMP ligands to determine whether perturbations could be demonstrated. The consequence of $BMPR2^{R899X}$ over-expression on downstream effectors could also be assessed by examining Id-1 expression, a common Smad target gene [59]. In addition, further characterization of the inflammatory processes taking place in this model should be pursued. For example, a cytokine array could be performed to identify which inflammatory mediators are involved as candidates in the mechanism of macrophage

infiltration. Similarly, the impact of IL-6 on disease manifestation should be further investigated by repeating IL-6 treatments with larger cohorts including saline controls. Of note, this model could be used to confirm a causal role for apoptosis in the pathogenesis of the PAH. One way to address this question would be to administer a pan-caspase inhibitor, such as Z-Vad, to mice over-expressing the $BMPR2^{R899X}$ transgene to determine whether preventing apoptosis would delay, inhibit or even reverse the progression of PAH, thereby pinpointing a key role for apoptosis in the pathogenesis of this disease. Along the same lines, this model could be used to validate the potential of EPC therapy as a regenerative treatment option. Eventually, this model could also be redeveloped using more potent ubiquitous promoters or more potent EC-specific promoters when these become available. One such promoter, Superscript Tie2, is currently being developed by our group. Together, these further studies would help unveil the intricacies of complex mechanisms and bring much needed understanding to the exact pathogenesis of PAH.

4.8. Conclusion

Altogether, over-expression of the $BMPR2^{R899X}$ transgene was shown to result in increased RVSP, pre-capillary arteriolar muscularization, alveolar septal thickening and infiltration of macrophages in lung tissue, therefore putting forth a new genetic murine model of PAH. Not only do BMPR2 mutations seem to predispose endothelial cells to apoptosis in this model, but they also appear to set the stage for excessive inflammation. This new model should be extremely useful in elucidating the early events leading to the initiation of PAH, notably by clarifying the yet undefined links between apoptosis, inflammation and disease pathogenesis, and serve as a platform to validate potential new treatments for this devastating disease.

5. References

1 Rubin LJ (1997) Primary pulmonary hypertension. *N Engl J Med* 336: 111-117

2 Simonneau G, Galie N, Rubin LJ, Langleben D, Seeger W, Domenighetti G, Gibbs S, Lebrec D, Speich R, Beghetti M et al (2004) Clinical classification of pulmonary hypertension. *J Am Coll Cardiol* 43: 5S-12S

3 Gaine SP, Rubin LJ (1998) Primary pulmonary hypertension. *Lancet* 352: 719-725

4 Runo JR, Loyd JE (2003) Primary pulmonary hypertension. *Lancet* 361: 1533-1544

5 Farber HW, Loscalzo J (2004) Pulmonary arterial hypertension. *N Engl J Med* 351: 1655-1665

6 Humbert M, Morrell NW, Archer SL, Stenmark KR, MacLean MR, Lang IM, Christman BW, Weir EK, Eickelberg O, Voelkel NF et al (2004) Cellular and molecular pathobiology of pulmonary arterial hypertension. *J Am Coll Cardiol* 43: 13S-24S

7 Hong KH, Lee YJ, Lee E, Park SO, Han C, Beppu H, Li E, Raizada MK, Bloch KD, Oh SP (2008) Genetic ablation of the BMPR2 gene in pulmonary endothelium is sufficient to predispose to pulmonary arterial hypertension. *Circulation* 118: 722-730

8 Atkinson C, Stewart S, Upton PD, Machado R, Thomson JR, Trembath RC, Morrell NW (2002) Primary pulmonary hypertension is associated with reduced pulmonary vascular expression of type II bone morphogenetic protein receptor. *Circulation* 105: 1672-1678

9 Scott J (2000) Pulling apart pulmonary hypertension. *Nat Genet* 26: 3-4

10 Zhang S, Fantozzi I, Tigno DD, Yi ES, Platoshyn O, Thistlethwaite PA, Kriett JM, Yung G, Rubin LJ, Yuan JX (2003) Bone morphogenetic proteins induce apoptosis in human pulmonary vascular smooth muscle cells. *Am J Physiol Lung Cell Mol Physiol* 285: L740-754

11 McLaughlin VV, Presberg KW, Doyle RL, Abman SH, McCrory DC, Fortin T, Ahearn G (2004) Prognosis of pulmonary arterial hypertension: ACCP evidence-based clinical practice guidelines. *Chest* 126: 78S-92S

12 Chen YF, Oparil S (2000) Endothelial dysfunction in the pulmonary vascular bed. *Am J Med Sci* 320: 223-232

13 Veyssier-Belot C, Cacoub P (1999) Role of endothelial and smooth muscle cells in the physiopathology and treatment management of pulmonary hypertension. *Cardiovasc Res* 44: 274-282

14 Nicod LP (2007) The endothelium and genetics in pulmonary arterial hypertension. *Swiss Med Wkly* 137: 437-442

15 Archer S, Rich S (2000) Primary pulmonary hypertension: a vascular biology and translational research "Work in progress". *Circulation* 102: 2781-2791

16 Stewart DJ, Levy RD, Cernacek P, Langleben D (1991) Increased plasma endothelin-1 in pulmonary hypertension: marker or mediator of disease? *Ann Intern Med* 114: 464-469

17 Christman BW, McPherson CD, Newman JH, King GA, Bernard GR, Groves BM, Loyd JE (1992) An imbalance between the excretion of thromboxane and prostacyclin metabolites in pulmonary hypertension. *N Engl J Med* 327: 70-75

18 Giaid A, Saleh D (1995) Reduced expression of endothelial nitric oxide synthase in the lungs of patients with pulmonary hypertension. *N Engl J Med* 333: 214-221

19 Tuder RM, Cool CD, Geraci MW, Wang J, Abman SH, Wright L, Badesch D, Voelkel NF (1999) Prostacyclin synthase expression is decreased in lungs from patients with severe pulmonary hypertension. *Am J Respir Crit Care Med* 159: 1925-1932

20 Humbert M, Montani D, Perros F, Dorfmuller P, Adnot S, Eddahibi S (2008) Endothelial cell dysfunction and cross talk between endothelium and smooth muscle cells in pulmonary arterial hypertension. *Vascul Pharmacol* 49: 113-118

21 Humbert M, Sitbon O, Simonneau G (2004) Treatment of pulmonary arterial hypertension. *N Engl J Med* 351: 1425-1436

22 Bellamy TC, Wood J, Goodwin DA, Garthwaite J (2000) Rapid desensitization of the nitric oxide receptor, soluble guanylyl cyclase, underlies diversity of cellular cGMP responses. *Proc Natl Acad Sci U S A* 97: 2928-2933

23 Vasquez-Vivar J, Kalyanaraman B, Martasek P, Hogg N, Masters BS, Karoui H, Tordo P, Pritchard KA, Jr. (1998) Superoxide generation by endothelial nitric oxide synthase: the influence of cofactors. *Proc Natl Acad Sci U S A* 95: 9220-9225

24 Xue C, Johns RA (1995) Endothelial nitric oxide synthase in the lungs of patients with pulmonary hypertension. *N Engl J Med* 333: 1642-1644

25 Ozaki M, Kawashima S, Yamashita T, Ohashi Y, Rikitake Y, Inoue N, Hirata KI, Hayashi Y, Itoh H, Yokoyama M (2001) Reduced hypoxic pulmonary vascular remodeling by nitric oxide from the endothelium. *Hypertension* 37: 322-327

26 Steudel W, Ichinose F, Huang PL, Hurford WE, Jones RC, Bevan JA, Fishman MC, Zapol WM (1997) Pulmonary vasoconstriction and hypertension in mice with targeted disruption of the endothelial nitric oxide synthase (NOS 3) gene. *Circ Res* 81: 34-41

27 Quinlan TR, Li D, Laubach VE, Shesely EG, Zhou N, Johns RA (2000) eNOS-deficient mice show reduced pulmonary vascular proliferation and remodeling to chronic hypoxia. *Am J Physiol Lung Cell Mol Physiol* 279: L641-650

28 Budhiraja R, Tuder RM, Hassoun PM (2004) Endothelial dysfunction in pulmonary hypertension. *Circulation* 109: 159-165

29 Nakayama T (2005) Prostacyclin synthase gene: genetic polymorphisms and prevention of some cardiovascular diseases. *Curr Med Chem Cardiovasc Hematol Agents* 3: 157-164

30 Hoshikawa Y, Voelkel NF, Gesell TL, Moore MD, Morris KG, Alger LA, Narumiya S, Geraci MW (2001) Prostacyclin receptor-dependent modulation of pulmonary vascular remodeling. *Am J Respir Crit Care Med* 164: 314-318

31 Geraci MW, Gao B, Shepherd DC, Moore MD, Westcott JY, Fagan KA, Alger LA, Tuder RM, Voelkel NF (1999) Pulmonary prostacyclin synthase overexpression in transgenic mice protects against development of hypoxic pulmonary hypertension. *J Clin Invest* 103: 1509-1515

32 Giaid A, Yanagisawa M, Langleben D, Michel RP, Levy R, Shennib H, Kimura S, Masaki T, Duguid WP, Stewart DJ (1993) Expression of endothelin-1 in the lungs of patients with pulmonary hypertension. *N Engl J Med* 328: 1732-1739

33 Galie N, Manes A, Branzi A (2004) The endothelin system in pulmonary arterial hypertension. *Cardiovasc Res* 61: 227-237

34 Davies RJ, Morrell NW (2008) Molecular mechanisms of pulmonary arterial hypertension: role of mutations in the bone morphogenetic protein type II receptor. *Chest* 134: 1271-1277

35 Higenbottam T, Wheeldon D, Wells F, Wallwork J (1984) Long-term treatment of primary pulmonary hypertension with continuous intravenous epoprostenol (prostacyclin). *Lancet* 1: 1046-1047

36 McLaughlin VV, Shillington A, Rich S (2002) Survival in primary pulmonary hypertension: the impact of epoprostenol therapy. *Circulation* 106: 1477-1482

37 Sitbon O, Humbert M, Nunes H, Parent F, Garcia G, Herve P, Rainisio M, Simonneau G (2002) Long-term intravenous epoprostenol infusion in primary pulmonary hypertension: prognostic factors and survival. *J Am Coll Cardiol* 40: 780-788

38 Channick RN, Simonneau G, Sitbon O, Robbins IM, Frost A, Tapson VF, Badesch DB, Roux S, Rainisio M, Bodin F et al (2001) Effects of the dual endothelin-receptor antagonist bosentan in patients with pulmonary hypertension: a randomised placebo-controlled study. *Lancet* 358: 1119-1123

39 Hasuda T, Satoh T, Shimouchi A, Sakamaki F, Kyotani S, Matsumoto T, Goto Y, Nakanishi N (2000) Improvement in exercise capacity with nitric oxide inhalation in patients with precapillary pulmonary hypertension. *Circulation* 101: 2066-2070

40 Ghofrani HA, Wiedemann R, Rose F, Olschewski H, Schermuly RT, Weissmann N, Seeger W, Grimminger F (2002) Combination therapy with oral sildenafil and inhaled iloprost for severe pulmonary hypertension. *Ann Intern Med* 136: 515-522

41 Cerinic Matucci M, Del Rosso A, Federico P, Livi R, Fiori G, Bartoli F, Blagojevic J, Tempestini A, Pignone A (2007) Therapeutic challenges for systemic sclerosis: facts and future targets. *Ann N Y Acad Sci* 1110: 448-454

42 Macchia A, Marchioli R, Marfisi R, Scarano M, Levantesi G, Tavazzi L, Tognoni G (2007) A meta-analysis of trials of pulmonary hypertension: a clinical condition looking for drugs and research methodology. *Am Heart J* 153: 1037-1047

43 Sitbon O, Humbert M, Jais X, Ioos V, Hamid AM, Provencher S, Garcia G, Parent F, Herve P, Simonneau G (2005) Long-term response to calcium channel blockers in idiopathic pulmonary arterial hypertension. *Circulation* 111: 3105-3111

44 Sakao S, Taraseviciene-Stewart L, Lee JD, Wood K, Cool CD, Voelkel NF (2005) Initial apoptosis is followed by increased proliferation of apoptosis-resistant endothelial cells. *Faseb J* 19: 1178-1180

45 Masri FA, Xu W, Comhair SA, Asosingh K, Koo M, Vasanji A, Drazba J, Anand-Apte B, Erzurum SC (2007) Hyperproliferative apoptosis-resistant endothelial cells in idiopathic pulmonary arterial hypertension. *Am J Physiol Lung Cell Mol Physiol* 293: L548-554

46 McMurtry MS, Archer SL, Altieri DC, Bonnet S, Haromy A, Harry G, Bonnet S, Puttagunta L, Michelakis ED (2005) Gene therapy targeting survivin selectively induces pulmonary vascular apoptosis and reverses pulmonary arterial hypertension. *J Clin Invest* 115: 1479-1491

47 Ley K, Laudanna C, Cybulsky MI, Nourshargh S (2007) Getting to the site of inflammation: the leukocyte adhesion cascade updated. *Nat Rev Immunol* 7: 678-689

48 Dorfmuller P, Perros F, Balabanian K, Humbert M (2003) Inflammation in pulmonary arterial hypertension. *Eur Respir J* 22: 358-363

49 Tuder RM, Voelkel NF (1998) Pulmonary hypertension and inflammation. *J Lab Clin Med* 132: 16-24

50 Mouthon L, Guillevin L, Humbert M (2005) Pulmonary arterial hypertension: an autoimmune disease? *Eur Respir J* 26: 986-988

51 Teder P, Noble PW (2000) A cytokine reborn? Endothelin-1 in pulmonary inflammation and fibrosis. *Am J Respir Cell Mol Biol* 23: 7-10

52 Miyata M, Sakuma F, Yoshimura A, Ishikawa H, Nishimaki T, Kasukawa R (1995) Pulmonary hypertension in rats. 2. Role of interleukin-6. *Int Arch Allergy Immunol* 108: 287-291

53 Golembeski SM, West J, Tada Y, Fagan KA (2005) Interleukin-6 causes mild pulmonary hypertension and augments hypoxia-induced pulmonary hypertension in mice. *Chest* 128: 572S-573S

54 Savale L, Tu L, Rideau D, Izziki M, Maitre B, Adnot S, Eddahibi S (2009) Impact of interleukin-6 on hypoxia-induced pulmonary hypertension and lung inflammation in mice. *Respir Res* 10: 6

55 Steiner MK, Syrkina OL, Kolliputi N, Mark EJ, Hales CA, Waxman AB (2009) Interleukin-6 overexpression induces pulmonary hypertension. *Circ Res* 104: 236-244, 228p following 244

56 Lane KB, Machado RD, Pauciulo MW, Thomson JR, Phillips JA, 3rd, Loyd JE, Nichols WC, Trembath RC (2000) Heterozygous germline mutations in BMPR2, encoding a TGF-beta receptor, cause familial primary pulmonary hypertension. *Nat Genet* 26: 81-84

57 Deng Z, Morse JH, Slager SL, Cuervo N, Moore KJ, Venetos G, Kalachikov S, Cayanis E, Fischer SG, Barst RJ et al (2000) Familial primary pulmonary hypertension (gene PPH1) is caused by mutations in the bone morphogenetic protein receptor-II gene. *Am J Hum Genet* 67: 737-744

58 Teichert-Kuliszewska K, Kutryk MJ, Kuliszewski MA, Karoubi G, Courtman DW, Zucco L, Granton J, Stewart DJ (2006) Bone morphogenetic protein receptor-2 signaling promotes pulmonary arterial endothelial cell survival: implications for loss-of-function mutations in the pathogenesis of pulmonary hypertension. *Circ Res* 98: 209-217

59 Miyazono K, Maeda S, Imamura T (2005) BMP receptor signaling: transcriptional targets, regulation of signals, and signaling cross-talk. *Cytokine Growth Factor Rev* 16: 251-263

60 Miyazawa K, Shinozaki M, Hara T, Furuya T, Miyazono K (2002) Two major Smad pathways in TGF-beta superfamily signalling. *Genes Cells* 7: 1191-1204

61 Kawabata M, Imamura T, Miyazono K (1998) Signal transduction by bone morphogenetic proteins. *Cytokine Growth Factor Rev* 9: 49-61

62 Miyazono K, Kusanagi K, Inoue H (2001) Divergence and convergence of TGF-beta/BMP signaling. *J Cell Physiol* 187: 265-276

63 West J, Harral J, Lane K, Deng Y, Ickes B, Crona D, Albu S, Stewart D, Fagan K (2008) Mice expressing BMPR2R899X transgene in smooth muscle develop pulmonary vascular lesions. *Am J Physiol Lung Cell Mol Physiol* 295: L744-755

64 Thomson J, Machado R, Pauciulo M, Morgan N, Yacoub M, Corris P, McNeil K, Loyd J, Nichols W, Trembath R (2001) Familial and sporadic primary pulmonary hypertension is caused by BMPR2 gene mutations resulting in haploinsufficiency of the bone morphogenetic protein tuype II receptor. *J Heart Lung Transplant* 20: 149

65 Long L, MacLean MR, Jeffery TK, Morecroft I, Yang X, Rudarakanchana N, Southwood M, James V, Trembath RC, Morrell NW (2006) Serotonin increases susceptibility to pulmonary hypertension in BMPR2-deficient mice. *Circ Res* 98: 818-827

66 Liu D, Wang J, Kinzel B, Mueller M, Mao X, Valdez R, Liu Y, Li E (2007) Dosage-dependent requirement of BMP type II receptor for maintenance of vascular integrity. *Blood* 110: 1502-1510

67 West J, Fagan K, Steudel W, Fouty B, Lane K, Harral J, Hoedt-Miller M, Tada Y, Ozimek J, Tuder R et al (2004) Pulmonary hypertension in transgenic mice expressing a dominant-negative BMPRII gene in smooth muscle. *Circ Res* 94: 1109-1114

68 Song Y, Jones JE, Beppu H, Keaney JF, Jr., Loscalzo J, Zhang YY (2005) Increased susceptibility to pulmonary hypertension in heterozygous BMPR2-mutant mice. *Circulation* 112: 553-562

69 Song Y, Coleman L, Shi J, Beppu H, Sato K, Walsh K, Loscalzo J, Zhang YY (2008) Inflammation, endothelial injury, and persistent pulmonary hypertension in heterozygous BMPR2-mutant mice. *Am J Physiol Heart Circ Physiol* 295: H677-690

70 Jurasz P, Courtman DW, Babaei S, Stewart DJ (2010) Role of Apoptosis in Pulmonary Hypertension: From Experimental Models to Clinical Trials. *Pharmacology & Therapeutics* [in press]

71 Thomas HC, Lame MW, Dunston SK, Segall HJ, Wilson DW (1998) Monocrotaline pyrrole induces apoptosis in pulmonary artery endothelial cells. *Toxicol Appl Pharmacol* 151: 236-244

72 Jones PL, Rabinovitch M (1996) Tenascin-C is induced with progressive pulmonary vascular disease in rats and is functionally related to increased smooth muscle cell proliferation. *Circ Res* 79: 1131-1142

73 Taraseviciene-Stewart L, Kasahara Y, Alger L, Hirth P, Mc Mahon G, Waltenberger J, Voelkel NF, Tuder RM (2001) Inhibition of the VEGF receptor 2 combined with chronic hypoxia causes cell death-dependent pulmonary endothelial cell proliferation and severe pulmonary hypertension. *Faseb J* 15: 427-438

74 Partovian C, Adnot S, Raffestin B, Louzier V, Levame M, Mavier IM, Lemarchand P, Eddahibi S (2000) Adenovirus-mediated lung vascular endothelial growth factor overexpression protects against hypoxic pulmonary hypertension in rats. *Am J Respir Cell Mol Biol* 23: 762-771

75 Campbell AI, Zhao Y, Sandhu R, Stewart DJ (2001) Cell-based gene transfer of vascular endothelial growth factor attenuates monocrotaline-induced pulmonary hypertension. *Circulation* 104: 2242-2248

76 Papapetropoulos A, Fulton D, Mahboubi K, Kalb RG, O'Connor DS, Li F, Altieri DC, Sessa WC (2000) Angiopoietin-1 inhibits endothelial cell apoptosis via the Akt/survivin pathway. *J Biol Chem* 275: 9102-9105

77 Thurston G, Rudge JS, Ioffe E, Zhou H, Ross L, Croll SD, Glazer N, Holash J, McDonald DM, Yancopoulos GD (2000) Angiopoietin-1 protects the adult vasculature against plasma leakage. *Nat Med* 6: 460-463

78 Thistlethwaite PA, Lee SH, Du LL, Wolf PL, Sullivan C, Pradhan S, Deutsch R, Jamieson SW (2001) Human angiopoietin gene expression is a marker for severity of pulmonary hypertension in patients undergoing pulmonary thromboendarterectomy. *J Thorac Cardiovasc Surg* 122: 65-73

79 Du L, Sullivan CC, Chu D, Cho AJ, Kido M, Wolf PL, Yuan JX, Deutsch R, Jamieson SW, Thistlethwaite PA (2003) Signaling molecules in nonfamilial pulmonary hypertension. *N Engl J Med* 348: 500-509

80 Sullivan CC, Du L, Chu D, Cho AJ, Kido M, Wolf PL, Jamieson SW, Thistlethwaite PA (2003) Induction of pulmonary hypertension by an angiopoietin 1/TIE2/serotonin pathway. *Proc Natl Acad Sci U S A* 100: 12331-12336

81 Chu D, Sullivan CC, Du L, Cho AJ, Kido M, Wolf PL, Weitzman MD, Jamieson SW, Thistlethwaite PA (2004) A new animal model for pulmonary hypertension based on the overexpression of a single gene, angiopoietin-1. *Ann Thorac Surg* 77: 449-456; discussion 456-447

82 Dewachter L, Adnot S, Fadel E, Humbert M, Maitre B, Barlier-Mur AM, Simonneau G, Hamon M, Naeije R, Eddahibi S (2006) Angiopoietin/Tie2 pathway influences smooth muscle hyperplasia in idiopathic pulmonary hypertension. *Am J Respir Crit Care Med* 174: 1025-1033

83 Kugathasan L, Dutly AE, Zhao YD, Deng Y, Robb MJ, Keshavjee S, Stewart DJ (2005) Role of angiopoietin-1 in experimental and human pulmonary arterial hypertension. *Chest* 128: 633S-642S

84 Kugathasan L, Ray JB, Deng Y, Rezaei E, Dumont DJ, Stewart DJ (2009) The angiopietin-1-Tie2 pathway prevents rather than promotes pulmonary arterial hypertension in transgenic mice. *J Exp Med* 206: 2221-2234

85 Zhao YD, Campbell AI, Robb M, Ng D, Stewart DJ (2003) Protective role of angiopoietin-1 in experimental pulmonary hypertension. *Circ Res* 92: 984-991

86 Abdulmalek K, Ashur F, Ezer N, Ye F, Magder S, Hussain SN (2001) Differential expression of Tie-2 receptors and angiopoietins in response to in vivo hypoxia in rats. *Am J Physiol Lung Cell Mol Physiol* 281: L582-590

87 Yamamoto A, Takahashi H, Kojima Y, Tsuda Y, Morio Y, Muramatsu M, Fukuchi Y (2008) Downregulation of angiopoietin-1 and Tie2 in chronic hypoxic pulmonary hypertension. *Respiration* 75: 328-338

88 Fournet-Bourguignon MP, Castedo-Delrieu M, Bidouard JP, Leonce S, Saboureau D, Delescluse I, Vilaine JP, Vanhoutte PM (2000) Phenotypic and functional changes in regenerated porcine coronary endothelial cells : increased uptake of modified LDL and reduced production of NO. *Circ Res* 86: 854-861

89 Boutet K, Montani D, Jais X, Yaici A, Sitbon O, Simonneau G, Humbert M (2008) Therapeutic advances in pulmonary arterial hypertension. *Ther Adv Respir Dis* 2: 249-265

90 Hansmann G, de Jesus Perez VA, Alastalo TP, Alvira CM, Guignabert C, Bekker JM, Schellong S, Urashima T, Wang L, Morrell NW et al (2008) An antiproliferative BMP-2/PPARgamma/apoE axis in human and murine SMCs and its role in pulmonary hypertension. *J Clin Invest* 118: 1846-1857

91 Nisbet RE, Bland JM, Kleinhenz DJ, Mitchell PO, Walp ER, Sutliff RL, Hart CM Rosiglitazone attenuates chronic hypoxia-induced pulmonary hypertension in a mouse model. *Am J Respir Cell Mol Biol* 42: 482-490

92 (2010) JAX Mice database. The Jackson Laboratory, http://jaxmice.jax.org/strain/006965.html

93 Mei SH, McCarter SD, Deng Y, Parker CH, Liles WC, Stewart DJ (2007) Prevention of LPS-induced acute lung injury in mice by mesenchymal stem cells overexpressing angiopoietin 1. *PLoS Med* 4: e269

94 Abdalla SA, Gallione CJ, Barst RJ, Horn EM, Knowles JA, Marchuk DA, Letarte M, Morse JH (2004) Primary pulmonary hypertension in families with hereditary haemorrhagic telangiectasia. *Eur Respir J* 23: 373-377

95 Goumans MJ, Mummery C (2000) Functional analysis of the TGFbeta receptor/Smad pathway through gene ablation in mice. *Int J Dev Biol* 44: 253-265

96 Vandivier RW, Henson PM, Douglas IS (2006) Burying the dead: the impact of failed apoptotic cell removal (efferocytosis) on chronic inflammatory lung disease. *Chest* 129: 1673-1682

97 Hagen M, Fagan K, Steudel W, Carr M, Lane K, Rodman DM, West J (2007) Interaction of interleukin-6 and the BMP pathway in pulmonary smooth muscle. *Am J Physiol Lung Cell Mol Physiol* 292: L1473-1479

98 Itoh T, Nagaya N, Ishibashi-Ueda H, Kyotani S, Oya H, Sakamaki F, Kimura H, Nakanishi N (2006) Increased plasma monocyte chemoattractant protein-1 level in idiopathic pulmonary arterial hypertension. *Respirology* 11: 158-163

99 Wang XX, Zhang FR, Shang YP, Zhu JH, Xie XD, Tao QM, Zhu JH, Chen JZ (2007) Transplantation of autologous endothelial progenitor cells may be beneficial in patients with idiopathic pulmonary arterial hypertension: a pilot randomized controlled trial. *J Am Coll Cardiol* 49: 1566-1571

Appendix 1 – Endothelial cell-specific over-expression of the BMPR2^{R899X} transgene in mice using the V-Cad promoter

Background

Over the years, ECs were increasingly suspected as being the cellular origin of PAH pathogenesis. It was shown that BMPR2 expression is prominent on the lung vascular endothelium with minimal expression in arterial smooth muscle [8]. Moreover, lung vascular endothelium has recently been reported to exhibit high levels of activation of downstream signaling molecules, such as Smads [58]. Mutations in the BMPR1, Alk-1, an endothelial restricted gene, have also been identified in patients with PAH [94]. Furthermore, a recent study has shown that the genetic ablation of BMPR2 in pulmonary endothelial cells is sufficient to predispose to PAH in mice [7]. Together, these data support a critical role for the endothelium in the pathogenesis of PAH. Therefore, we originally sought to determine the effect of targeted over-expression of BMPR2 mutations on EC survival in relation to the development of PAH. Our initial hypothesis was that EC-targeted loss-of-function mutations in BMPR2 would lead to PAH by increasing the susceptibility of ECs to apoptosis, particularly at the level of fragile pulmonary arterioles.

Methods

All experiments were performed as previously described, with the following exceptions. TetO$_7$-BMPR2^{R899X} mice were bred to driver mice harbouring the tetracycline transactivator (tTA) under the control of an endothelial selective promoter (V-Cad). This model uses a Dox-off transgene expression system; therefore, mice were put on doxycycline during gestation until 5 weeks of age to prevent embryonic lethality. Data points were

collected 8 weeks following the removal of doxycycline. Yupu Deng was responsible for performing α-SMA staining and imaging on these samples, in addition to gathering hemodynamic measurements. No quantification of muscularization was performed.

Results

To confirm the expression of the $BMPR2^{R899X}$ transgene in V-Cad mice, Western blots using a Flag antibody were performed. After a high exposure, bands were detected in BT mice, with some leakiness detected in NBT-$BMPR2^{R899X}$ mice, and an absence of expression in the CD1 control (Figure S1). β-actin was used as a loading control. However, this was a single finding amongst several attempts. In other blots, very little or no expression was detected specifically in BT mice. RVSP was measured after 8 weeks of transgene induction as an indicator of pulmonary artery pressure. RVSP was only elevated in 1 out of 12 BT mice, and the average RVSP was not significantly increased in BT mice compared to NBT-$BMPR2^{R899X}$ mice (26 ± 1.0 mmHg, n=12, 25 ± 0.61 mmHg, n=12, respectively, Figure S2A and S2B). Right ventricular hypertrophy was also assessed by calculating the RV/LV+S ratio, which was significantly increased in BT mice compared to NBT-$BMPR2^{R899X}$ mice (0.28 ± 0.01, n=5, 0.25 ± 0.006, n=7, respectively, $p<0.05$, Figure S2C and S2D). Staining for α-SMA also revealed qualitative thickening of the smooth muscle layer surrounding the small pulmonary arterioles of BT mice (Figure S3). The degree of muscularization was relatively consistent within the 4 mice in each group. Lastly, TUNEL staining was performed to detect apoptotic cells. The number of TUNEL-positive cells per high power field was significantly increased in BT mice compared to NBT-$BMPR2^{R899X}$ mice (6 ± 1 cells/HPF, n= 6, 1 ± 1 cells/HPF, n= 4, respectively, $p<0.05$, Figure S4).

Conclusion

Overall, the PAH phenotype observed in V-Cad BT mice was not as severe as originally anticipated. Indeed, only a portion of the BT mice displayed the characteristic features of PAH. That was not necessarily surprising since incomplete penetrance is a universal feature of BMPR2 mutations in humans. However, in this model, that could also be due to low levels of transgene expression. We therefore decided to pursue further experiments using the ROSA model, which ubiquitously expresses the transgene, in hopes of getting a more robust, consistent expression of the transgene as well as a more severe PAH phenotype.

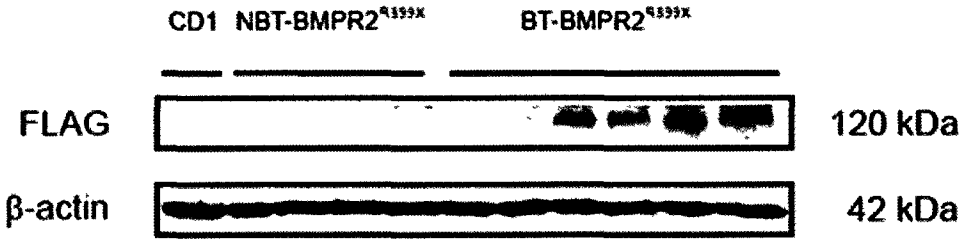

Figure S1.1. Expression of the BMPR2^{R899X} transgene in V-Cad mice. Western blot with an anti-Flag antibody on total protein extracts from the lungs of CD1 (n=1), NBT-BMPR2^{R899X} (n=4) and BT (n=6) mice following 8 weeks of transgene induction. β-actin was used as a loading control.

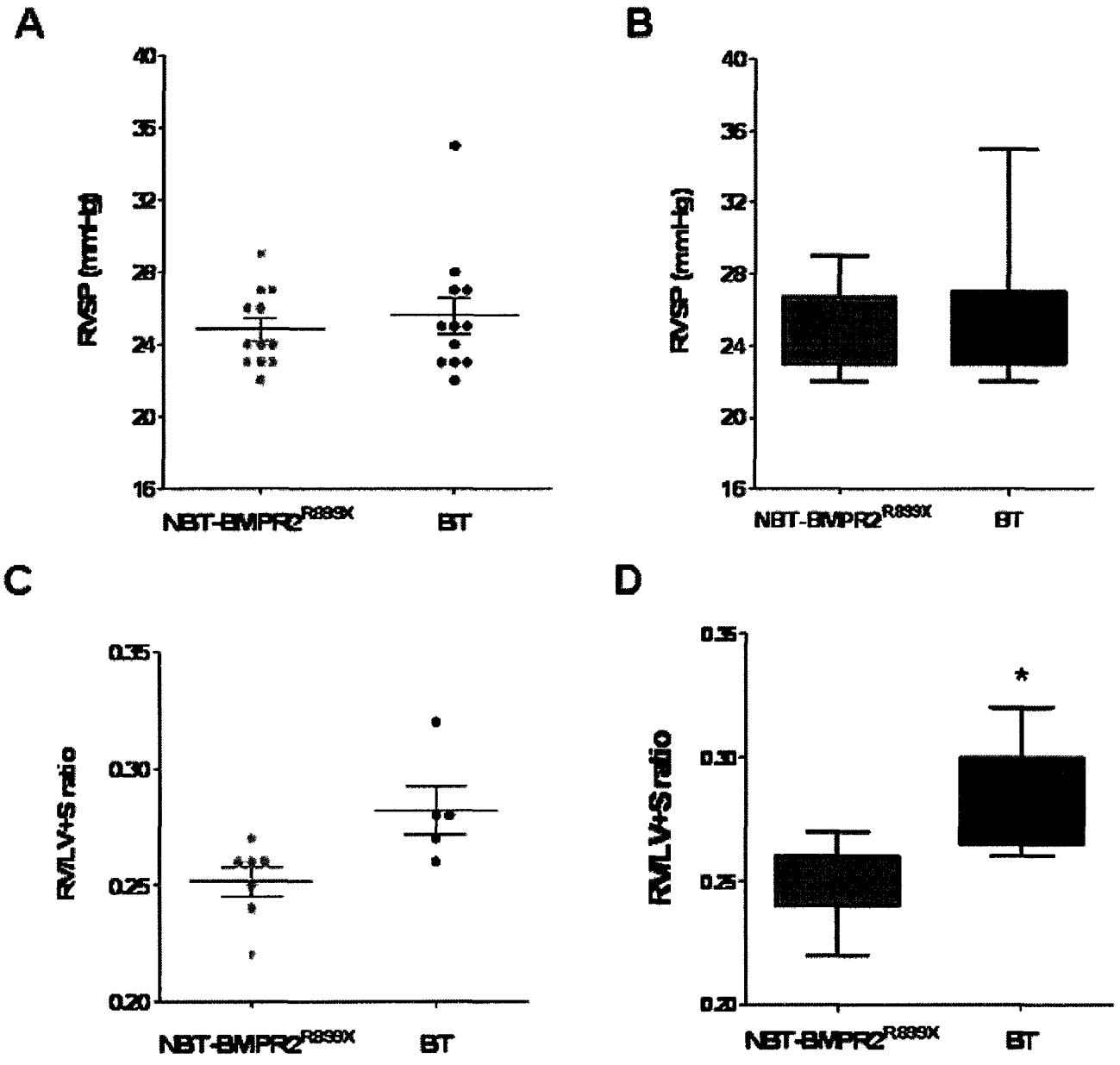

Figure S1.2. Distribution of RVSP and RV/LV+S values in V-Cad mice. **(A)** Scatter plot showing the distribution of RVSP values in BT mice (n=12) compared to NBT-BMPR2^{R899X} mice (n=12). Mean ± SEM. **(B)** Box plots summarizing RVSP values of each group. Whiskers represent sample minimum and maximum, line at sample median. **(C)** Scatter plot showing the distribution of RV/LV+S values in BT mice (n=5) compared to NBT-BMPR2^{R899X} mice (n=7). Mean ± SEM. **(D)** Box plots summarizing RV/LV+S values of each group. Whiskers represent sample minimum and maximum, line at median. * = $p<0.05$ by t-test with Welch's correction.

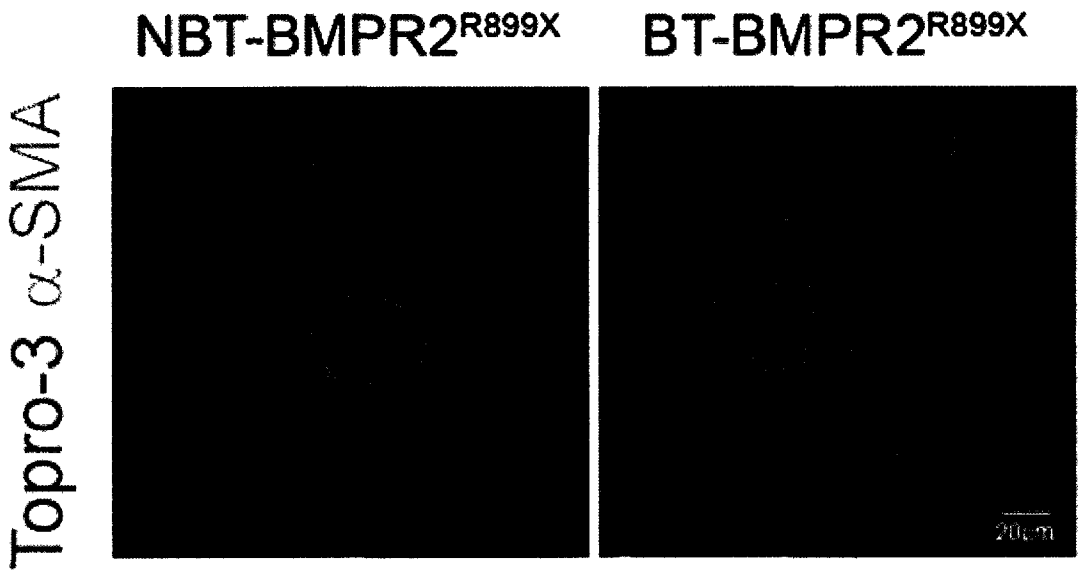

Figure S1.3. Arteriolar smooth muscle hypertrophy in V-Cad BT mice after 8 weeks of transgene induction. Immunofluorescence using an antibody against α-smooth muscle actin (α-SMA, red) combined with Topro-3 nuclear counterstaining (blue) on paraffin lung sections after 8 weeks of transgene induction. Bar = 20μm.

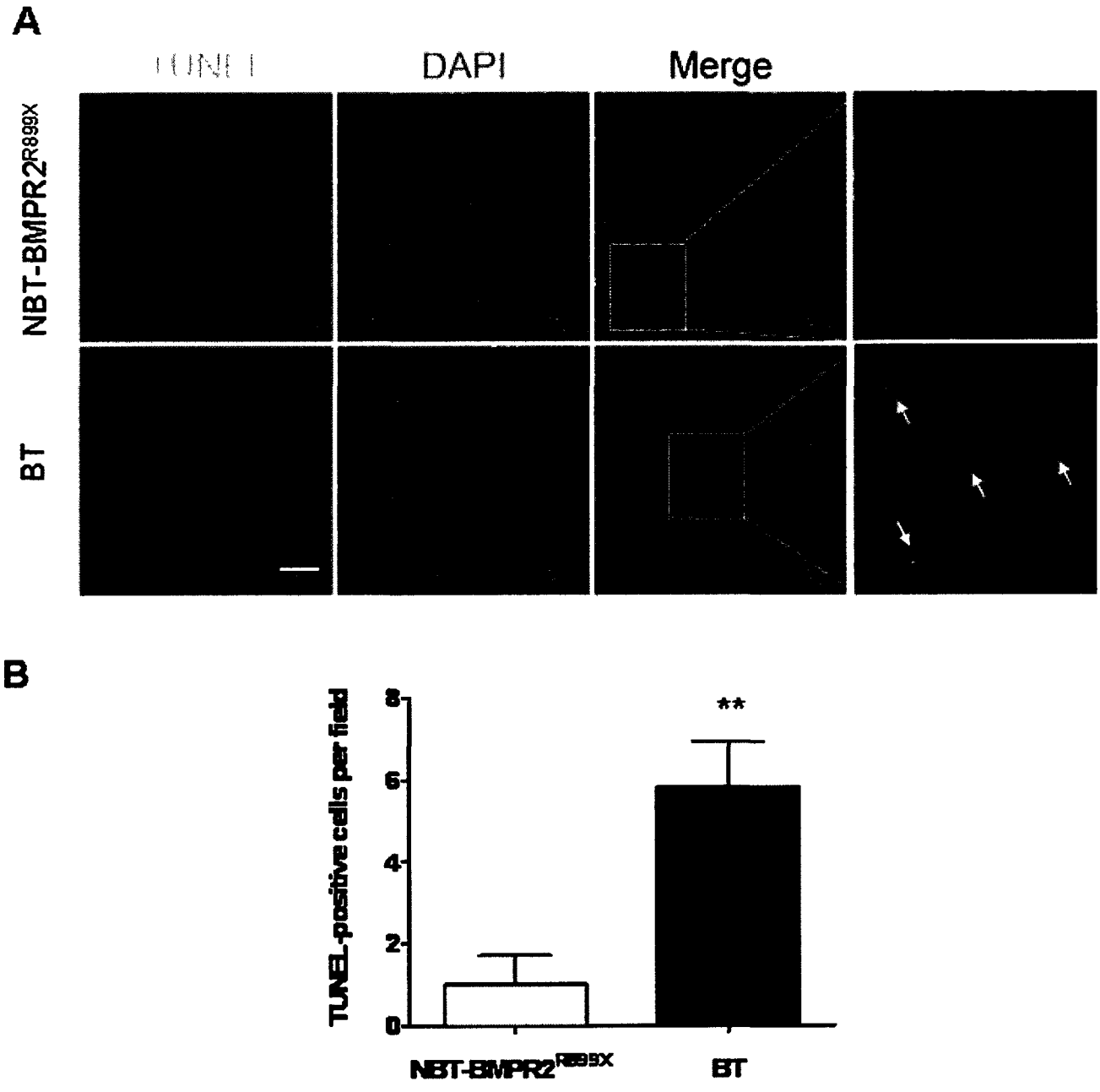

Figure S1.4. Apoptosis is increased in V-Cad BT mice after 8 weeks of transgene induction. **(A)** TUNEL staining combined with DAPI nuclear counterstaining on paraffin lung sections after 8 weeks of transgene induction. Bar = 50μm **(B)** Quantification of TUNEL-positive cells. Bar = mean + SEM. ** = $p<0.01$ by t-test with Welch's correction.

Appendix 2 – Supplemental Western blot figures

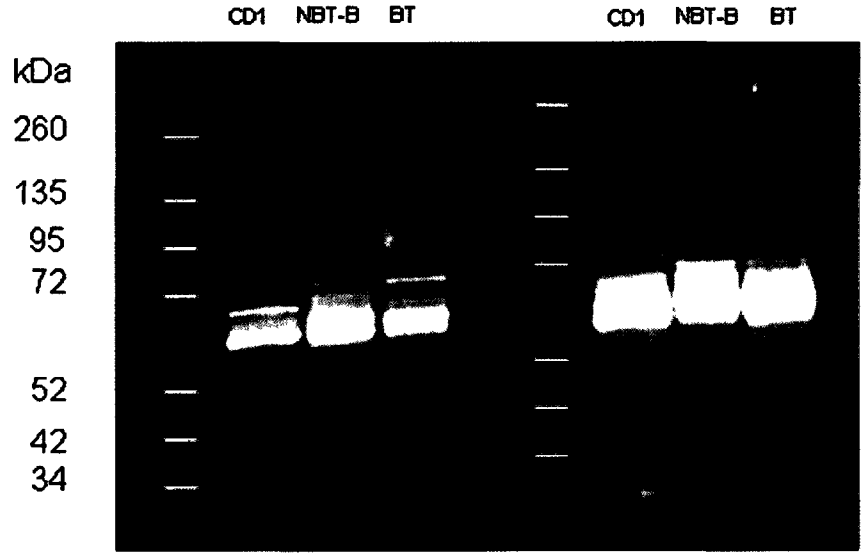

Figure S2.1. Expression of the BMPR2^{R899X} transgene in total protein extracts from ROSA mice. Western blot with an anti-DDK antibody on total protein extracts from the lungs of CD1, NBT-BMPR2^{R899X} and BT mice (n=2 replicates) following 8 weeks of transgene induction.

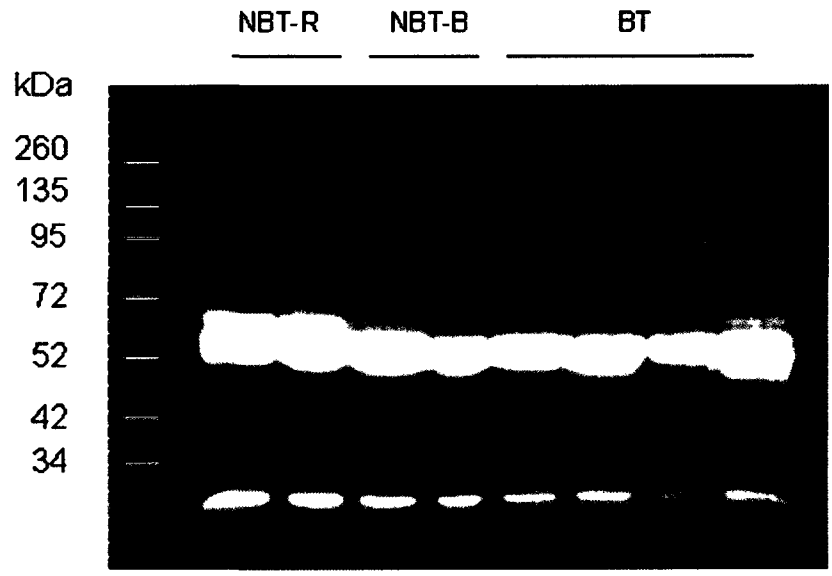

Figure S2.2. Expression of the BMPR2^{R899X} transgene in the membrane fraction of subcellular extracts from ROSA mice. Western blot with an anti-DDK antibody on the membrane fraction of subcellular protein extracts from the lungs of NBT-ROSA, NBT-BMPR2^{R899X} and BT mice (n=3) following 8 weeks of transgene induction.

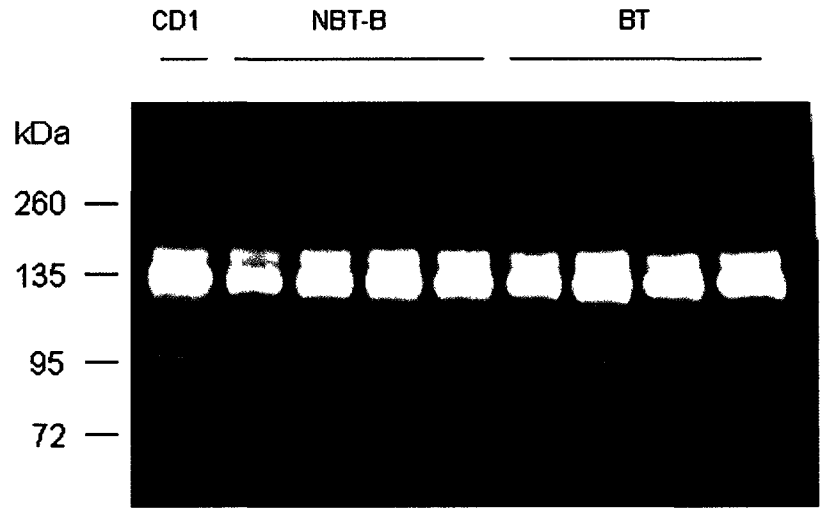

Figure S2.3. BMPR2 expression in total protein extracts from ROSA mice. Western blot with an anti-BMPR2 antibody on total protein extracts from the lungs of CD1, NBT-BMPR2^{R899X} and BT mice (n=4) following 8 weeks of transgene induction.

Appendix 3 – Solutions and Reagents

Histology

10X PBS
2.013 g KCl
81.816 g NaCl
21.714 g $Na_2HPO_4*7H_2O$
2.024 g KH_2PO_4
Fill to 1 L with dH_2O
Store at room temperature

4% PFA
40g Paraformaldehyde
1L 1X PBS
Heat slightly to dissolve
Adjust pH to 7.4

Mowiol mounting medium
2.4 g Mowiol (Calbiochem, 475904)
6 g Glycerol
12 mL H_2O
12 mL 0.2M Tris pH 8.5
2.5 % DABCO (Sigma, D2522)

Acid alcohol
2.5 mL 12N HCl
500 mL 70% EtOH

Scott's solution
6 g $MgSO_4$
1.05 g $NaHCO_3$
Fill to 300 mL with dH_2O

Western Immunoblotting

RIPA lysis buffer
25 mL 1M Tris-HCl pH 7.4
5 mL NP-40
15 mL 5M NaCl
1 mL 0.5M EDTA
449 mL dH_2O
5 mL glycerol
Add the following to 0.9 mL stock
50 µL 5% sodium deoxycholate
50 µL 1M NaF

10 µL 0.2M Na_3VO_4
10 µL protease inhibitor cocktail

BCA Reagent Mix
1 mL BCA
1 mL dH_2O
40 uL 4% $CuSO_4$

Laemmli buffer
781 µL 2M Tris-HCL pH6.5
0.5 g 10% SDS
0.0125 g 0.25% Bromophenol Blue
1.25 mL β-mercaptoethanol
2.5 mL Glycerol

5% Stacking Gel
1.8 mL 30% Acrylamide
2.5 mL 4X Stacking Buffer
5.7 mL dH_2O
75 µL 10% Ammonium Persulfate
10 µL TEMED

10% Separating Gel
5 mL 30% Acrylamide
3.75 mL 4X Separating Buffer
6.25 mL dH_2O
75 µL 10% Ammonium Persulfate
15 µL TEMED

4X Stacking Buffer – 500 mL
30 g Tris base
2 g SDS
Add to 300 mL dH_2O
Adjust pH to 6.8
Fill to 500 mL with dH_2O
Store at 4 °C

4X Separating Buffer – 500 mL
90 g Tris base
2 g SDS
Add to 300 mL dH_2O
Adjust pH to 8.8
Fill to 500 mL with dH_2O
Store at 4 °C

5X Running Buffer – 1 L
15 g Tris base
72 g Glycine
5 g SDS
Add to 700 mL dH_2O
Fill to 1L with dH_2O
Store at 4 °C
Dilute to 1X before use

Transfer Buffer – 800 mL
5.82 g Tris base
2.93 g Glycine
3.75 mL 10% SDS
Add to 250 mL dH_2O
Fill to 800 mL
Store at room temperature
Add 20% methanol before use

0.1% TBS-T – 1 L
10 mL 1M Tris-HCl pH 8.0
30 mL 5M NaCl
1 mL Tween-20
Fill to 1 L with dH_2O

5M NaCl – 500 mL
146.1 g NaCl
Add to 450 mL dH_2O
Heat slightly to dissolve
Fill to 500 mL with dH_2O
Store at room temperature

1M Tris-HCl – 500 mL
60.55 g Tris base
Add to 300 mL dH_2O
Adjust pH to 8.0
Fill to 500 mL with dH_2O
Store at room temperature